OXIDATIVE ENERGY PATHWAYS IN THE HUMAN BRAIN

QUANTIFYING CEREBRAL OXYGEN AND GLUCOSE DYNAMICS UNDER METABOLIC CHALLENGES

Antonia Bose

Graduate School of
Systemic Neurosciences
LMU Munich

Dissertation at the
Graduate School of Systemic Neurosciences
Ludwig-Maximilians-Universität München

16.05.2024

First Reviewer:	Prof. Dr. Dr. Valentin Riedl
Second Reviewer:	Prof. Dr. Tobias Staudigl
External Reviewer	Prof. Dr. Marc Tittgemeyer

Date of Defense : 30.09.2024

Abstract

The human body relies on oxidized glucose as its primary fuel. Therefore, oxygen and glucose metabolism are tightly coupled. Here, we examine this coupling in the human brain under metabolic challenges. To ensure energy homeostasis even in cases of glucose deficiency (hypoglycemia), the body has developed several fallback systems for adenosine triphosphate (ATP) production. To this end, it can oxidize alternate energy substrates, such as fatty acids, ketone bodies or lactate. Evidence on the extent to which the brain utilizes these alternate energy pathways is sparse. According to the Selfish Brain Theory, the brain prioritizes its own energy demand over that of other organs. Previous studies do, however, find decreases in cerebral glucose metabolism during hypoglycemia. It is unclear whether these findings imply a general downregulation of cerebral energy metabolism – an energy-saving measure – or whether the brain indeed switches to oxidation of alternate energy substrates. Therefore, the first project presented in this thesis investigated alterations in cerebral oxygen metabolism during hypoglycemia, using multiparametric quantitative BOLD (mqBOLD) MR imaging. Results demonstrate stable levels of the cerebral metabolic rate of oxygen (CMR_{O2}), concomitant with widespread changes in cerebral blood flow and oxygen extraction fraction in response to hypoglycemia. Further, while acute hypoglycemia is known to largely impair cognitive function, it was long unclear how long these cognitive deficits persist. We present evidence that memory consolidation, but neither encoding nor attention, is impaired under restored euglycemia following hypoglycemia. In favor of the Selfish Brain Theory, steady CMR_{O2} rates suggest the utilization of alternate energy pathways in the brain under hypoglycemia, such as astrocytic glycogenolysis and ketolysis. As a limiting factor, the first study did not quantify cerebral glucose metabolism (CMR_{glc}) concurrently, mainly due to the lack of imaging methods to do so fully quantitatively. The second project presented in this thesis demonstrates a novel way to simultaneously measure CMR_{O2} and CMR_{glc}. For the first time, we successfully combined mqBOLD and ^{18}F-FDG functional PET (fPET) for simultaneous quantification of cerebral oxygen and glucose metabolism under different conditions in one single scanning session, aiming for this unique setup to be applied to future studies, thereby expanding current knowledge about the mechanisms behind cerebral energy metabolism.

Table of Contents

List of abbreviations

^{18}F-FDG	[^{18}F]Fluorodeoxyglucose
^{31}P-MRS	Phosphorus-31 magnetic resonance spectroscopy
Acetyl-CoA	Acetyl coenzyme A
AIF	Arterial input function
AD	Alzheimer's disease
ATP	Adenosine triphosphate
BBB	Blood brain barrier
BGA	Blood gas analysis
BOLD	Blood oxygenation level dependent
BSR	Bootstrap ration
CA	Contrast agent
C_aO_2	Arterial oxygen content
CBF	Cerebral blood flow
CBV	Cerebral blood volume
CMR_{O2}	Cerebral metabolic rate of oxygen
CMR_{glc}	Cerebral metabolic rate of glucose
CNS	Central nervous system
CRP	C-reactive protein
CSF	Cerebrospinal fluid
Deoxy-hb	Deoxygenated hemoglobin
DM	Diabetes mellitus
FA	Fatty acid
FDG	Fluorodeoxyglucose
fMRI	Functional magnetic resonance imaging
fPET	Functional positron emission tomography
GLM	Generalized linear model
GM	Grey matter
GLUT	Glucose transporter
Hb	Hemoglobin

Hct	Hematocrit
HPA axis	Hypothalamus-pituitary-adrenal axis
IGF-1	Insulin-like growth factor 1
LHPA system	Limbic-hypothalamus-pituitary-adrenal system
LMM	Linear mixed modeling
MBq	Megabecquerel
MRI	Magnetic resonance imaging
MRS	Magnetic resonance spectroscopy
mqBOLD	Multiparametric quantitative blood oxygenation level dependent
O2sat	Oxygen saturation
OEF	Oxygen extraction fraction
OGI	Oxygen-to-glucose index
Oxy-hb	Oxygenated hemoglobin
PET	Positron emission tomography
PPP	Pentose phosphate pathway
R2’	Transverse relaxation rate
ROS	Reactive oxygen species
ROI	Region of interest
SNR	Signal-to-noise ratio
SNS	Sympathetic nervous system
SWR	Sharp wave ripple
TCA cycle	Tricarboxylic acid cycle, also known as Krebs cycle or citric acid cycle
T1DM	Type 1 diabetes mellitus
T2DM	Type 2 diabetes mellitus
TAC	Time activity curve
tSNR	Temporal signal-to-noise ratio
VASO	Vascular space occupancy
WM	White matter

1 General introduction

The human body's energy metabolism is fundamentally driven by the production and utilization of adenosine triphosphate (ATP) as the universal currency of cellular energy. ATP fuels a wide range of physiological processes, such as muscle contraction, biosynthesis of macromolecules (such as proteins and lipids), and neurotransmission (Khakh & Burnstock, 2009; O. H. Petersen & Verkhratsky, 2016). Hence, through ATP, the heart is able to pump blood, the body is able to repair muscle fibers after a workout, and we are able to perceive and interact with our environment. In short, ATP powers the entire body and mind. Consequently, we rely heavily on it and cannot tolerate ATP deficiency. Insufficient ATP levels lead to cellular dysfunction, metabolic imbalances, and, ultimately, cell death. To meet those energy demands required to maintain ATP homeostasis even under adverse circumstances, the body has developed several backup systems that tightly regulate intracellular energy levels at all times.

One organ that is particularly interesting when studying energetics is the brain, the driving force behind energy allocation. The human brain accounts for only ~2% of the body's weight while consuming about 20% of its total energy (Padamsey & Rochefort, 2023). Hence, it consumes a disproportionally large amount of energy relative to its mass. Any disruption in the brain's ATP supply has detrimental effects, leading to cognitive impairment, neurological dysfunction or other adverse outcomes (Johnson et al., 2019; Sharma et al., 2021). To expand the knowledge about the energetics of the human brain, this thesis examines the interplay between oxygen and glucose, two crucial substrates in energy metabolism. More specifically, the first chapter serves as a general introduction to human energy metabolism, laying the groundwork for the subsequent exploration of cerebral energy metabolism. The first research project investigates the relationship between brain and peripheral energy metabolism by examining the effects of systemic glucose deficiency on the brain's oxygen metabolism and neurovascular function, using a novel magnetic resonance imaging (MRI) technique. Further, it explores the relationship between glucose deficiency and cognitive functioning. The second project introduces a method for simultaneous quantification of oxygen and glucose metabolism in the human brain, using hybrid positron emission tomography (PET)-MR imaging. Findings from both studies are then tied together in a general discussion. Ultimately, with this thesis, I aim to

add to the understanding of human energy metabolism, particularly how it affects brain function.

1.1 Cellular respiration

Energy cannot be generated out of nowhere but can only be converted from one form to another. Usually, our main way to provide our bodies with energy is through food, particularly through carbohydrates, as found in legumes or grains. The human body needs a considerable amount of energy: on average 2250 kcal per day (Bernardin & Moller, 2013) which is equivalent to approximately 253 sugar cubes. This is not to say that it is a good idea to consume the daily 2250 kcal primarily in the form of sugar cubes. On the contrary, that would result in a number of health issues, including metabolic disorders, as we shall learn later. A balanced diet appears to be the better option. *Balanced* in this case means that it consists of the three macronutrients: proteins, fats and carbohydrates – each of which contributes distinctly to the maintenance of energy homeostasis.

After ingestion, proteins are broken down into their constituent amino acids, which mainly serve as building blocks for the synthesis of new proteins (Norton et al., 2015). They are essential for facilitating tissue growth and repair across the body, and, in the presence of energy deficiency, can be metabolized into simple sugar molecules to provide an additional source of energy (Schutz, 2011). In contrast to proteins, fats are often perceived as more harmful to our health. It is commonly known that high levels of some fats, such as cholesterol, are related to various health problems, including cardiovascular diseases (Berger et al., 2015). However, the body needs a certain amount of fat for healthy functioning (Schwingshackl et al., 2021). After ingestion, fat is broken down into fatty acids as well as glycerol (Friedman & Nylund, 1980). These fat molecules are important building blocks for cell membranes and serve as precursors for the synthesis of various lipid-based molecules, such as certain hormones. Additionally, they can be stored as triglycerides in adipose tissue as an energy reserve. Lastly, carbohydrates play the most important role when it comes to meeting acute energy requirements. After ingestion, the digestive system breaks them down into simple sugars, called glucose, which are absorbed into the bloodstream, distributed across the body and, ultimately, taken up by cells (Gray, 1970).

A summary of glucose metabolism within the cell can be found in Figure 1. In the cytoplasm of the cell, one mole of glucose is broken down into two pyruvates. This process is called glycolysis because glucose is lysed, meaning that it is broken down. Glycolysis produces 2 ATP. In the mitochondria, the two pyruvates are further metabolized into acetyl coenzyme A (acetyl-CoA). Acetyl-CoA subsequently enters the tricarboxylic acid (TCA) cycle, which is also commonly known as the Krebs or citric acid cycle. Via the TCA cycle, acetyl-CoA undergoes oxidative phosphorylation, leading to a net amount of 32 ATP molecules. This last step, oxidative phosphorylation, requires oxygen, hence the entire process from glycolysis to the end result of 32 ATP molecules is termed *aerobic* cellular respiration (Brady et al., 2012; Gibney, 2009).

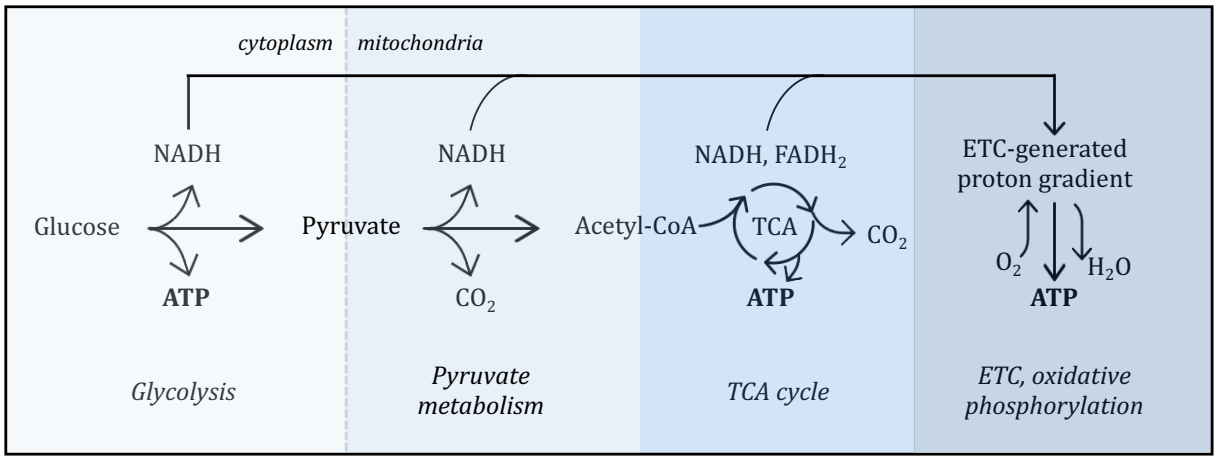

Figure 1. Schematic depiction of pathways involved in aerobic cellular respiration. During glycolysis, glucose is converted into pyruvate, a process that produces 2 ATP. Further, pyruvate is converted into acetyl-CoA, which is fed into the TCA cycle. The final step, oxidative phosphorylation, requires oxygen to finally generate a net amount of 32 ATP.

1.1.1 Metabolic challenges

In the face of metabolic challenges, such as during intense exercise, prolonged fasting or a ketogenic diet, aerobic cellular respiration is not possible to the same extent.

1.1.1.1 Oxygen deficiency

During intense exercise, muscles demand a higher amount of oxygen in order to meet the increased energy demands associated with muscle contraction and movement (Bangsbo, 2000). This can create an imbalance between oxygen demand and oxygen supply, requiring an alternate way of sustaining ATP levels since oxygen is necessary for

oxidative phosphorylation, the last step of aerobic cellular respiration (see Figure 1). Conversely, in anaerobic cellular respiration (see Figure 2), glucose is still lysed into two pyruvates, thereby producing 2 ATPs, but then not further metabolized into acetyl-CoA. Instead, pyruvate is converted into lactate, which can subsequently be used for gluconeogenesis, which is the synthesis of new glucose. The energy yield of non-oxidative glucose metabolism is thus 2 ATP (Byrne et al., 2014).

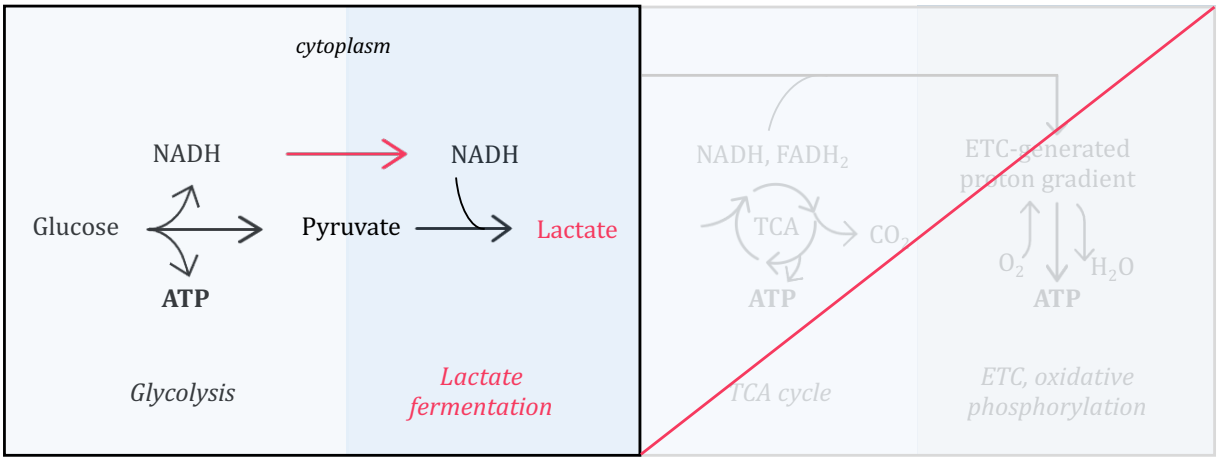

Figure 2. Anaerobic cellular respiration, yielding a total of 2 ATP. The difference to aerobic cellular respiration is that here, pyruvate is metabolized into lactate instead of acetyl-CoA. This process does not require oxygen and only takes place in the cytoplasm of the cell. As a consequence, cells that do not have mitochondria can undergo anaerobic cellular respiration but not aerobic cellular respiration.

Apart from the ability to adapt to an increased oxygen demand (e.g. during exercise or heightened neuronal activity), anaerobic cellular respiration is crucial for those cells lacking mitochondria (Fernie et al., 2004; Melkonian et al., 2024), for example erythrocytes (red blood cells) and Escherichia coli bacteria, as found in the digestive tract. They depend exclusively on anaerobic respiration due to their inability to further metabolize pyruvate into acetyl-CoA – a process occurring in the mitochondria of a cell. Thus, ATP production under anaerobic conditions is possible, albeit less efficient compared to aerobic conditions (2 vs. 32 ATP). It must be noted that even with sufficient oxygen available, cells still undergo anaerobic cellular respiration (Brady et al., 2012; Byrne et al., 2014). This is called aerobic glycolysis because it takes place under aerobic conditions. Aerobic glycolysis is particularly interesting in the context of increased neuronal activity, as we will discuss later.

1.1.1.2 Glucose deficiency

During prolonged fasting or when following a ketogenic diet, the body lacks its main glucose source: carbohydrates. While this might seem problematic at first, we only need to think a few thousands of years back: Before the agricultural revolution and subsequent progress in food preservation techniques, food availability was naturally limited, with periods of hunger being the norm. Consequently, the body has developed ways of dealing with these periods of food scarcity without compromising its energy balance. Specifically, four alternate pathways of ATP production when glucose availability is limited have been observed.

The first pathway, which would be the primary response to glucose deficiency, is glycogenolysis, the consumption of glycogen storages (Hems et al., 1980; Petersen et al., 2017). Even though glucose cannot be stored directly, it can be converted to glycogen and then stored inside cells. Most glycogen is found in the liver and muscles, while other organs, such as the brain, may contain smaller amounts, too (Brown, 2004; Brown & Ransom, 2007). When blood glucose levels drop, the hormones glucagon and epinephrine (adrenaline) trigger glycogenolysis, the process of breaking down glycogen into glucose molecules (Exton et al., 1972). These are released into the bloodstream and used by cells to produce ATP (see Figure 1). The time it takes for glycogen storages to be depleted depends on various factors, such as an individual's metabolic rate, muscle mass and current level of physical activity. During exercise, glycogen storages can be depleted within an hour, while during rest, the body usually has enough glycogen to last for a day (Browning et al., 2012; Melanson et al., 1999).

In case the carbohydrate scarcity persists, the body switches into the other three alternate pathways of ATP production: gluconeogenesis, fatty acid oxidation and ketogenesis. These three processes can take place concurrently or separately, depending on the specific metabolic conditions. They are depicted schematically in Figure 3. Gluconeogenesis refers to the synthesis of new glucose molecules from non-carbohydrate sources, such as amino acids, lactate or glycerol (X. Zhang et al., 2019). Once converted into glucose molecules, they undergo aerobic cellular respiration, as previously discussed.

Fatty acids first need to be released from triglycerides in adipose tissue, where they are primarily stored. Once released, fatty acids are metabolized directly inside the mitochondria. There, they undergo a process called beta-oxidation, which results in acetyl-CoA. As previously described, acetyl-CoA can enter the TCA cycle, producing ATP

through oxidative phosphorylation. Thus, in fatty acid oxidation, glycolysis and pyruvate metabolism are skipped (see Figure 3). During beta-oxidation, large amounts of acetyl-CoA are produced, sometimes exceeding the immediate capacity of the TCA cycle to metabolize them (Masino & Rho, 2012). As a result, there is a surplus of acetyl-CoA. In a process called ketogenesis, the liver then converts these additional acetyl-CoA molecules into ketone bodies since, after all, the body does not let any energy substrates go to waste. Ketone bodies are water-soluble and can be transported through the bloodstream as well as across the blood brain barrier (BBB) (Auestad et al., 1991; Kolb et al., 2021; Krebs, 1966). In this way, ketone bodies are a highly efficient form of transporting energy to tissues that have limited capacity to oxidize fatty acids directly, such as the brain (Schönfeld & Reiser, 2013). Once ketogenesis has been set in motion, the body enters the metabolic state of ketosis. Via ketolysis – the lysing of ketone bodies back into acetyl-CoA – the body is eventually able to perform the TCA cycle and oxidative phosphorylation to produce ATP in the respective tissue (see Figure 3). Almost all cell types are capable of using ketone bodies as an energy resource. Solely hepatocytes (liver cells) and erythrocytes are incapable of metabolizing them (Orii et al., 2008; Z. Zhang et al., 2011). Erythrocytes lack mitochondria and are thus dependent on anaerobic metabolic pathways, and hepatocytes lack the necessary enzyme to process ketones. This is an advantage though, since the liver is the main site for ketogenesis. It would be disadvantageous if it used up parts of the ketone bodies itself before providing them to other tissues.

In summary, in order to ensure energy balance in the face of prolonged carbohydrate deficiency, the body has developed four fallback systems (see Figure 3), varying in energetic efficiency:

1. Glycogenolysis: the production of glucose from glycogen
2. Gluconeogenesis: the formation of glucose molecules from non-carbohydrate sources
3. Fatty acid oxidation: the formation of acetyl-CoA from fatty acids
4. Ketogenesis: the formation of ketone bodies from excess acetyl-CoA

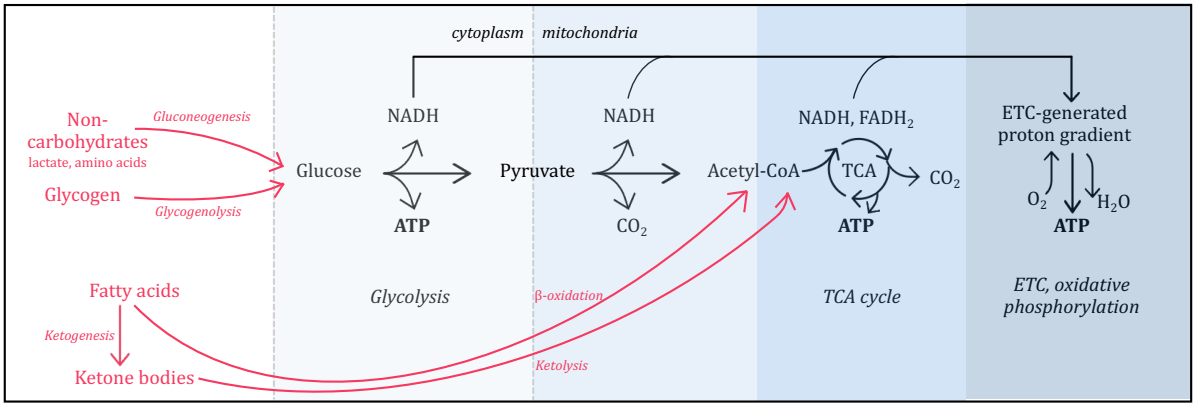

Figure 3. Schematic depiction of alternate pathways of ATP production: gluconeogenesis, glycogenolysis, fatty acid oxidation and ketolysis. During gluconeogenesis, new glucose is synthesized from substrates like lactate and amino acids. Glycogenolysis refers to the process of glycogen breakdown into glucose. In both cases, the newly gained glucose is metabolized as depicted in Figure 1. Fatty acids from adipose tissue can either be converted into acetyl-CoA via beta-oxidation or undergo ketogenesis, thereby producing ketone bodies. Ketone bodies can be transported efficiently to cells. Within the cell, they undergo ketolysis and by that are converted into acetyl-CoA. Acetyl-CoA can then be fed into the TCA cycle and subsequently undergo oxidative phosphorylation.

1.1.1.3 Experimental models of metabolic challenges

In order to explore the implications of metabolic challenges in a controlled setting, researchers employ various experimental models. Oxygen deficiency can be studied using hypoxia setups, where subjects (usually rodents) are exposed to air containing reduced oxygen levels (Brierley, 1977). Additionally, an increased oxygen requirement can be simulated through intense exercise (Xu & Rhodes, 1999). In both scenarios, researchers can examine the physiological responses to the imbalance between oxygen supply and demand.

To investigate effects of glucose metabolism as well as the previously mentioned fallback systems, researchers often study individuals following specific dietary regimens, such as a ketogenic diet (Su et al., 2000; Zajac et al., 2014). In this specific type of diet, people consume disproportionally small amounts of carbohydrates relative to proteins and particularly fats, leading to ketosis (Masood et al., 2023). Alternatively, ketone bodies can be infused directly into the bloodstream. Through this approach, for example, it has been discovered that the brain exhibits a preference for ketone bodies: When injecting ketone bodies, the cerebral metabolic rate of glucose (CMR_{glc}) decreased, even under conditions of normal blood sugar levels (euglycemia) (Hasselbalch et al., 1996). Hence, even when there is sufficient glucose available, the brain prefers metabolizing ketone bodies over glucose to produce ATP.

Studies that examine the implications of acute alterations in glucose metabolism, such as during low and high blood glucose levels (hypo- and hyperglycemia, respectively) typically use hyperinsulinemic glucose clamping (Heise et al., 2016). This technique involves intravenous infusions of glucose and insulin, a hormone crucial for regulating blood sugar levels. Glucose levels are monitored closely and glucose infusion rates are adjusted accordingly to reach the target blood glucose level. In healthy individuals, normal fasting blood glucose levels typically range between 70mg/dl and 100mg/dl, with postprandial levels of up to 140mg/dl still considered normal (World Health Organization, n.d.). By deviating from these levels researchers can induce hypo- or hyperglycemia, respectively. Hyperinsulinemic glucose clamping is particularly useful in studying insulin-induced hypoglycemia, a common side effect of Type 1 Diabetes Mellitus (T1DM) (Genuth, 2006).

The aforementioned models can be used across a spectrum of experimental settings to study the body's adaptive responses to metabolic challenges. They allow researchers to investigate various aspects of metabolic regulation both in healthy as well as diseased individuals (e.g. patients of diabetes mellitus) (e.g. Anderson et al., 2006; Heise et al., 2016; Laitinen et al., 2008). Furthermore, these challenges can be applied to study distinct adaptive responses of different organs, such as the brain when including them in neuroimaging studies, adding to a comprehensive understanding of how the body maintains energy homeostasis (Anderson et al., 2006; T. M. Blazey & Raichle, 2019). In the first research project later presented in this thesis, we applied hyperinsulinemic glucose clamping to study the effects of systemic glucose deficiency on cerebral energy metabolism. More detailed information about the study design as well as the scientific background will be provided below.

1.1.2 Glucose uptake

Whether derived from carbohydrates, glycogen or proteins, glucose must pass the cell membrane to fuel following metabolic pathways. There is a common conception that glucose transport into the cell is driven by insulin. However, the process is more complex. Glucose uptake into the cell is controlled by a family of membrane proteins, called glucose transporters (GLUT), comprising 14 subtypes distributed across the body. Among these GLUT subtypes, only GLUT4 is an insulin-dependent transporter (Huang & Czech, 2007;

Koepsell, 2020). When blood glucose levels rise, insulin is secreted from pancreatic beta cells into the bloodstream. Insulin then binds to receptors, activating GLUT4 proteins. These are primarily expressed in tissues like skeletal muscle, adipose tissue and the heart muscle (Abel, 2004; Kraegen et al., 1993; Laybutt, 1993). Thus, insulin-dependent glucose transport is crucial for general physiological functioning. Nevertheless, it is important to note that many cellular processes are regulated by insulin-independent glucose transporters, such as GLUT1, GLUT2 and GLUT3. GLUT1, the most common transporter, is predominantly found in the BBB, astrocytes and erythrocytes. GLUT2 is primarily located in the kidneys, liver, and pancreas, and GLUT3 in the placenta, neurons and kidneys (Koepsell, 2020; Thorens & Mueckler, 2010).

1.1.2.1 Disordered glucose uptake: Diabetes mellitus

Diabetes mellitus (DM) is a common metabolic disorder that currently affects ~9% of the world population (Standl et al., 2019). While both type 1 and type2 DM (T1DM and T2DM) are disorders of insulin metabolism, they differ in their underlying mechanisms, prognosis and treatment. T1DM is a chronic autoimmune disease characterized by the destruction of insulin-producing beta cells in the pancreas. Due to their vital involvement in insulin production and secretion, this leads to an absolute deficiency of insulin, resulting in high levels of blood glucose and insufficient levels of intracellular glucose (Alam et al., 2014). Common symptoms include sudden weight loss, dizziness, extreme thirst and hunger, and blurry vision. T1DM is typically treated with insulin therapy adminstered by the patients themselves. It must be noted however, that both insufficient as well as excessive levels of insulin have adverse consequences. Therefore, the biggest challenge in managing T1DM comes from the risk of insulin-induced hypoglycemia, especially considering the self-administrations of insulin injections. Various situational factors (such as exact food intake, alcohol consumption, stress, dysregulated circadian rhythm or exercise) affect insulin metabolism (Borghouts & Keizer, 2000; Catalano et al., 2022; Pei et al., 2003; Schrieks et al., 2015), making a precise calculation of the required insulin dose difficult which frequently results in hypoglycemia. Therefore, patients must monitor their blood glucose levels carefully at all times.

T2DM is the more common type of DM and is characterized by a decreased insulin sensitivity, usually caused by poor diet and insufficient physical activity. In T2DM, while pancreatic beta cells are intact, cells develop a resistance to insulin (Ginter, 2012). As a

result, they require higher amounts of insulin to enable glucose transport across the cell membrane. Many T2DM patients manage the condition well without therapy. Symptoms often improve with lifestyle alterations, such as dietary change and increased physical activity.

Despite being classified as a metabolic disorder, DM has far-reaching implications for various aspects of health. Particularly hypoglycemia as a result of insulin therapy seems to pose a problem. DM patients with recurrent episodes of hypoglycemia are, for instance, at a higher risk for cognitive and neurological impairments, such as memory deficits and Alzheimer's disease (AD) compared to DM patients without recurrent hypoglycemia (Chen et al., 2017; Profenno et al., 2010; Yaffe, 2013). Regarding underlying mechanisms of this relationship, it has been found that recurrent events of severe hypoglycemia lead to elevated levels of oxidative stress and necrosis, particularly in the hippocampus, a brain region crucial for memory processing (Auer, 2004; Dickerson & Eichenbaum, 2010; Won et al., 2012) . The adverse consequences of hypoglycemia are not limited to recurrent hypoglycemic episodes, though. Studies showed acute cognitive performance deficits under hypoglycemia in DM patients when compared to euglycemic conditions (Sommerfield et al., 2003b), a finding that has been replicated in healthy participants (Sommerfield et al., 2003a). Thus, low glucose availability in the periphery appears to have large effects on brain function and integrity, a relationship that this thesis aims to explore further.

1.2 Cerebral energy metabolism

The human brain's disproportionately high energy demand relative to its size, as well as compared to other species, has made the understanding of how it spends this energy a focal point in neuroscience for years. It is known that the majority of the brain's energy – 60% overall and 75% within gray matter – is spent on signaling (Engl & Attwell, 2015). Within this, 74% are allocated to postsynaptic information integration, a number that is notably lower, at 34%, in rodents (Attwell & Iadecola, 2002).

To provide this energy, the brain generally relies on a constant supply of energy substrates from the periphery, such as oxygen and glucose. It can tolerate some levels of hypoxia (Hochachka, 1998), but anaerobic cellular respiration, yielding only 2 ATP, is soon insufficient to cover cerebral energy demands. Under anoxic conditions, lacking oxygen

entirely, the brain can manage three to six minutes before the occurrence of irreparable damages (White et al., 1984) . Glucose transport across the BBB and into neurons mainly occurs via insulin-independent transporters (GLUT1 and GLUT3) (Koepsell, 2020). It is important to note that insulin-dependent GLUT4 can also be found in the central nervous system, albeit not as widespread as in the periphery (Koepsell, 2020; McNay & Pearson-Leary, 2020). Astrocytes play an important role in regulating cerebral glucose metabolism due to their ability to store glycogen and shuttle lactate to neurons (Bak et al., 2018; Brown & Ransom, 2007; Dienel, 2017). Moreover, astrocytes are able to metabolize fatty acids via beta-oxidation and ketogenesis (Allaman & Magistretti, 2013; Brocchi et al., 2022). The resulting ketone bodies can be used to fuel neurons. In that sense, astrocytes act as a buffer for neuronal energy demands, which can rapidly change due to spontaneous changes in neuronal activity.

In contrast to the periphery, the brain was long assumed to be a generally insulin-insensitive organ. In more recent years, however, studies found insulin receptors distributed throughout the central nervous system as well as transport mechanisms of insulin across the BBB (Rhea et al., 2018; Schulingkamp et al., 2000). Contrary to its primary role as a regulator of cellular glucose uptake in the periphery, insulin's actions within the brain appear to be more diverse. To a small extent, insulin is still involved in glucose uptake, recognizable by the expression of insulin-dependent GLUT4 transporters in some brain regions, particularly the hippocampus (McNay & Pearson-Leary, 2020). The majority of cerebral glucose consumption is, however, mediated by insulin-independent GLUT1 and GLUT3, predominantly found in astrocytes and neurons, respectively. Further, astrocytic insulin signaling was shown to play a crucial role in glucose sensing and the control of systemic energy homeostasis (García-Cáceres et al., 2016; Herrera Moro Chao et al., 2022). Additionally, insulin possesses neuroprotective properties (Adzovic et al., 2015; McNay, 2007). For instance, in stroke patients, these neuroprotective mechanisms act both indirectly and directly (Yu & Pei, 2015). Hyperglycemia is a common side effect of ischemic stroke, with hyperglycemic stroke patients at higher mortality risk compared to euglycemic stroke patients. Studies show that insulin injections alleviate this effect not only by lowering blood glucose levels but also by reducing inflammatory markers, neuronal cell death and cortical infarction, thereby improving subjects' chances of survival (Garg et al., 2006; LeMay et al., 1988; Voll et al., 1989). In addition to this rather indirect effect via the periphery, other studies showed a direct neuroprotective effect of

insulin on the brain independent of its regulatory effect on blood glucose levels: Insulin injected directly into cerebral ventricles, without changing blood glucose concentrations, reduced the amount of neuronal cell death following ischemia (Zhu & Auer, 1994).

Taken together, these examples show the importance of insulin balance for intact brain functioning. Insulin's signaling, glucose-regulatory and neuroprotective functions suggest that its role within the central nervous system is manifold and cannot be equated to insulin function in the periphery.

1.2.1 The oxygen-to-glucose index (OGI)

As previously discussed, cellular respiration can occur aerobically (via glycolysis, TCA cycle, oxidative phosphorylation; requiring oxygen) and anaerobically (via glycolysis, lactic acid fermentation; not requiring oxygen). Since the former pathway involves oxygen, whereas the latter one does not, the molar ratio between oxygen and glucose consumption can provide insights into the nature of its energy metabolism. This ratio, known as the oxygen-to-glucose index (OGI), serves as a measure of oxidative vs. non-oxidative glucose metabolism. It is calculated as

$$\mathrm{OGI} = \frac{\mathrm{CMRO2}}{\mathrm{CMRglc}}$$

In purely oxidative cellular respiration, the ratio between oxygen and glucose consumption would be 6:1, as oxidizing one mole of glucose requires 6 moles of oxygen (Brady et al., 2012). Theoretically, the OGI would hence be 6. If glucose metabolism is at least in part nonoxidative, less oxygen would be consumed and the OGI would thus be <6. Conversely, an OGI of >6 would indicate a higher consumption of oxygen, a lower consumption of glucose, or both. Such a deviation can indicate the utilization of alternative substrates other than glucose for ATP production.

Particularly in neuroenergetics, the OGI has been studied to gain insight into the metabolic efficiency (32 vs. 2 ATP) and substrate preference of brain tissue under different conditions. In healthy adults, neuroimaging studies have found a resting OGI of approximately 5.5 (T. Blazey, Snyder, Goyal, et al., 2018; Shulman et al., 2001; Sokoloff, n.d.), which is close to the theoretical value of 6 and suggests parts of glucose metabolism

to be non-oxidative. During increased neuronal activity, the OGI has been suggested to drop substantially, one study reporting a decrease of 90% (Fox et al., 1988). This would imply a strong uncoupling between oxygen and glucose metabolism during neuronal activation. However, findings from other studies suggest a weaker OGI drop during stimulation (Davis et al., 1998; Donahue et al., 2009; Fujita et al., 2006; Kim et al., 1999), albeit still implying a decrease. It is not entirely clear why the brain switches to higher rates of non-oxidative glucose metabolism upon heightened neuronal activity. It seems less efficient to convert glucose into lactate, thereby producing only 2 ATP. One explanation for a preference towards lactate fermentation over oxidative phosphorylation is its speed. Lactate fermentation has been found to be more rapid (Pfeiffer 2001). Consequently, despite non-oxidative glucose metabolism only generating 2 ATP per mole of glucose, it might eventually be more efficient and better suited for supporting rapid bursts of activity in neurons. Empirical data regarding the exact extent of glucose/oxygen uncoupling during neuronal activity is lacking. This is mainly due to the inability of previous studies to measure oxygen and glucose dynamics simultaneously, which will be described in detail below. Moreover, there is a disagreement about the uniformity of the OGI across the cortex, with some studies stating equal OGI across the brain and others finding differences between functional brain networks (T. Blazey, Snyder, Su, et al., 2018; Hyder et al., 2016). Again, consecutive data acquisition of CMR_{O2} and CMR_{glc}, opposed to simultaneous acquisition, impedes result interpretation. We addressed this gap in literature in the second manuscript of this thesis, where we combined recent advances in neuroimaging to, for the first time, measure oxygen and glucose metabolism in the human brain simultaneously and dynamically.

1.2.2 The selfish brain

Given its high energy demand and importance for overall well-being and functioning, researchers proposed that the brain has evolved to prioritize its own energy demand, which can come at the expense of other bodily systems, including other vital organs, such as the heart. This idea was summarized as the Selfish Brain Theory (Peters et al., 2004). First evidence for this theory came from early post-mortem studies in humans showing the preservation of human brain mass during inanition, while other organs, including the heart, liver and kidneys, lost about 40% of their mass (Krieger,

1921). More recent in-vivo studies in animals and humans provided further evidence for neuroprotection during metabolic challenges (Kind et al., 2005; Miller et al., 2002; Peters et al., 2011). According to the Selfish Brain Theory, the CNS has regulatory mechanisms to ensure coverage of the brain's energy demands.

One such mechanism is the limbic-hypothalamus-pituitary-adrenal (LHPA) system. If ATP levels in the brain drop, neurons in the ventromedial hypothalamus are disinhibited which activates the sympathetic nervous system (SNS) and subsequently suppresses pancreatic insulin production (Hitze et al., 2010). Reduced insulin levels lead to decreased glucose uptake by the insulin-dependent GLUT4 transporters, thereby leaving more glucose available for other tissues, such as neuronal tissue. This cerebral insulin suppression is one example of the brain's active pull-mechanisms, supporting the Selfish Brain Theory. In this context, the brain is not considered as solely relying on passive supply mechanisms (push factors). Instead, according to the energy-on-demand principle, it is depicted as an organ engaging in active pull mechanisms to cover its energy requirements (Peters et al., 2022). Another example for a pull mechanism is the increase of subcutaneous lipolysis, triggered by the SNS and hypothalamus-pituitary-adrenal (HPA) axis (Lopaschuk et al., 2010) which provides more fatty acids for cardiac and skeletal muscles – two tissue types with high energy demands – thereby increasing glucose availability for the brain. For more examples on the brain's pull mechanisms, please consult the review paper by Peters et al. (2022).

According to the Selfish Brain Theory, the cerebral energy metabolism should remain largely unaffected by decreased levels of glucose availability. A recent PET study, however, found decreased levels of glucose consumption (cerebral metabolic rate of glucose, CMR_{glc}) during acute hypoglycemia (T. M. Blazey & Raichle, 2019). It is unclear whether these results imply a general downregulation of cerebral energy metabolism during glucose deficiency. This would be a kind of energy-saving measure and contradict the Selfish Brain Theory. Potentially, a general reduction in cerebral energy metabolism could explain cognitive deficits during hypoglycemia. Alternatively, decreased CMR_{glc} levels could mean that, during hypoglycemia, the brain utilizes other energy substrates. In fact, it is quite likely that it metabolizes, for instance, astrocytic glycogen during glucose deficiency (Choi et al., 2003; Öz et al., 2007), but what remains unclear is to what extent alternate substrates are utilized for ATP production and whether they are able to compensate for the lack of glucose entirely. These open questions were our motivation

for the first projected presented in this thesis. The metabolism of alternate substrates, such as lactate, fatty acids or ketone bodies, would still require oxidative phosphorylation for ATP production (see Figure 3). Consequently, oxygen metabolism should remain unaffected. Therefore, in the first project, we measured cerebral oxygen metabolism under hypoglycemia. To this end, we applied a novel neuroimaging technique to measure the cerebral metabolic rate of oxygen (CMR_{O2}), as described in the next section.

1.2.3 Measuring cerebral energy metabolism in vivo

Ideally, direct measurement of ATP within the human brain in vivo would provide detailed insights into cellular energy metabolism. However, such direct measurement is not yet possible. One approach to approximate ATP levels in vivo is 31-phosphorus magnetic resonance spectroscopy (^{31}P-MRS). MRS is a non-invasive imaging technique that measures specific metabolite concentrations within tissues based on their chemical composition (Dappert et al., 1992). While ^{31}P-MRS is able to detect phosphorus-containing compounds, such as ATP, phosphocreatine or inorganic phosphate, it cannot distinguish between the individual compounds. Thus, ATP levels can only be approximated from this technique. Moreover, MRS has limited spatial resolution and sensitivity, which affects the precision of ATP level estimations.

Even if direct ATP measurements were feasible, it would not offer any insight into the mechanisms underlying ATP synthesis: e.g. oxidative vs. non-oxidative cellular respiration or the utilization of glucose vs. alternate substrates. Therefore, measuring underlying metabolic compounds, such as oxygen and glucose, not only aligns with current technical possibilities but also provides valuable information about the specific pathways involved in ATP synthesis.

1.2.3.1 Measuring cerebral oxygen metabolism

The current standard to study changes in brain tissue oxygenation is functional magnetic resonance imaging (fMRI). This non-invasive MR technique picks up changes in the oxygenation status of hemoglobin (Hb), a protein that transports oxygen from the lungs to tissues throughout the body and carbon dioxide back to the lungs for exhalation. fMRI is mainly applied to approximate neuronal activity. The underlying idea is that neuronal activation requires oxygen, which is extracted from the bloodstream for

oxidative phosphorylation and, ultimately, ATP production. In response to the elevated oxygen demand, cerebral blood flow (CBF) increases, delivering new oxy-Hb to the brain. This increase in CBF often overcompensates for the required oxygen, resulting in a decrease in deoxy-Hb concentrations in the blood. Fortunately for MR researchers, oxy-Hb and deoxy-Hb have distinct magnetic properties, with the paramagnetic nature of deoxy-Hb causing localized magnetic field distortions, thereby increasingly dephasing protons, which mitigates the MR signal (Byrne et al., 2014; Drew, 2019). These changes in deoxy-Hb between different conditions can then be picked up by the MR scanner and are reflected in the Blood Oxygen Level Dependent (BOLD) contrast. Despite its advantages, such as non-invasiveness, relatively short acquisition time as well as robust spatial and temporal resolution, the BOLD contrast has its limitations. It neither directly measures neuronal activity nor oxygen consumption (Buxton, 2010). Instead, it relies entirely on the assumption that changes in deoxy-Hb concentrations reflect changes in oxygen consumption, complicating data interpretation. Changes in deoxy-Hb, and with that in the BOLD signal, could come from both increased oxygen consumption and/or increased provision with oxy-Hb. The BOLD signal thus mixes hemodynamic and metabolic signals. Moreover, due to its relative nature, BOLD imaging can only provide information about its percentage change between conditions, limiting its utility for absolute comparisons across brain regions, subjects and studies.

Quantitative measurements of oxygen consumption. A more direct method for measuring oxygen metabolism in the human brain is via oxygen-15 PET ($^{15}O_2$-PET) (Herscovitch et al., 1983; Raichle et al., 1983). The underlying principle of PET imaging is the administration of radiotracers, which are radioactively labeled molecules. Radiotracers decay by releasing positrons, which then interact with nearby electrons in the body, producing gamma rays. These gamma rays are picked up by the PET scanner to create images. $^{15}O_2$-PET combines the inhalation of $^{15}O_2$-labeled gas and the injection of $[^{15}O]H_2O$ in order to measure cerebral blood volume (CBV), the oxygen extraction fraction (OEF) and CBF, separately (Herscovitch et al., 1983; Raichle et al., 1983). Using these parameters, one can then calculate the cerebral metabolic rate of oxygen (CMR_{O2}) via Fick's principle:

$$CMR_{O2} = Ca_{O2} * CBF * OEF$$

where Ca_{O2} represents the arterial oxygen content (Fick, 1870, p. 18). CMR_{O2}, expressed in µmol/100g/min, provides a direct and absolute measure of oxygen metabolism, offering insights into cellular energy metabolism. However, PET generally comes with some drawbacks, particularly concerning its invasiveness. One of the primary challenges in PET is the administration of the radiotracer. Due to its short decay time of approximately two minutes, $^{15}O_2$-PET typically requires higher tracer doses to ensure an adequate amount of tracer available for imaging. This results in rather high levels of absolute radiation exposure which is particularly ethically problematic when studying healthy participants. The short decay time also leads to difficulties in coordinating tracer production and administration. Moreover, compared to MRI, PET offers poorer spatial resolution.

In recent years, researchers have developed a way of measuring CMR_{O2} using MRI, thereby addressing the aforementioned drawbacks. Multiparametric quantitative BOLD (mqBOLD) involves the acquisition of separate MR sequences to gain information on CBF, CBV and tissue oxygenation (Christen et al., 2012; Hirsch et al., 2014; Kaczmarz et al., 2020). CBV is measured via the administration of a gadolinium-based contrast agent and, when combined with information on tissue oxygenation, yields the oxygen extraction fraction (OEF). As previously described, using Fick's principal ($CMR_{O2} = Ca_{O2} * CBF * OEF$), these parameters can be combined to yield voxelwise CMR_{O2} maps. Ca_{O2}, the arterial oxygen capacity can be measured via the individual's hematocrit value and arterial oxygen saturation, determined by blood sampling and pulse oximetry, respectively. In Fick's principle, by multiplying absolute oxygen provision to a brain region (voxelwise CBF maps in ml/100g/min and Ca_{O2}) with relative oxygen extraction from that brain region (voxelwise OEF maps), we can calculate how much oxygen was consumed in absolute terms, yielded as CMR_{O2} in µmol/100g/minute. The advancement of mqBOLD avoids previous limitations of both $^{15}O_2$-PET as well as the BOLD contrast. Compared to $^{15}O_2$-PET, mqBOLD does not require the injection of a radiotracer and is thus notably less invasive. mqBOLD does, however, involve the administration of a contrast agent which must be noted when evaluating its invasiveness. Gadolinium-based contrast agents are generally well-tolerated and the newer, macrocyclic agents, which are primarily used nowadays, only lead to small amounts of gadolinium residue in the brain (Thomsen, 2017). So far, there have been no indications of adverse effects of these residues. Moreover, the BOLD signal is not only a compound signal of different processes, thereby

complicating interpretations, but it is also a relative signal. Hence, in BOLD imaging, one contrasts different conditions and calculates the relative change between them. Percent change values are, however, heavily affected by the baseline value, impeding comparability. Also, they are not physiologically interpretable. Unlike the BOLD contrast, mqBOLD yields absolute and quantitative maps of oxygen consumption. Therefore, CMR_{O2} values are interpretable and comparable across brain regions, subjects, sessions and studies. In the two manuscripts presented in this thesis, we therefore employed mqBOLD to measure quantitative brain maps of oxygen metabolism.

1.2.3.2 Measuring cerebral glucose metabolism

The gold standard for measuring the cerebral metabolic rate of glucose (CMR_{glc}) is [^{18}F]fluorodeoxyglucose PET (^{18}F-FDG-PET). ^{18}F-FDG, commonly referred to as FDG, is a radiotracer that closely mimics glucose. After injection, the body processes FDG like glucose, as it cannot differentiate between the two substances. As a consequence, more FDG is brought to those cells with increased CMR_{glc}. However, once inside the cell, FDG cannot be further metabolized since, unlike glucose, it cannot undergo glycolysis. As a result, the PET tracer is trapped within the cell and accumulates until it decays. With a half-time of 109 minutes, FDG has a substantially longer decay time than $^{15}O_2$, allowing for single intravenous bolus injection just before the scan. This significantly reduces radiation exposure for patients and participants compared to PET scans using other radiotracers. Furthermore, because of the longer decay time, coordination of tracer production and injection timing is easier.

Typically, PET images are averaged over the entire scanning duration. Thus, when studying alterations in glucose metabolism between multiple conditions, at least two scanning sessions are necessary to ensure complete tracer decay. This not only increases total radiation exposure but is also more expensive and time-consuming. Additionally, acquiring data under different conditions on different days can introduce inaccuracies in the data due to potential variations between scanning sessions. In order to enable continuous monitoring of glucose metabolism, researchers have developed ^{18}F-FDG functional PET (fPET) (Hahn et al., 2016; Jamadar, Ward, Carey, et al., 2019; Rischka et al., 2018; Villien et al., 2014). Instead of a bolus injection, acquiring fPET data involves an initial bolus followed by a continuous infusion of FDG into the participant's bloodstream. This constant infusion maintains a steady-state level of tracer in the bloodstream,

allowing for dynamic imaging of glucose metabolism over an extended period. In this way, fPET allows for the measurement of multiple conditions within a single scanning session, as successfully applied in various studies (Hahn et al., 2016, 2017; Jamadar et al., 2021). To accurately model tracer delivery to brain tissue, continuous arterial sampling is required to obtain the arterial input function (AIF). This arterial sampling must be noted regarding the invasiveness of this method.

1.3 Aims of the current work

A healthy energy metabolism and intact brain function seem to be closely linked. As mentioned in the context of diabetes, a dysregulated energy metabolism is associated with various pathologies, including neurodegenerative diseases, as well as cognitive deficits (Chen et al., 2017; Profenno et al., 2010; Yaffe, 2013). Conversely, optimizing the body's metabolism has shown promising results in the therapy of various medical conditions. This has, for instance, been shown for depression, anxiety disorder and autism, disorders that are often associated with a disrupted gut microbiome (Peirce & Alviña, 2019; Pulikkan et al., 2019). Taking probiotics, thereby supporting the gut microbiome, alleviated symptoms of depression, anxiety and autism in these patients (Dinan et al., 2013; Dinan & Cryan, 2013; Gao et al., 2023; Navarro et al., 2016). Conversely, anti-depressants have been used to successfully treat inflammatory bowel disease (Ford et al., 2009). Further, patients with neurological disorders, such as epilepsy and autism, have shown improvement of symptoms after following a ketogenic diet (Barañano & Hartman, 2008; Napoli et al., 2014). These are just some examples to illustrate the tight connection between peripheral energy metabolism and healthy brain function.

The current thesis explores this relationship further in the healthy individual by investigating the effect of systemic glucose deficiency on brain energy metabolism and cognitive function. We were interested in whether a downregulated cerebral energy metabolism under metabolic challenges could be a link between peripheral energy metabolism and healthy cerebral functioning. Therefore, we first needed to establish whether decreased systemic glucose availability generally reduces rates of cerebral energy metabolism or whether the brain is capable of keeping up its ATP production through the oxidation of alternate energy substrates other than glucose.

Project I examines the impact of acute hypoglycemia on oxygen metabolism in healthy individuals, using mqBOLD.

⇒ **Aim I.** Quantify oxygen metabolism (CMR_{O2}) in the healthy human brain in response to hypoglycemia compared to euglycemia.

⇒ **Aim II.** Quantify oxygen metabolism (CMR_{O2}) in the healthy human brain in response to hyperinsulinemia compared to normal insulin levels.

⇒ **Aim III.** Investigate the impact of restored euglycemia (after hypoglycemia) on memory processing as well as attention.

Project II integrates recent advancements in MR and PET imaging. For the first time, CMR_{O2} and CMR_{glc} are measured simultaneously under different conditions within a single scanning session, applying mqBOLD and ^{18}F-FDG-fPET at the same time.

⇒ **Aim IV.** Demonstrate the feasibility of simultaneously quantifying task-induced changes in oxygen and glucose metabolism.

⇒ **Aim V.** Investigate how the oxygen-to-glucose index (OGI) changes upon increased neuronal activation and whether the OGI follows a uniform distribution across the cortex.

2 Manuscript I: Quantifying the effects of hypoglycemia on cerebral oxygen metabolism

Antonia Bose[1,2], Stefanie J. Haschka[3], Johanna Köhler[3], Felix A. Hesse[3], Santiago Martin[1], Lea Steinberg[1], Roman Iakoubov[3], Valentin Riedl[1,4]

1 Department of Neuroradiology, Neuroimaging Center, Technical University of Munich, Munich, Germany

2 Graduate School of Systemic Neurosciences, Ludwig-Maximilians-Universität, Munich, Germany

3 Department of Internal Medicine, Technical University of Munich, Munich, Germany

4 Department of Neuroradiology, Friedrich-Alexander-Universität, Erlangen, Germany

Abstract

The continuous supply with glucose and oxygen is essential for healthy brain function. Accordingly, the Selfish Brain Theory states that the brain prioritizes its own energy demand and is thus not susceptible to alterations in systemic availability of energy substrates. However, previous studies report whole-brain decreases of cerebral glucose metabolism under hypoglycemia. It remains unclear whether this implies a general decrease in cerebral energy metabolism or, alternatively, the utilization of different energy substrates. In this context, information on cerebral oxygen metabolism (CMR_{O2}) is sparse. The present study investigates CMR_{O2} under hypoglycemia, providing insights into the oxidation of energy substrates. Additionally, it explores the effects of restored euglycemia after prior hypoglycemia on cognitive function. Results indicate no changes in CMR_{O2} under hypoglycemia, even when considering potentially confounding effects of hyperinsulinemia in insulin-induced hypoglycemia. Hypoglycemia increased blood flow (CBF) in large parts of the brain, while only severe hypoglycemia reduced the oxygen extraction fraction (OEF). Further, memory consolidation, but neither encoding nor attention, was impaired under restored euglycemia in comparison to maintained euglycemia. In favor of the Selfish Brain Theory, the steady CMR_{O2} rates suggest utilization of alternate energy pathways in the brain under hypoglycemia, such as ketones and astrocytic glycogen. Despite this adaptability to alternative energy substrates, prior hypoglycemia has long-lasting effects specifically on memory consolidation, potentially resulting from glycogen depletion and impaired glutamate synthesis.

Introduction

The brain is the energetically most expensive organ relative to its size. Under normal conditions, it relies on oxidized glucose as its primary fuel and thus depends on a constant supply with glucose and oxygen to meet its metabolic demands. Therefore, during periods of glucose deficiency, the body initiates a number of counterregulatory mechanisms to maintain energy homeostasis (Cryer, 1993). This involves the utilization of alternative energy substrates, such as ketone bodies, fatty acids and lactate (Kersten et al., 1999; Kolb et al., 2021; Pan et al., 2000). These energy substrates are eventually, just like glucose, oxidized for adenosine triphosphate (ATP) production. Despite the body's ability to metabolize these substrates efficiently in the face of prolonged starvation, questions remain regarding the brain's reliance on them under acutely low blood glucose levels (hypoglycemia), which is a common side effect in diabetes mellitus (Genuth, 2006). The present study examines whether hypoglycemia results in reduced oxygen metabolism, and therefore reduced ATP production, or whether the utilization of alternative energy substrates is sufficient to maintain normal levels of cerebral energy metabolism.

Previous studies on cerebral energy metabolism have shown reductions in brain glucose utilization during hypoglycemia. An infrared spectroscopy study for instance found a decrease in brain glucose uptake among healthy participants experiencing hypoglycemia (Boyle et al., 1994), a finding that was confirmed by a more recent PET study (Blazey & Raichle, 2019). The latter study reported a significant 20-30% reduction in the cerebral metabolic rate of glucose (CMR_{glc}) across the entire brain during hypoglycemia. These findings could imply a whole-brain reduction in cerebral energy metabolism, hence a kind of energy conservation measure the brain takes under circumstances of restricted energy substrate availability. Alternatively, however, they could mean that the brain switches to a different pathway for energy production, such as those described above. This would be in line with the Selfish Brain Theory, which states that the brain always prioritizes its own energy demand over that of other bodily systems (Peters et al., 2004). First evidence for this theory came from early post-mortem studies in humans showing the preservation of human brain mass during inanition, while other organs, including the heart, liver and kidneys, lost about 40% of their mass (Krieger, 1921). More recent in-vivo studies in animals and humans provided further evidence for neuroprotection during metabolic challenges (Kind et al., 2005; Miller et al., 2002; Peters

et al., 2011). The Selfish Brain Theory views the brain as an organ that actively demands energy substrates (pull mechanisms), instead of being passively supplied with them (push mechanisms) (Peters et al., 2022). These pull mechanisms then allow the brain to adapt to fluctuations in energy substrate availability and maintain energy homeostasis, even under metabolically challenging conditions. They are mainly orchestrated by the ventromedial hypothalamus (Miki et al., 2001), which, for instance, limits peripheral glucose utilization, thereby sparing more for the brain (Ahrén, 2000; Mulder et al., 2005). Moreover, astrocytes have been shown to actively increase their glucose uptake in response to energetic demands, driven by both their own energy requirements and those of adjacent neurons (Blodgett et al., 2007; Pellerin & Magistretti, 1997). Hence, according to the Selfish Brain Theory, cerebral energy metabolism should not be largely affected by decreased levels of systemic glucose availability. Considering studies demonstrating decreased glucose uptake under hypoglycemia (Blazey & Raichle, 2019; Boyle et al., 1994), this would imply that the brain must rely on alternative substrates (such as ketones, lactate and fatty acids) during acute glucose deficiency. Since alternative substrates would still need to be oxidized, cerebral oxygen metabolism should be maintained in that case. However, experimental evidence about the brain's oxygen metabolism under glucose deficiency is lacking.

The present study was designed to answer the question whether hypoglycemia would induce reductions in cerebral oxygen metabolism to a similar extent as it does to CMR_{glc}, and how hypoglycemia differentially impacts functional brain networks. Previous studies have measured the cerebral metabolic rate of oxygen (CMR_{O2}) of the entire brain in fetal lambs, finding significant decreases in both CMR_{glc} and CMR_{O2} in hypoglycemia compared to euglycemia (Richardson et al., 1985). In humans, however, cerebral oxygen metabolism under hypoglycemia has not been studied directly. One study approximated brain oxygen uptake by combining measurements of cerebral blood flow (CBF) with the arterio-venous differences in plasma oxygen content and found no changes in CMR_{O2} and CBF in response to hypoglycemia (Lubow et al., 2006). While this method may give an estimate of oxygen consumption of the brain, it is neither a direct measurement of CMR_{O2}, nor can it provide information on spatial variations in cerebral oxygen metabolism. Using fMRI, other studies measured the blood oxygen level dependent (BOLD) contrast during hypoglycemia. They found a lower BOLD signal under hypoglycemia compared to euglycemia during a visual task (Anderson et al., 2006). The BOLD signal is a compound

signal, though, mixing information about both hemodynamic and metabolic changes. A positive BOLD signal could result from either increased oxygen consumption and/or increased CBF. It is thus not a direct measure of cerebral oxygen metabolism. In the present study, we measured CMR_{O2} via multiparametric quantitative BOLD (mqBOLD) (Christen et al., 2012; Hirsch et al., 2014; Kaczmarz et al., 2020). To this end, we acquired data on oxygenation and CBF separately. In this way, we were able to differentiate between purely hemodynamic processes and actual oxygen consumption.

We induced hypoglycemia using hyperinsulinemic glucose clamping (Heise et al., 2016) and compared it to euglycemia. Previous studies measured euglycemia in one of two ways: While some studies applied hyperinsulinemic glucose clamping to induce artificial euglycemia (Bolo et al., 2011; Graveling et al., 2013), other studies did not apply any intervention and therefore measured a rather natural euglycemia (McManus et al., 2020). Despite contrasting natural euglycemia with hypoglycemia better mimicking hypoglycemia resulting from insulin therapy in diabetics, this setup does not allow controlling for potential confounding effects of insulin. The majority of cellular glucose uptake within the brain occurs independently of insulin via the glucose transporters GLUT1 and GLUT3. Further studies found, however, a widespread distribution of insulin-dependent glucose transporters GLUT4 across the brain, particularly in the hippocampus (El Messari et al., 2002; Koepsell, 2020). In addition to its role in glucose uptake, insulin in the brain seems to act as a signaling molecule. In this context, it has been demonstrated that astrocytic insulin signaling plays an important role in glucose sensing and the control of systemic energy homeostasis (García-Cáceres et al., 2016; Herrera Moro Chao et al., 2022). Moreover, insulin has also been found to affect the neurovasculature, with intra-nasal administrations altering regional CBF (Akintola et al., 2017; Kullmann et al., 2015, 2017). Insulin is thus a factor that should be accounted for. Consequently, in the present study, we measured insulin-induced hypoglycemia as well as both artificial euglycemia and natural euglycemia. Artificial euglycemia involved the same amount of insulin, enabling us to isolate the sole effect of glucose when comparing it to hypoglycemia. For natural euglycemia, we neither infused insulin nor glucose but merely sodium chloride, while keeping all other experimental parameters constant. By comparing the two euglycemic conditions we were able to examine the insulin effect on our measures of interest.

In addition to effects on energy metabolism, acute hypoglycemia has been found to impair cognition. While a general cognitive impairment during hypoglycemia has been consistently found in diabetics (Broadley et al., 2022; Sommerfield et al., 2003b), additional studies suggest a similar effect in healthy adults, with memory systems and processing speed being compromised in particular (Graveling et al., 2013; McAulay et al., 2001; Sommerfield et al., 2003a). Still, it is unclear whether these cognitive deficits pertain only to acute hypoglycemic periods or whether they are more enduring. Therefore, in the present study, we examine the effects of restored euglycemia after hypoglycemia on cognition and contrast it with consistently maintained euglycemia. Previous experiments on a drosophila model demonstrated that the knockout of glucose transporter expression leads to impaired long-term memory formation (de Tredern et al., 2021). This suggests a strong involvement of specifically glucose in memory consolidation. In the current study, we therefore examined whether hypoglycemia affects long-term memory even when euglycemia has already been restored, while controlling for potential attention deficits following hypoglycemia.

Methods

Participants

A total of 38 participants was recruited for the study, which consisted of three sessions on separate days. Seven participants had to be excluded due to abnormal reactions to the experimental setup, such as signs of insulin resistance or poor vein status, and one participant dropped out after the first session. For imaging analyses, four more participants had to be excluded due to insufficient MR data quality. Moreover, to ensure hypoglycemia during MR scans, we only included subjects that did not exceed a blood glucose concentration of 65mg/dl during hypoglycemic MR acquisition. This leads to a final imaging sample size of 25 participants (mean age=23.96 ±2.3 years), with 23 sessions for hypo, 25 for eu_{nat} and 19 for eu_{art}. Cognitive data collection was initiated only after eight subjects, which resulted in a final cognition sample size of 23 participants (mean age=23.65 ±2.08 years).

All participants were healthy males with no family history of metabolic disorders. Their glucose metabolism was checked for large abnormalities prior to study participation via a glucose sensor (FreeStyle Libre 2, Abbott Laboratories) that subjects

wore continuously for seven days. The sensor was attached to the upper arm, allowing for the measurement of tissue glucose levels every 15 minutes via the integrated needle. The ethics board of the university hospital of the Technical University of Munich approved the experimental protocol and all participants gave written informed consent prior to study initiation.

Experimental protocol

On three separate days, we induced hypoglycemia (*hypo*; 55mg/dl blood glucose concentration), artificial euglycemia (eu_{art}; 90mg/dl) and natural euglycemia (eu_{nat}; ~90mg/dl) in each subject, using hyperinsulinemic glucose clamping (Heise et al., 2016). Participants were blind to the counterbalanced order of conditions. Given that insulin sensitivity decreases throughout the day (A. Lee et al., 1992; Saad et al., 2012), all data were acquired in the early morning after participants had fasted overnight. Upon the participant's arrival at the study site, intravenous catheters were placed in both arms, and baseline parameters were measured. That included baseline levels of epinephrine, norepinephrine, cortisol, IGF-1, insulin, c-peptide, CRP, creatinine, hematocrit and arterial oxygen saturation, as well as the performance of a baseline blood gas analysis (BGA; Epoc®, Epocal Inc), yielding real-time blood glucose levels. Acquisition of the stress hormones epinephrine, norepinephrine and cortisol served to control for stress effects on our outcome measures. Particularly epinephrine is known to increase during hypoglycemia, thereby inducing gluconeogenesis from kidneys and liver (Cryer, 1993). IGF-1 was measured to control for its potential effects in glucose utilization and insulin sensitivity (Clemmons, 2004; Hernandez-Garzón et al., 2016). Insulin and c-peptide provided further information on insulin levels and synthesis. While each of these parameters was measured repeatedly throughout the course of the experiment, CRP, creatinine and hematocrit were only measured at baseline level. CRP served as a control for effects of acute infections on energy metabolism (Powanda & Beisel, 2003). Creatinine and hematocrit values were required for the MRI protocol. Once all baseline parameters had been measured, we started the one-step hyperinsulinemic glucose clamping procedure, using a 20% glucose solution. Insulin infusion rates were body weight adapted to 0.12ml/h per kilogram body weight and kept steady within as well as across sessions. At 6-minute intervals, we performed BGAs, adjusting glucose infusion rates accordingly to reach or maintain the targeted blood glucose levels of 55mg/dl and 90mg/dl,

respectively (Spinner et al., 2016). Moreover, every 24 minutes, we took additional blood samples for epinephrine, norepinephrine, cortisol, IGF-1, insulin and c-peptide which were processed and analyzed in our in-house clinical chemistry laboratory.

For the eu_{nat} condition, we followed the same protocol, but instead of infusing glucose and insulin, we only infused sodium chloride (NaCl), thereby maintaining subjects' natural euglycemic levels. By conducting the three conditions, we established the following intrasubject contrasts: Firstly, comparing hypo and eu_{art} allowed us to isolate the effect of reduced blood glucose levels (glucose contrast), as both conditions involved the same amount of insulin. Secondly, contrasting eu_{art} and eu_{nat} provided an insulin contrast. In both conditions, subjects maintained euglycemia, while hyperinsulinemia was induced in eu_{art}.

Once blood glucose levels were stabilized in the target range, we transferred the subjects into the MR scanner and started with MRI acquisition, which will be described in detail below. During MR scanning, we continued with the clamping setup as before, including infusions as well as blood sampling at 6-minute intervals. See Figure 1 for information on blood glucose levels across participants and conditions.

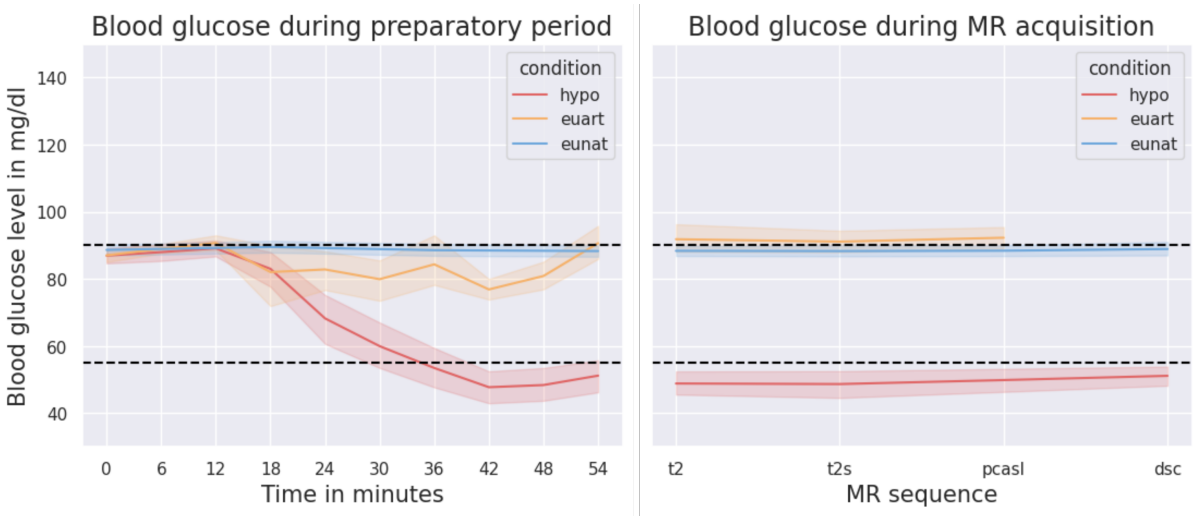

Figure 1. Blood glucose levels across subjects during hyperinsulinemic glucose clamping. Dashed lines represent the targeted glucose levels of 90mg/dl and 55mg/dl. **Left:** Blood glucose levels during the preparatory phase before MR scanning. Clamping began at t=0. On average, MR scanning was started 54 minutes after clamping onset. **Right:** Blood glucose levels during the MR scan per sequence. The blood glucose level during an MR sequence was calculated as the average of the blood glucose levels before and after the respective sequence.

In the scanner, participants performed an oddball task. During this task, they focused on a white fixation cross on dark background which turned red every 30 seconds on average. They were instructed to press a key on a button box whenever they saw the fixation cross turning red. This undemanding task enabled us to ensure participants' wakefulness while still acquiring resting state data. It is a necessary measure of control as hypoglycemia can induce neuroglycopenic symptoms, such as fatigue and drowsiness (Mitrakou et al., 1991), which in turn substantially lower cerebral energy metabolism (Madsen et al., 1991). Once the MR scan was completed, we stopped all infusions and transferred the participant into another room where we continued glucose infusions until they were stably euglycemic. At that point, we started cognitive testing, which comprised a memory and an attention task. Hence, the cognitive tasks were administered outside the scanner as well as under restored or maintained euglycemia.

For the memory task, participants learned a list of 15 concrete nouns, presented successively on a screen (adapted from Sommerfield et al., 2003a). They were instructed to note down the words immediately. This procedure of encoding and immediate recall was repeated one more time. After 20 minutes, they were prompted to recall the words another time without learning them again. Approximately 24 hours later, participants were contacted again and asked to recall the learned words one last time. During the 20-minute period of initial consolidation, participants performed a visual attention task (Quirk, 2020). In this task, they were instructed to find the *T* embedded within *L*s, and subsequently indicate with the four arrow keys on the keyboard in which direction the *T* was rotated. The leftover time of the 20-minute initial consolidation period was filled with the same undemanding oddball task as in the MR scanner. This ensured standardization of how participants spent that initial consolidation period. For a schematic depiction of the experimental setup, see Figure 2. An internist was present for the entire duration of glucose clamping.

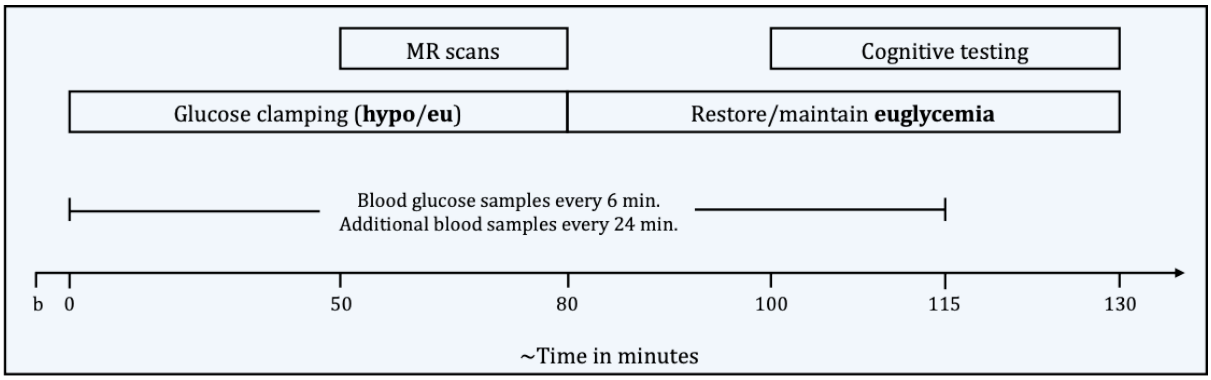

Figure 2. Schematic depiction of the experimental setup, where b denotes baseline measurements. After baseline measurements, glucose clamping was initiated at t=0, inducing either hypo- or euglycemia. In eunat, only NaCl was infused. Once blood glucose levels were stable, MR scanning was started. During the MR scan, glucose clamping was continued. After the MR scan, euglycemia was either restored (prior hypoglycemia) or maintained (prior euglycemia). Finally, we conducted cognitive tests. This procedure was repeated three times per participant, thereby inducing hypo, euart and eunat on three separate days. The order of conditions was counterbalanced and participants were blind to it.

Image acquisition

In the present study, we quantified subjects' cerebral oxygen metabolism. To this end, we calculated voxelwise CMR_{O2} parameter maps using mqBOLD (Christen et al., 2012; Hirsch et al., 2014; Kaczmarz et al., 2020), which requires several separate MR sequences. MR data acquisition was performed on a 3T Ingenia Elition MRI scanner (Philips Healthcare, The Netherlands), using a 32-channel head coil. Each session consisted of the following MR sequences:

- Multi-echo spin-echo T2 mapping: 3D gradient spin echo (GRASE) readout as previously described (Kaczmarz et al., 2020). 8 echoes, TE1 = ΔTE = 6 ms, TR = 251 ms, α=90°, voxel size 2x2x3.3 mm^3, 35 slices.
- Multi-echo gradient-echo T2* mapping: As previously described (Hirsch et al., 2014; Kaczmarz et al., 2020), 12 echoes, TE1 = 6ms, ΔTE = 5 ms, TR=2229 ms, α=30°, voxel size 2x2x3 mm^3, gap 0.3 mm, 35 slices.
- Pseudo-continuous arterial spin labelling (pCASL): As previously described (Alsop et al., 2015). Implementation according to previous literature (Göttler et al., 2019; Kaczmarz et al., 2020). PLD: 1800 ms, label duration: 1800 ms, 4 background suppression pulses, 2D EPI readout, TE=11 ms, TR=4500 ms, α=90°, 20 slices, EPI factor: 29, acquisition voxel size: 3.28x3.50x6.00 mm^3, gap: 0.6 mm, 30 dynamic scans, including a proton density weighted M0 scan.

- Dynamic susceptibility contrast (DSC): As previously described (Hedderich et al., 2019). Injection of a gadolinium-based contrast agent as a bolus after 5 dynamic scans. Dosage: 0.2ml/kg body weight, split into two injections of 0.1ml/kg body weight for two conditions (hypo, eu_{nat}). For the third condition (eu_{art}), DSC data could not be acquired without exceeding the recommended dosage for healthy participants. Neither could the total dosage of 0.2ml/kg body weight be further divided without compromising signal quality. For data processing of eu_{art}, the DSC from eu_{nat} was used. Flow rate: 4ml/s, plus 25ml NaCl. Single-shot GRE-EPI, EPI factor: 49, 80 dynamic scans, TR=2.0s, α=60°, acquisition voxel size: 2x2x3.5 mm^3, 35 slices. Prior to CA administration, healthy kidney function was ensured. The CA was only injected at creatinine levels of ≤ 1.2mg/dl.
- Additionally, anatomical data was acquired in one session for anatomical reference and to exclude brain lesions. This included a T1-weighted 3D MPRAGE pre- and post-gadolinium (TI=100 ms, TR=9 ms, TE=4 ms, α=8°; 170 slices, FOV=240x252x170 mm^3; voxel size: 1.0x1.0x1.0 mm^3; acquisition time: 2.05 minutes) and a T2-weighted 3D fluid-attenuated inversion recovery (FLAIR) image (TR = 4800 ms; TE = 293 ms, α=40°; 140 slices; FOV=240x248.9x168 mm^3; acquisition voxel size: 1.2x1.2x1.2 mm^3; turbo spin-echo factor: 170; inversion delay 1650 ms; acquisition time: 2:09 minutes).

Data processing and statistical analyses

Imaging data

CMR_{O2} calculation. The quantification of all parameter maps was performed with in-house MATLAB scripts and SPM12 (Wellcome Trust Centre for Human Neuroimaging, UCL, London, UK). Cerebral blood flow (CBF) parameter maps were derived from pCASL data by building average pairwise differences of motion-corrected label and control images and a proton-density weighted image (Alsop et al., 2015). The resulting CBF values are expressed in ml/100g/minute. R2', the transverse, reversible relaxation rate, was calculated via

$$R2' = \frac{1}{T2*} - \frac{1}{T2}$$

as described previously (Blockley et al., 2013, 2015; Bright et al., 2019). Cerebral blood volume (CBV) parameter maps were calculated from the DSC maps (Hedderich et al., 2019, p. 20; Kluge et al., 2016) and, when combined with R2', subsequently yielded the oxygen extraction fraction (OEF) (Christen et al., 2012; Hirsch et al., 2014; Yablonskiy & Haacke, 1994) via the following formula

$$OEF = \frac{R2'}{CBV}$$

Ultimately, voxelwise CMR_{O2} parameter maps were calculated by combining OEF and CBF via Fick's principle (Fick, 1870):

$$CMR_{O2} = CBF * OEF * C_aO_2$$

CMR_{O2} is expressed in units of $\mu mol/100g/minute$. C_aO_2, the arterial oxygen content, is calculated as $C_aO_2 = 0.335*Hct*55.6*O_2sat$, where Hct is the subject's hematocrit level and O_2sat the arterial oxygen saturation measured with a pulse oximeter (Bright et al., 2019; Ma et al., 2020). All individual parameter maps were registered to the first echo of the subject's respective multi echo T2 data. Further, we masked out the cerebellum and only considered voxels with a grey matter (GM) probability of >0.5. Additionally, in native space, we discarded voxels influenced by cerebrospinal fluid (T2>90ms), susceptibility artefacts ($R2'>9s^{-1}$), voxels with elevated blood volume (CBV>10%, probably driven by larger vessels) and voxels with physiologically unexpected values (T2*>90ms, OEF>0.9, CBF>90). See Figure 3 for schematic depiction of CMR_{O2} calculation.

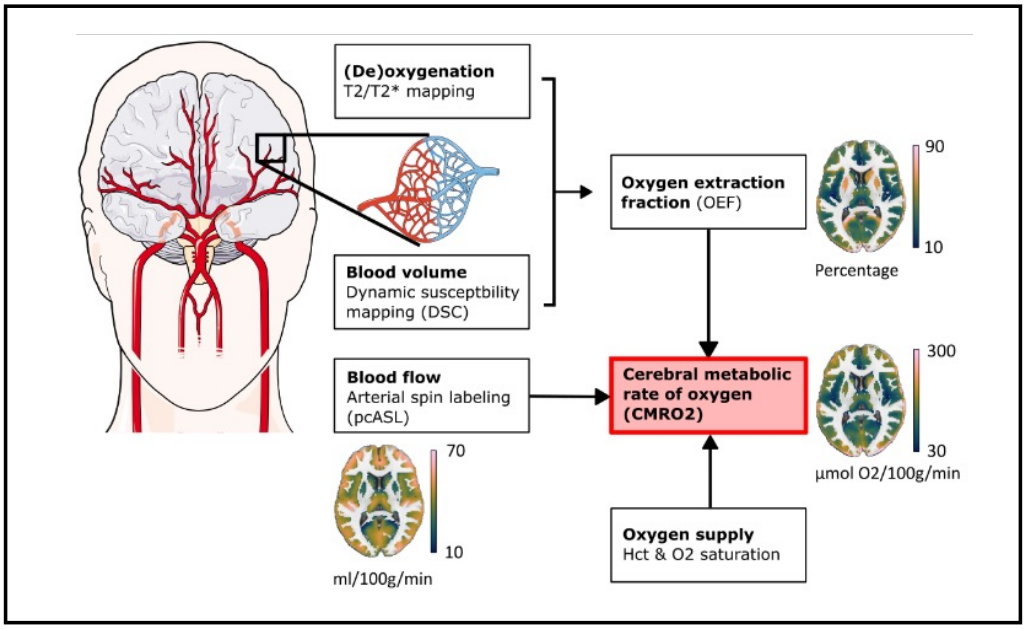

Figure 3. Schematic depiction of CMR_{O2} calculation. Deoxygenation mapping, CBV and CBF are acquired separately to produce voxelwise CMR_{O2} maps. Figure is from Hechler et al. (2023).

Statistical analyses. For statistical analyses of the imaging data, we performed linear mixed modeling (LMM) on a network level. Specifically, we used the R package robustlmer (Koller, 2016) to predict CMR_{O2}. LMM allows for the inclusion of fixed as well as random effects in predicting an outcome variable. In our model, we included the interaction between condition and brain network (7 networks according to Thomas Yeo et al., 2011; with the limbic network excluded due to susceptibility artefacts) as a fixed effect. We set eu_{art} as a reference condition to enable both glucose (hypo vs. eu_{art}) and insulin (eu_{nat} vs. eu_{art}) contrasting. Further, we specified the visual network as a reference for the network variable since previous work investigating CBF changes in response to hypoglycemia suggested the least effect in that particular network (Blazey & Raichle, 2019). The random model term (1|subject/condition) treats conditions as nested within subjects and was included to account for the repeated measures design of the study. For the dependent variable, regional CMR_{O2} values were calculated as the median voxel value within 400 Schaefer regions of interest (ROIs) (Schaefer et al., 2018) to reduce voxel-level noise. These medians were then entered as a predictor variable per subject and condition which yielded a total of 26,310 entries to the model. This resulted in the following LMM:

$$CMR_{O2} \sim condition*network + (1|subject/condition)$$

For ROI and network parcellations, we registered the atlases into native space and subsequently performed all analyses in native space.

Additional data

All other data were analyzed using Python (Python Software Foundation, version 3.8). For the analysis of the visual attention task, we applied a repeated measures ANOVA from the statsmodels module to test for condition effects on attention. As the predictor variable, we used reaction time in seconds because our main interest lay in changes in processing speed, as suggested by previous literature (Graveling et al., 2013). For analyses of the memory data, we applied the non-parametric Friedman's test (Friedman, 1937) to investigate whether condition had a significant impact on memory performance. Generally, memory scores were expressed as the number of words remembered. The learning score was calculated as the average performance on the two immediate recall tasks. Additionally, for performance on the delayed recall tasks (after 20 minutes and 24 hours), we used a generalized linear model (GLM; Nelder & Wedderburn, 1972) to include the learning score as a predictor.

Similarly, blood parameters were analyzed using a repeated measures ANOVA or Friedman's test, depending on adherence of the data to statistical assumptions. Post-hoc testing was performed using paired t-tests or the Wilcoxon signed-rank test (Wilcoxon, 1945), depending on the statistical method applied in the primary analysis. Blood parameters during MR acquisition were calculated by averaging blood values from timepoints 48 and 72 minutes (see supplementary Figures S1-S6).

Results

In the present study, we employed mqBOLD to study the effects of hypoglycemia on cerebral oxygen metabolism quantitatively. Specifically, we were interested in whether oxygen consumption in the brain would be decreased to a similar extent as previous literature has suggested for glucose (Blazey & Raichle, 2019; Boyle et al., 1994). To this end, we performed hyperinsulinemic glucose clamping and acquired mqBOLD MR scans concurrently.

Subjects presented with average fasting blood glucose levels of 87.33 mg/dl (std=4.8), which is in a healthy range. More information on subjects' physiological

characteristics as well as all blood parameters can be found in the supplements (Table S1 and Figures S1-S6). Apart from the changes explicitly stated here, no significant differences between conditions were observed in blood parameters. Most importantly, during MR acquisition, hypo, compared to eu_{art}, significantly increased epinephrine (Wilcoxon signed-rank test; W=3.0, p<0.001) and significantly decreased c-peptide (Wilcoxon signed-rank test; W=9.0, p<0.01). These changes were as expected, as hypoglycemia is known to affect stress hormones like epinephrine to trigger gluconeogenesis (Cryer, 1993). Decreases in c-peptide show a reduction in endogenous insulin production in response to hypoglycemia (Woods et al., 1974). Consequently, these results can be considered a validation of the hypoglycemic condition. Moreover, as expected, insulin levels were significantly different between insulin contrast conditions (eu_{art} vs. eu_{nat}; Wilcoxon signed-rank test; W=0, p<0.001). Importantly, insulin levels did not differ between hypo and eu_{art} (Wilcoxon signed-rank test; W=61.0, p=0.49), thereby creating a pure glucose contrast. No differences between conditions in oddball task performance during the MR scan were observed (Friedman's test; χ^2_F=0.49, p=0.78), suggesting similar levels of wakefulness in all conditions.

Imaging data

CMR_{O2}

For imaging analyses, we performed an LMM analysis. As previously described, we specified the model CMR_{O2} ~ condition*network + (1|subject/condition) to examine the effect of conditions (hypo, eu_{art}, eu_{nat}) on CMR_{O2} in each brain network (Thomas Yeo et al., 2011), while taking into account the within-subjects design. CMR_{O2} input data was provided as grey matter (GM) voxel medians per ROI (400 ROI parcellation; Schaefer et al., 2018) to reduce voxel-level noise.

First, we tested our model against a null model lacking the condition term, thereby examining whether the model improves significantly when including our intervention as a predictor. Including the condition term explained significantly more variance (χ^2=865.88, p<0.001), with the fixed and random effects combined accounting for 22.51% of variance in CMR_{O2}. We also tested whether including epinephrine in the interaction term increased the explained variance since epinephrine differed between conditions during MR scanning. However, this did not significantly increase the amount of explained variance (χ^2=25.26, p=0.24).

Across conditions, participants had an average CMR_{O2} of 130.58 µmol/100g/min (see intercept, Table 1). In healthy individuals, CMR_{O2} is expected to vary between 120 and 160 µmol/100g/min (Christen et al., 2012; Xu et al., 2009). Thus, our group average fits with previous literature, validating the applied methodologies. See Tables S2 in the supplements for values on all imaging parameters across subjects and conditions. We found no significant associations between the fixed effects and our outcome variable. This suggests that neither hypoglycemia nor hyperinsulinemia significantly affected CMR_{O2} (see Table 1 and Figure 4).

Table 1.

Results of the linear model predicting CMR_{O2} in the main group.

Fixed effect	**Estimate** µmol/100g/min	**95% CI**	**p-value**
(Intercept)	130.58	121.99 – 139.13	<0.001***
Condition[eunat]	-3.34	-10.49 – 3.79	0.35
Condition[hypo]	-0.73	-8.08 – 6.62	0.84
Condition[eunat]:network[Cont]	0.35	-4.30 – 4.99	0.88
Condition[hypo]:network[Cont]	-0.43	-5.16 – 4.30	0.86
Condition[eunat]:network[Default]	1.39	-2.68 – 5.45	0.50
Condition[hypo]:network[Default]	2.51	-1.63 – 6.65	0.23
Condition[eunat]:network[DorsAttn]	3.14	-1.65 – 7.93	0.20
Condition[hypo]:network[DorsAttn]	-1.76	-6.63 – 3.12	0.48
Condition[eunat]:network[SalVentAttn]	0.94	-3.82 – 5.70	0.70
Condition[hypo]:network[SalVentAttn]	0.23	-4.62 – 5.08	0.93
Condition[eunat]:yeo_nw[SomMot]	1.86	-2.34 – 6.07	0.39
Condition[hypo]: network[SomMot]	0.20	-4.08 – 4.49	0.93

Note. Result parameters of the following model: CMR_{O2} ~ condition*network + (1|subject/condition) for the main group. Not shown here are the parameters for main effects of the individual networks. The entire model results can be found in the supplements. In summary, condition had neither a main- nor an interaction effect on CMR_{O2}. R^2=22.51%. Network abbreviations: Cont ≙ Control; Default ≙ Default mode; DorsAttn ≙ Dorsal attention; SalVentAttn ≙ Salience; SomMot ≙ Somatomotor. Significant codes: <0.001: ***; <0.01: **, <0.05: *. Analyses were performed in native space.

Next, we were interested in whether more severe hypoglycemia would affect CMR_{O2} or whether the brain would still be able to keep up its regular levels of oxygen metabolism. For that purpose, we created a more severely hypoglycemic subgroup according to previously defined glycemic thresholds for neuroglycopenic symptoms (Mitrakou et al., 1991). Accordingly, in this subgroup, we included subjects that had constant blood glucose levels of below 49mg/dl during MR scanning. This comprised six participants in total. Similar to the main group, the subgroup did not show differences in CMR_{O2} in response to hypoglycemia or hyperinsulinemia, suggesting the maintenance of regular levels of cerebral energy metabolism even under more severely low blood glucose levels. For detailed information on all model results, please consult the supplementary material (Table S4).

CBF and OEF

Further, we were interested in whether hypoglycemia and hyperinsulinemia did not affect cerebral dynamics at all or whether solely CMR_{O2} was spared. Therefore, we investigated the effect of our interventions on the subcomponents of CMR_{O2}: CBF and OEF. For that, we used the same linear model as previously described, only changing the predictor variable to CBF and OEF, respectively.

The model CBF ~ condition*network + (1|subject/condition) explained a total variance of 44.7% in CBF. Across conditions, subjects had an average CBF of 43.56 ml/100g/min, fitting well to the range of 38-54 ml/100/min reported in previous literature (Gusnard & Raichle, 2001; K. Zhang et al., 2014). We found a significant increase in CBF under hypo compared to eu_{art} in the control network (46.18 ml/100g/min; $p<0.001$), default mode network (45.84 ml/100g/min; $p<0.001$) and salience network (44.09 ml/100g/min; $p<0.05$) (see Figure 4). Hyperinsulinemia did not affect CBF. For the purpose of conciseness, Table 2 only includes significant interaction effects. The entire model output can be found in the supplements (Table S5).

Table 2.

Results of the linear model predicting CBF in the main group.

Fixed effect	**Estimate** ml/100g/min	**95% CI**	**p-value**
(Intercept)	43.56	40.27 – 46.87	<0.001***
Condition[eunat]	-1.23	-4.23– 1.80	0.42
Condition[hypo]	0.33	-2.75 – 3.46	0.83
Condition[hypo]:network[Cont]	2.29	1.16 – 3.41	<0.001***
Condition[hypo]:network[Default]	1.95	0.95 – 2.92	<0.001***
Condition[hypo]:network[SalVentAttn]	1.20	0.04 – 2.35	0.04*

Note. Result parameters of the following model: CBF ~ condition*network + (1|subject/condition) for the main group. Not shown here are the parameters for main effects of the individual networks as well as nonsignificant interaction effects. All model results can be found in the supplements. R^2=44.7%. Network abbreviations: Cont ≙ Control; Default ≙ Default mode; DorsAttn ≙ Dorsal attention; SalVentAttn ≙ Salience; SomMot ≙ Somatomotor. Significant codes: <0.001: ***; <0.01: **, <0.05: *. Analyses were performed in native space.

In the severely hypoglycemic subgroup (average CBF: 43.08 ml/100g/min), we found significant CBF increases in the control network (51 ml/100g/min; p<0.001), default mode network (50.1 ml/100g/min; p<0.001), dorsal attention network (48.24 ml/100g/min; p<0.05), salience network (48.14 ml/100g/min; p<0.05) and somatomotor network (47.84 ml/100g/min; p<0.05) (see Table 3 and Figure 5). Hence, CBF increased in every network but the visual network in response to hypoglycemia. Again, hyperinsulinemia had no effect.

Table 3.

Results of the linear model predicting CBF in the subgroup.

Fixed effect	**Estimate** ml/100g/min	**95% CI**	**p-value**
(Intercept)	43.08	39.83 – 46.33	<0.001***
Condition[eunat]	-0.64	-3.56 – 2.26	0.66
Condition[hypo]	3.13	-1.28 – 7.48	0.16
Condition[hypo]:network[Cont]	4.79	3.15 – 6.42	<0.001***
Condition[hypo]:network[Default]	3.89	2.46 – 5.33	<0.001***
Condition[hypo]:network[DorsAttn]	2.03	0.34 – 3.72	0.01*
Condition[hypo]:network[SalVentAttn]	1.93	0.25 – 3.61	0.02*
Condition[hypo]: network[SomMot]	1.63	0.15 – 3.12	0.03*

Note. Result parameters of the following model: CBF ~ condition*network + (1|subject/condition) for the subgroup. Not shown here are the parameters for main effects of the individual networks as well as nonsignificant interaction effects. All model results can be found in the supplements. Network abbreviations: Cont ≙ Control; Default ≙ Default mode; DorsAttn ≙ Dorsal attention; SalVentAttn ≙ Salience; SomMot ≙ Somatomotor. Significant codes: <0.001: ***; <0.01: **, <0.05: *. Analyses were performed in native space.

The model OEF ~ condition*network + (1|subject/condition) explained a total variance of 18.88% in OEF. Usually, OEF values range between 0.3 and 0.5 (Epp et al., 2023; Gusnard & Raichle, 2001). In line with that, in our data, subjects' average OEF across conditions was 0.42. Neither hypoglycemia nor hyperinsulinemia affected OEF in the main group (see Figures S6 and S7 in the supplements). In the more severely hypoglycemic subgroup, however, OEF was reduced in every network under hypoglycemia (see Table 4 and Figure 5). In this case, the main effect of hypo was significant ($p<0.01$), meaning that OEF in hypo was significantly lower than during eu_{art} in the reference network, i.e. the visual network. Since the effects in the remaining networks are compared to this main effect, nonsignificant interaction terms mean that effects in these networks are not different from the main effect. Hence, they all show significant reductions in hypo compared to eu_{art}. Again, hyperinsulinemia did not have any effect.

Table 4.

Results of the linear model predicting OEF in the subgroup.

Fixed effect	Estimate ratio	95% CI	p-value
(Intercept)	0.42	39.83 – 46.33	<0.001***
Condition[eunat]	-0.01	-3.56 – 2.26	0.39
Condition[hypo]	-0.03	-1.28 – 7.48	0.002**
Condition[hypo]:network[Cont]	-0.01	3.15 – 6.42	0.24
Condition[hypo]:network[Default]	-0.001	2.46 – 5.33	0.87
Condition[hypo]:network[DorsAttn]	-0.002	0.34 – 3.72	0.77
Condition[hypo]:network[SalVentAttn]	-0.01	0.25 – 3.61	0.46
Condition[hypo]: network[SomMot]	-0.01	0.15 – 3.12	0.10

Note. Result parameters of the following model: OEF ~ condition*network + (1|subject/condition) for the subgroup. Not shown here are the parameters for main effects of the individual networks as well as nonsignificant interaction effects. All model results can be found in the supplements. R^2=20.7%. Network abbreviations: Cont ≙ Control; Default ≙ Default mode; DorsAttn ≙ Dorsal attention; SalVentAttn ≙ Salience; SomMot ≙ Somatomotor. Significant codes: <0.001: ***; <0.01: **, <0.05: *. Analyses were performed in native space.

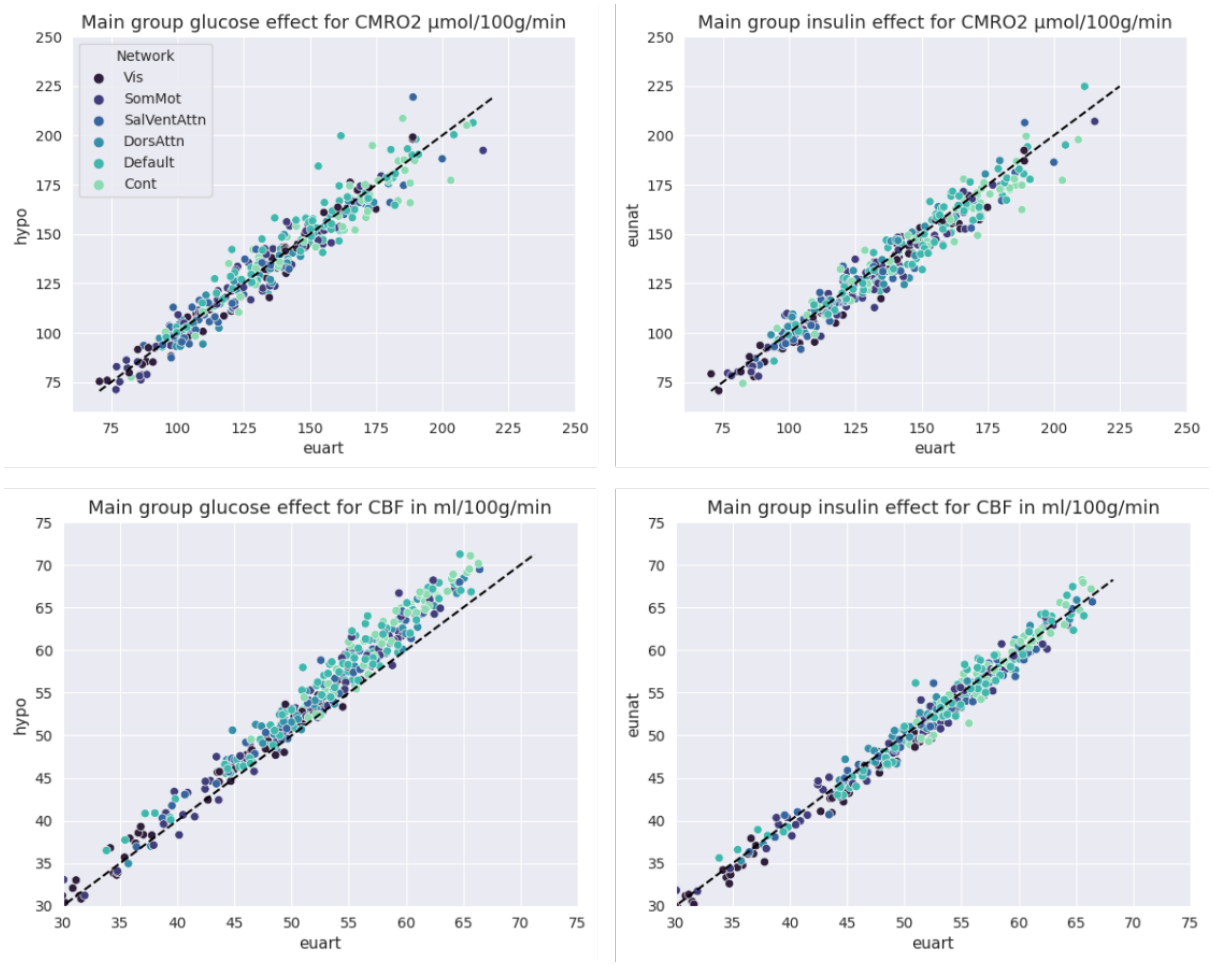

Figure 4. Glucose (left plots) and insulin (right plots) contrasts (main group) for CMR_{O2} (upper row) and CBF (lower row) per brain network. Datapoints reflect parameter averages per ROI across subjects. The dashed line represents the angle bisector. CMR_{O2} was maintained in both contrasts, while CBF increased significantly in response to hypoglycemia (glucose contrast) in the control, default mode and salience networks. OEF was maintained as well. OEF plots can be found in the supplements (Figure S7, Table S7). Network abbreviations: Cont ≙ Control; Default ≙ Default mode; DorsAttn ≙ Dorsal attention; SalVentAttn ≙ Salience; SomMot ≙ Somatomotor. Analyses were performed in native space. Detailed parameters can be found in supplementary Tables S3 and S5.

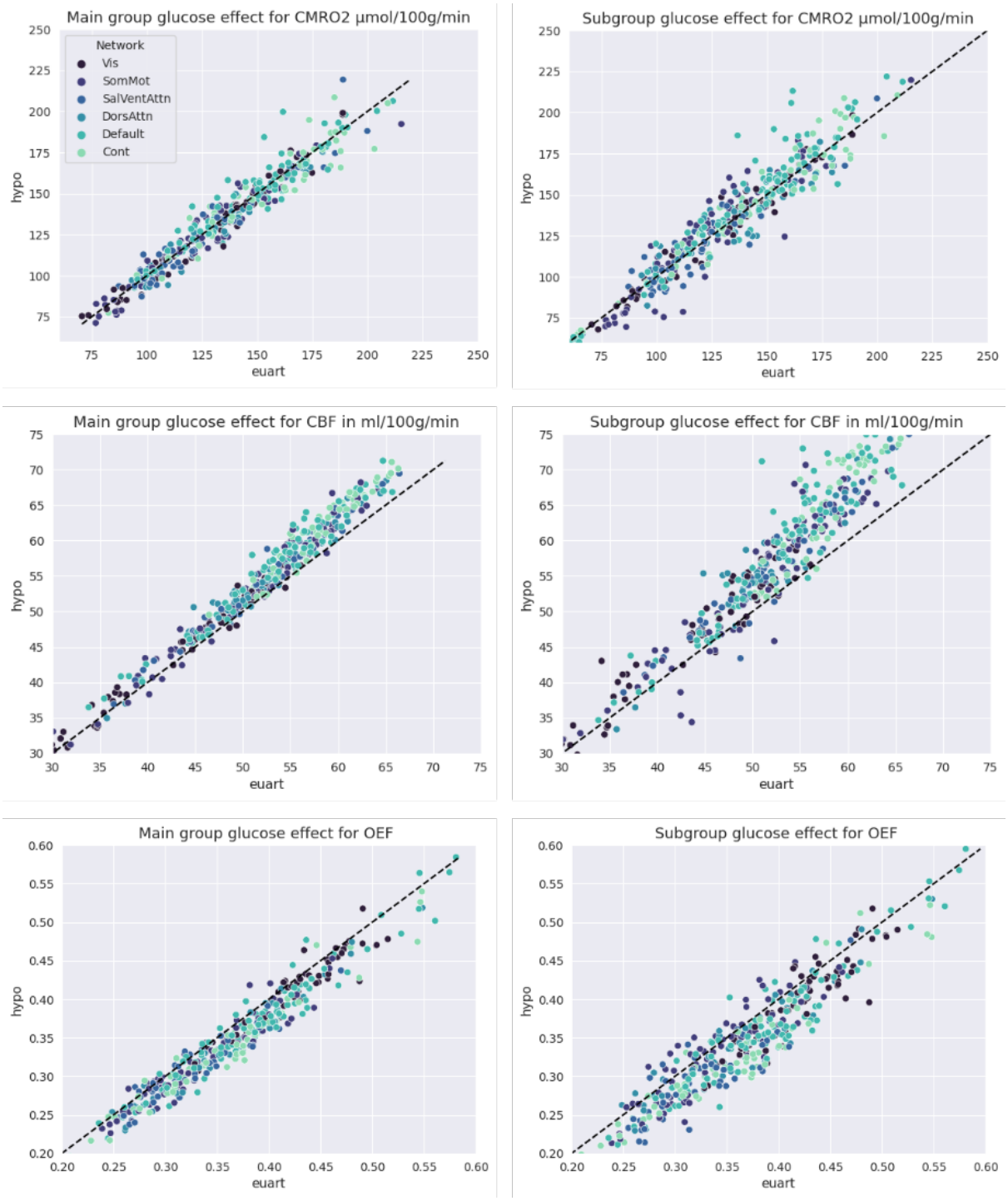

Figure 5. Glucose contrasts for the main group (left plots) and severely hypoglycemic subgroup (right plots) for CMR_{O2} (upper row), CBF (middle row) and OEF (lower row) per yeo network. Datapoints reflect parameter averages per ROI across subjects. The dashed line represents the angle bisector. In the subgroup, CMR_{O2} was maintained again, while CBF increases were amplified compared to the main group. In the subgroup, CBF increased in all but the visual network. OEF decreased significantly in all networks in the subgroup. Network abbreviations: Cont ≙ Control; Default ≙ Default mode; DorsAttn ≙ Dorsal attention; SalVentAttn ≙ Salience; SomMot ≙ Somatomotor. Analyses were performed in native space. Detailed parameters can be found in supplementary Tables S4, S6 and S8.

Cognitive data

Cognitive data was acquired after the MR scan, once euglycemia was restored (if previously hypoglycemic) or maintained (if previously euglycemic). From now on, we will therefore refer to the conditions as *restored euglycemia* (prior hypo) and *maintained euglycemia* (prior eu_{art}), respectively. At the point of cognitive testing, there were no differences anymore in epinephrine (Friedman's test; χ^2_F=1.69, p=0.43) or any other stress parameter between conditions. Further, the previously observed reductions in c-peptide in response to hypoglycemia disappeared once euglycemia had been restored (restored vs. maintained euglycemia: Wilcoxon signed-rank test; W=27.0, p=0.35). These findings demonstrate that not only had blood glucose levels been restored but also that physiological reactions to prior hypoglycemia had stopped.

Memory

In the memory task, subjects were instructed to learn a list of 15 concrete nouns presented to them successively on a screen. Subjects did not show differences in encoding (Friedman's test; χ^2_F=1.37, p=0.5) between restored and maintained euglycemia. After 20 minutes of consolidation, subjects still showed no differences between restored and maintained euglycemia in memory performance (Friedman's test; χ^2_F=2.63, p=0.27). However, recall after a 24-hour consolidation period was significantly impaired in restored vs. maintained hypoglycemia (Wilcoxon signed-rank test; W=14.0, p<0.01), even when controlling for initial learning performance (GLM, p=0.03 for the effect of restored vs. maintained euglycemia on memory consolidation 24 hours later). Including condition and learning performance as predictors explained 60.7% of the variance in memory recall after 24 hours. See Figure 6 for a summary of the memory performance. There were no differences in memory performance for the insulin contrast.

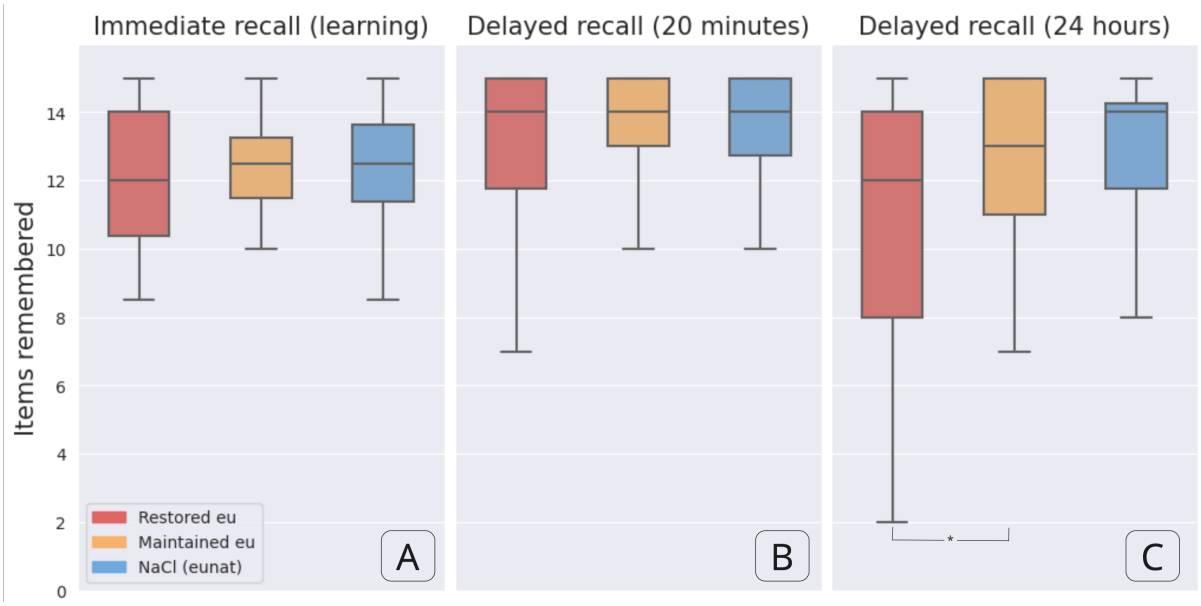

Figure 6. Memory performance after hyperinsulinemic glucose clamping. **A.** Immediate memory performance, considered as learning. **B.** Memory performance after a 20-minute consolidation period. **C.** Memory performance after a 24-hour consolidation period. Performance was significantly worse (p=0.03) in restored euglycemia than in maintained euglycemia.

Attention

Previous literature suggests decreased speed of information processing under acute hypoglycemia (Graveling et al., 2013; McAulay et al., 2001). It is thus difficult to say whether other cognitive impairments under acute hypoglycemia are caused by this delayed processing speed. Here, subjects performed a visual attention task, instructed to find a specific stimulus within similarly looking stimuli. Statistical testing showed no differences between conditions in reaction times (repeated measures ANOVA; F=1.39, p=0.26). This suggests a) that impairments in processing speed might be limited to acute periods of hypoglycemia and b) that the previously described effects of restored euglycemia after hypoglycemia are rather memory-specific instead of a more general cognitive impairment.

Discussion

CMR_{O2}

The present study was conducted to investigate whether hypoglycemia in healthy individuals reduces CMR_{O2} to a similar extent as it reduces CMR_{glc} (Blazey & Raichle, 2019). Hence, if cerebral energy metabolism generally decreases in response to hypoglycemia, we would find decreases in CMR_{O2} in accordance with those in CMR_{glc}. Steady levels of CMR_{O2}, however, would imply the utilization of alternate energy substrates, like ketone bodies, lactate and/or fatty acids, because these substrates still need to be oxidized for ATP production. Our results show no changes of CMR_{O2} in response to hypoglycemia. Even in severe hypoglycemia, CMR_{O2} levels were maintained. This suggests that, even in the face of low systemic glucose availability, the brain is able to keep up its energy metabolism and ATP production at normal levels by using alternative energy substrates. This is in line with the Selfish Brain Theory (Peters et al., 2004), which states that the brain prioritizes its own energy requirements even under conditions of low energy availability. According to this theory, the brain is depicted as an organ that actively demands energy substrates (pull mechanisms), instead of being passively supplied with them (push mechanisms) (Peters et al., 2022). These active pull mechanisms are initiated mainly by the ventromedial hypothalamus and the sympathetic nervous system (SNS). They are, for example, responsible for decreased pancreatic insulin secretion in response to hypoglycemia (Hitze et al., 2010). The brain mainly comprises glucose transporters GLUT1 and GLUT3, which are insulin-independent in contrast to the insulin-dependent GLUT4. While GLUT4 are present in the brain, glucose transport into neural cells still happens mainly independent of insulin (Koepsell, 2020). With lower levels of circulating insulin due to reduced pancreatic insulin secretion, more glucose is spared for insulin-insensitive tissues, like large parts of the brain (Koepsell, 2020). In accordance with the concept of SNS-mediated insulin suppression, our data revealed decreased levels of c-peptide, a byproduct of insulin synthesis. Other examples of these active pull mechanisms that have been found to be driven by the SNS include increases of glucagon secretion (Chan et al., 2007, 2011) and consequently increased glycogenolysis, higher rates of gluconeogenesis (X. Zhang et al., 2019) and ketogenesis (Kubera et al., 2014) as well as increased muscular lactate release (Qvisth et al., 2008), thereby providing alternate energy resources.

Further, we find no significant effect of hyperinsulinemia on any of our parameters, suggesting that all described effects are mainly glucose-driven. While our results suggest that cerebral energy metabolism is maintained under hypoglycemia by the utilization of alternative substrates, our data cannot provide information on which specific substrates are metabolized. Most likely, as suggested by previous literature on prolonged fasting, the brain uses astrocytic glycogen, ketone bodies and fatty acids to compensate for glucose deficiency (Aizawa et al., 2016; Cahill, 2006; Garcia Corrales et al., 2021; Lima et al., 2015; Öz et al., 2007). The exact extent to which each of the substrates is used is unclear. However, even with sufficient levels of glucose available, the brain exhibits a preference for ketone bodies compared to glucose (Hasselbalch et al., 1996). Further, studies found significantly higher levels of lactate in the extracellular fluid surrounding neurons compared to plasma lactate levels under hypoglycemia (Abi-Saab et al., 2002). This is in line with the theory that the brain readily depletes astrocytic glycogen storages during hypoglycemia and shuttles them to neurons in the form of lactate. Although fatty acids are probable contributors to the maintenance of cerebral energy metabolism, their slow transportation across the blood brain barrier, slow rates of metabolism (Alberghina et al., 1993) and high oxygen requirement (Kolwicz, 2021) make it unlikely for them to serve as the primary alternate source of energy under hypoglycemia.

CBF and OEF

Despite no changes in CMR_{O2}, we found alterations in its underlying components, CBF and OEF. During hypoglycemia, there were significant increases in CBF in the control, default mode and salience networks. These findings fit well with existing literature on hypoglycemia effects on CBF, reporting increases in the medial prefrontal cortex (Teves et al., 2004), anterior cingulate cortex (Dunn et al., 2018; Teh et al., 2010), dorsolateral prefrontal cortex, and angular gyrus (Dunn et al., 2018), all part of one of the three aforementioned networks. In contrast, animal studies report whole-brain increases in CBF in response to hypoglycemia in rats (Bryan et al., 1987; Choi et al., 2001). This might be due to generally lower hypoglycemia targets chosen for animal studies (~30mg/dl). In line with this, in our more severely hypoglycemic subgroup, the CBF effect was amplified. Here, we found significant CBF increases in every network, except for the visual network.

In the main group, the larger increases in the higher cognitive networks (control and default mode networks) may be due to their overall higher metabolic demand. As

Figure S7 in the supplements demonstrates, CBF increases during hypoglycemia correlate significantly and positively with baseline CMR_{O2} values ($p<0.001$). In general, higher rates of CBF could serve to provide the brain more efficiently with the remaining glucose and alternative substrates. Previous studies interpreted increased flow rates in brain areas during hypoglycemia as an indicator for heightened neuronal activity in these regions, implying their involvement in the autonomic response to hypoglycemia (Teves et al., 2004). If CBF increases were caused by neuronal activation, however, we would have found concomitant CMR_{O2} patterns. Instead, CBF and CMR_{O2} seem to be uncoupled during hypoglycemia. Alternatively, CBF alterations could be driven by ketone bodies. High levels of ketones have been shown to cause CBF surges even under euglycemia (Hasselbalch et al., 1996), thereby potentially acting as signaling molecules of glucose deficiency. Further, epinephrine increases blood flow (Thomas et al., 1997). Since we found higher levels of epinephrine in hypo vs. eu_{art}, this could explain the CBF results, too, but plasma epinephrine levels start rising at blood glucose concentrations of 75mg/dl already (J. J. Lee et al., 2017). Hence, elevated epinephrine alone cannot account for CBF alterations. Also, even acute hypoglycemia induces inflammatory processes (Iqbal et al., 2019; Ratter et al., 2017), which can increase blood flow (Fassbender et al., 1996). Lastly, certain neurological conditions, such as ischemic stroke and migraines, have been associated with the concept of luxury perfusion, which describes hyperperfusion of the brain as a result of lost cerebrovascular autoregulation (Haggenmüller et al., 2023). It has been hypothesized that this could be the case during hypoglycemia, too, but evidence is lacking.

In contrast to CBF, we did not find any significant OEF alterations in response to hypoglycemia. Typically, when CBF increases upon enhanced neuronal activity, it overcompensates for the increased oxygen demand, thereby overall decreasing the relative amount of oxygen extracted from the blood. In theory, the unaltered oxygen extraction *fraction* in our data would imply an increased *absolute* oxygen extraction. The extent was not large enough, though, to affect CMR_{O2}. Moreover, OEF does seem to decrease in all networks (see Table S7 in the supplements), but not to a statistically significant extent. Supporting this, in the more severely hypoglycemic subgroup, we find OEF reductions in all networks, reflecting the larger increases in CBF and thereby overcompensation of oxygen delivery.

Cognition

In addition to studying cerebral oxygen dynamics, the present study was conducted to investigate whether prior hypoglycemia, once restored to euglycemia, affects cognition. Previous studies showed memory as well as attention deficits during acute hypoglycemia (Graveling et al., 2013; Sommerfield et al., 2003b, 2003a), with the attentive deficit complicating the interpretation of such results. They could imply a general cognitive impairment due to decreased attention during task performance or an interference of hypoglycemia with e.g. memory-specific cellular processes.

Our results suggest that restored euglycemia after a hypoglycemic period impairs memory consolidation while encoding as well as attention remain unaffected. Unaltered processing speed in the attention task suggests three things: 1) Attention deficits appear to be restricted to periods of acute hypoglycemia. 2) Impaired consolidation during restored euglycemia seems to reflect a domain-specific issue instead of a general cognitive impairment. 3) The clear difference between attention and memory performance could indicate an uncoupling of these processes during acute hypoglycemia as well. Further, the fact that encoding did not differ between conditions rules out the possibility that impaired consolidation is mediated by poorer learning ability during restored euglycemia compared to maintained euglycemia.

The underlying mechanisms of decreased memory consolidation when learning under restored euglycemia are not entirely clear. It is well established that there is an increased energy demand during long-term memory formation in the hippocampus. This brain region is particularly important for memory formation, while comprising insulin-dependent GLUT4 glucose transporters (El Messari et al., 2002; McNay et al., 2000). The resulting decreased glucose metabolism during low blood glucose levels might thus account for memory deficits during acute hypoglycemia but it cannot explain the impairment of memory consolidation specifically during restored euglycemia, especially with learning remaining unaffected. In this context, past studies suggest an important role of lactate shuttling from glial cells to neurons in long-term but not short-term memory (Gao et al., 2016; Newman et al., 2011; Suzuki et al., 2011). This lactate comes primarily from glycogen stored in astrocytes. Under hypoglycemia, these glycogen repertoires are utilized and, depending on the duration and severity of hypoglycemia, depleted (Öz et al., 2007), sparing no glycogen for subsequent long-term memory formation. Further, it was shown that inhibiting glycogen breakdown leads to difficulties

in long-term memory formation, with glucose unable to substitute for the lack in glycogen (Gibbs et al., 2006; Suzuki et al., 2011). This demonstrates that glycogen is not solely a storage form of glucose but serves specific functions.

Moreover, about 30 minutes after learning, studies found a decrease of glycogen in the forebrain of neonate chicks, scaling with elevated levels of glutamate and glutamine, suggesting glutamate/glutamine synthesis from glycogen to promote memory consolidation (Bak et al., 2018; Hertz et al., 2003; O'Dowd et al., 1994). Supporting synaptic plasticity, glutamate contributes to memory formation (Barnes et al., 2020). Depleted glycogen reserves due to prior hypoglycemia would imply decreased de novo synthesis of glutamate after learning and, consequently, impaired memory consolidation. In addition, glutamate is essential for sharp wave ripples (SWRs) (Behrens et al., 2005; Colgin et al., 2004; Maier et al., 2003; Papatheodoropoulos & Kostopoulos, 2002). SWRs are oscillatory patterns of neural activity in the hippocampus observed during periods of rest. They are thought to play a crucial role in long-term memory formation (Schreiner et al., 2023; Yang et al., 2024). In fact, they are even considered a cognitive biomarker for episodic memory consolidation and retrieval (Buzsáki, 2015). Thus, the depletion of astrocytic glycogen storages due to hypoglycemia and following deficient glutamate-glutamine cycling could explain why we find impaired memory consolidation, specifically, while other cognitive domains remain unaffected.

Conclusion

The present study aimed to investigate quantified oxygen metabolism under hypoglycemia and hyperinsulinemia. Hypoglycemia did not affect CMR_{O2} levels. Taken together with previous literature demonstrating whole-brain CMR_{glc} decreases, this suggests the utilization of alternative energy substrates to maintain steady levels of cerebral energy metabolism even in the face of severe hypoglycemia. It must be noted, however, that we did not acquire data on cerebral glucose metabolism in this study. Future studies that simultaneously acquire oxygen and glucose metabolism during hypoglycemia would be able to evaluate this uncoupling of CMR_{O2} and CMR_{glc} more reliably. Hyperinsulinemia did not show any effects in the measured parameters, while hypoglycemia increased CBF in large parts of the brain. More severe hypoglycemia decreased OEF on a whole-brain level. Further, we examined the effect of restored euglycemia vs maintained euglycemia on cognition. Memory consolidation was

significantly impaired under restored euglycemia, while learning as well as attention remained unaffected. Taken together, these findings demonstrate the flexibility of cerebral energy metabolism, being able to adapt its energy resources even in the face of acute severe hypoglycemia. Still, our cognitive results show that brain function does not remain unimpaired and that these effects of hypoglycemia might even be more enduring than previously assumed.

Acknowledgements

The authors want to thank Christine Preibisch for the provision of MRI protocols as well as template code for acquisition and processing of mqBOLD MRI data.

References

Abi-Saab, W. M., Maggs, D. G., Jones, T., Jacob, R., Srihari, V., Thompson, J., Kerr, D., Leone, P., Krystal, J. H., Spencer, D. D., During, M. J., & Sherwin, R. S. (2002). Striking Differences in Glucose and Lactate Levels between Brain Extracellular Fluid and Plasma in Conscious Human Subjects: Effects of Hyperglycemia and Hypoglycemia. *Journal of Cerebral Blood Flow & Metabolism*, *22*(3), 271–279. https://doi.org/10.1097/00004647-200203000-00004

Ahrén, B. (2000). Autonomic regulation of islet hormone secretion—Implications for health and disease. *Diabetologia*, *43*(4), 393–410. https://doi.org/10.1007/s001250051322

Aizawa, F., Nishinaka, T., Yamashita, T., Nakamoto, K., Koyama, Y., Kasuya, F., & Tokuyama, S. (2016). Astrocytes Release Polyunsaturated Fatty Acids by Lipopolysaccharide Stimuli. *Biological & Pharmaceutical Bulletin*, *39*(7), 1100–1106. https://doi.org/10.1248/bpb.b15-01037

Akintola, A. A., van Opstal, A. M., Westendorp, R. G., Postmus, I., van der Grond, J., & van Heemst, D. (2017). Effect of intranasally administered insulin on cerebral blood flow and perfusion; a randomized experiment in young and older adults. *Aging*, *9*(3), 790–802. https://doi.org/10.18632/aging.101192

Akram M. A focused review of the role of ketone bodies in health and disease. J Med Food. 2013 Nov;16(11):965-7. doi: 10.1089/jmf.2012.2592. Epub 2013 Oct 18. PMID: 24138078.

Alberghina, M., Lupo, G., Anfuso, C. D., & Moro, F. (1993). Palmitate transport through the blood-retina and blood-brain barrier of rat visual system during aging. *Neuroscience Letters*, *150*(1), 17–20. https://doi.org/10.1016/0304-3940(93)90097-5

Alsop, D. C., Detre, J. A., Golay, X., Günther, M., Hendrikse, J., Hernandez-Garcia, L., Lu, H., MacIntosh, B. J., Parkes, L. M., Smits, M., van Osch, M. J. P., Wang, D. J. J., Wong, E. C., & Zaharchuk, G. (2015). Recommended implementation of arterial spin-labeled perfusion MRI for clinical applications: A consensus of the ISMRM perfusion study

group and the European consortium for ASL in dementia: Recommended Implementation of ASL for Clinical Applications. *Magnetic Resonance in Medicine*, *73*(1), 102–116. https://doi.org/10.1002/mrm.25197

Anderson, A. W., Heptulla, R. A., Driesen, N., Flanagan, D., Goldberg, P. A., Jones, T. W., Rife, F., Sarofin, H., Tamborlane, W., Sherwin, R., & Gore, J. C. (2006). Effects of hypoglycemia on human brain activation measured with fMRI. *Magnetic Resonance Imaging*, *24*(6), 693–697. https://doi.org/10.1016/j.mri.2006.03.013

Arbeláez, A. M., Su, Y., Thomas, J. B., Hauch, A. C., Hershey, T., & Ances, B. M. (2013). Comparison of Regional Cerebral Blood Flow Responses to Hypoglycemia Using Pulsed Arterial Spin Labeling and Positron Emission Tomography. *PLoS ONE*, *8*(3), e60085. https://doi.org/10.1371/journal.pone.0060085

Bak, L. K., Walls, A. B., Schousboe, A., & Waagepetersen, H. S. (2018). Astrocytic glycogen metabolism in the healthy and diseased brain. *Journal of Biological Chemistry*, *293*(19), 7108–7116. https://doi.org/10.1074/jbc.R117.803239

Barnes, J. R., Mukherjee, B., Rogers, B. C., Nafar, F., Gosse, M., & Parsons, M. P. (2020). The Relationship Between Glutamate Dynamics and Activity-Dependent Synaptic Plasticity. *The Journal of Neuroscience*, *40*(14), 2793–2807. https://doi.org/10.1523/JNEUROSCI.1655-19.2020

Behrens, C. J., van den Boom, L. P., de Hoz, L., Friedman, A., & Heinemann, U. (2005). Induction of sharp wave–ripple complexes in vitro and reorganization of hippocampal networks. *Nature Neuroscience*, *8*(11), 1560–1567. https://doi.org/10.1038/nn1571

Blazey, T. M., & Raichle, M. E. (2019). *Brain Blood Flow and Metabolism: Variable Relationships in Altered Metabolic States*.

Blockley, N. P., Griffeth, V. E. M., Simon, A. B., & Buxton, R. B. (2013). A review of calibrated blood oxygenation level-dependent (BOLD) methods for the measurement of task-induced changes in brain oxygen metabolism: A REVIEW OF CALIBRATED BOLD METHODS. *NMR in Biomedicine*, *26*(8), 987–1003. https://doi.org/10.1002/nbm.2847

Blockley, N. P., Griffeth, V. E. M., Simon, A. B., Dubowitz, D. J., & Buxton, R. B. (2015). Calibrating the BOLD response without administering gases: Comparison of hypercapnia calibration with calibration using an asymmetric spin echo. *NeuroImage*, *104*, 423–429. https://doi.org/10.1016/j.neuroimage.2014.09.061

Blodgett, D. M., De Zutter, J. K., Levine, K. B., Karim, P., & Carruthers, A. (2007). Structural Basis of GLUT1 Inhibition by Cytoplasmic ATP. *The Journal of General Physiology*, *130*(2), 157–168. https://doi.org/10.1085/jgp.200709818

Bolo, N. R., Musen, G., Jacobson, A. M., Weinger, K., McCartney, R. L., Flores, V., Renshaw, P. F., & Simonson, D. C. (2011). Brain Activation During Working Memory Is Altered in Patients With Type 1 Diabetes During Hypoglycemia. *Diabetes*, *60*(12), 3256–3264. https://doi.org/10.2337/db11-0506

Boyle, P. J., Nagy, R. J., O'Connor, A. M., Kempers, S. F., Yeo, R. A., & Qualls, C. (1994). Adaptation in brain glucose uptake following recurrent hypoglycemia. *Proceedings of the National Academy of Sciences*, *91*(20), 9352–9356. https://doi.org/10.1073/pnas.91.20.9352

Bright, M. G., Croal, P. L., Blockley, N. P., & Bulte, D. P. (2019). Multiparametric measurement of cerebral physiology using calibrated fMRI. *NeuroImage*, *187*, 128–144. https://doi.org/10.1016/j.neuroimage.2017.12.049

Broadley, M. M., Chatwin, H., Soeholm, U., Axelsen, J., Amiel, S. A., Choudhary, P., ... Pouwer, F. (2022). 373-P: A Systematic Review and Meta-analysis of the Impact of Acute Hypoglycemia on Cognitive Function in Adults with Type 1 Diabetes. *Diabetes*, *71*(Supplement_1), 373–P. https://doi.org/10.2337/db22-373-P

Bryan, R. M., Hollinger, B. R., Keefer, K. A., & Page, R. B. (1987). Regional Cerebral and Neural Lobe Blood Flow during Insulin-Induced Hypoglycemia in Unanesthetized Rats. *Journal of Cerebral Blood Flow & Metabolism*, *7*(1), 96–102. https://doi.org/10.1038/jcbfm.1987.14

Buzsáki, G. (2015). Hippocampal sharp wave-ripple: A cognitive biomarker for episodic memory and planning. *Hippocampus*, *25*(10), 1073–1188. https://doi.org/10.1002/hipo.22488

Cahill, G. F. (2006). Fuel Metabolism in Starvation. *Annual Review of Nutrition*, *26*(1), 1–22. https://doi.org/10.1146/annurev.nutr.26.061505.111258

Chan, O., Lawson, M., Zhu, W., Beverly, J. L., & Sherwin, R. S. (2007). ATP-Sensitive K+ Channels Regulate the Release of GABA in the Ventromedial Hypothalamus During Hypoglycemia. *Diabetes*, *56*(4), 1120–1126. https://doi.org/10.2337/db06-1102

Chan, O., Paranjape, S., Czyzyk, D., Horblitt, A., Zhu, W., Ding, Y., Fan, X., Seashore, M., & Sherwin, R. (2011). Increased GABAergic Output in the Ventromedial Hypothalamus Contributes to Impaired Hypoglycemic Counterregulation in Diabetic Rats. *Diabetes*, *60*(5), 1582–1589. https://doi.org/10.2337/db10-1579

Choi, I.-Y., Lee, S.-P., Kim, S.-G., & Gruetter, R. (2001). *In Vivo* Measurements of Brain Glucose Transport Using the Reversible Michaelis–Menten Model and Simultaneous Measurements of Cerebral Blood Flow Changes during Hypoglycemia. *Journal of Cerebral Blood Flow & Metabolism*, *21*(6), 653–663. https://doi.org/10.1097/00004647-200106000-00003

Christen, T., Schmiedeskamp, H., Straka, M., Bammer, R., & Zaharchuk, G. (2012). Measuring brain oxygenation in humans using a multiparametric quantitative blood oxygenation level dependent MRI approach. *Magnetic Resonance in Medicine*, *68*(3), 905–911. https://doi.org/10.1002/mrm.23283

Clemmons, D. R. (2004). The relative roles of growth hormone and IGF-1 in controlling insulin sensitivity. *Journal of Clinical Investigation*, *113*(1), 25–27. https://doi.org/10.1172/JCI20660

Colgin, L. L., Kubota, D., Jia, Y., Rex, C. S., & Lynch, G. (2004). Long-term potentiation is impaired in rat hippocampal slices that produce spontaneous sharp waves. *The Journal of Physiology*, *558*(3), 953–961. https://doi.org/10.1113/jphysiol.2004.068080

Cryer PE. Glucose counterregulation: prevention and correction of hypoglycemia in humans. Am J Physiol. 1993 Feb;264(2 Pt 1):E149-55. doi: 10.1152/ajpendo.1993.264.2.E149. PMID: 8447379.

de Tredern, E., Rabah, Y., Pasquer, L., Minatchy, J., Plaçais, P.-Y., & Preat, T. (2021). Glial glucose fuels the neuronal pentose phosphate pathway for long-term memory. *Cell Reports*, *36*(8), 109620. https://doi.org/10.1016/j.celrep.2021.109620

Dunn, J. T., Choudhary, P., Teh, M. M., Macdonald, I., Hunt, K. F., Marsden, P. K., & Amiel, S. A. (2018). The impact of hypoglycaemia awareness status on regional brain responses to acute hypoglycaemia in men with type 1 diabetes. *Diabetologia*, *61*(7), 1676–1687. https://doi.org/10.1007/s00125-018-4622-2

El Messari, S., Aït-Ikhlef, A., Ambroise, D.-H., Penicaud, L., & Arluison, M. (2002). Expression of insulin-responsive glucose transporter GLUT4 mRNA in the rat brain and spinal cord: An in situ hybridization study. *Journal of Chemical Neuroanatomy*, *24*(4), 225-242.

Epp, S. M., Castrillón, G., Yuan, B., Andrews-Hanna, J., Preibisch, C., & Riedl, V. (2023). *Two distinct modes of hemodynamic responses in the human brain* [Preprint]. Neuroscience. https://doi.org/10.1101/2023.12.08.570806

Fassbender, K., Ries, S., Schminke, U., Schneider, S., & Hennerici, M. (1996). Inflammatory cytokines in CSF in bacterial meningitis: Association with altered blood flow velocities in basal cerebral arteries. *Journal of Neurology, Neurosurgery & Psychiatry*, *61*(1), 57–61. https://doi.org/10.1136/jnnp.61.1.57

Fick, A. (1870). Ueber die Messung des Blutquantums in den Herzventrikeln. *Sitzungsberichte Der Physikalisch-Medizinischen Gesellschaft Zu Würzburg*, 16.

Friedman, M. (1937). The Use of Ranks to Avoid the Assumption of Normality Implicit in the Analysis of Variance. *Journal of the American Statistical Association*, *32*(200), 675–701. https://doi.org/10.2307/2279372

Gao, V., Suzuki, A., Magistretti, P. J., Lengacher, S., Pollonini, G., Steinman, M. Q., & Alberini, C. M. (2016). Astrocytic β_2 -adrenergic receptors mediate hippocampal long-term memory consolidation. *Proceedings of the National Academy of Sciences*, *113*(30), 8526–8531. https://doi.org/10.1073/pnas.1605063113

Garcia Corrales, A. V., Haidar, M., Bogie, J. F. J., & Hendriks, J. J. A. (2021). Fatty Acid Synthesis in Glial Cells of the CNS. *International Journal of Molecular Sciences*, *22*(15), 8159. https://doi.org/10.3390/ijms22158159

García-Cáceres, C., Quarta, C., Varela, L., Gao, Y., Gruber, T., Legutko, B., Jastroch, M., Johansson, P., Ninkovic, J., Yi, C.-X., Le Thuc, O., Szigeti-Buck, K., Cai, W., Meyer, C. W., Pfluger, P. T., Fernandez, A. M., Luquet, S., Woods, S. C., Torres-Alemán, I., … Tschöp, M. H. (2016). Astrocytic Insulin Signaling Couples Brain Glucose Uptake with Nutrient Availability. *Cell*, *166*(4), 867–880. https://doi.org/10.1016/j.cell.2016.07.028

Genuth, S. (2006). Insights from The Diabetes Control and Complications Trial/Epidemiology of Diabetes Interventions and Complications Study on The Use of Intensive Glycemic Treatment to Reduce The Risk of Complications of Type 1 Diabetes. *Endocrine Practice*, *12*, 34–41. https://doi.org/10.4158/EP.12.S1.34

Gibbs, M. E., Anderson, D. G., & Hertz, L. (2006). Inhibition of glycogenolysis in astrocytes interrupts memory consolidation in young chickens. *Glia*, *54*(3), 214–222. https://doi.org/10.1002/glia.20377

Göttler, J., Kaczmarz, S., Kallmayer, M., Wustrow, I., Eckstein, H.-H., Zimmer, C., Sorg, C., Preibisch, C., & Hyder, F. (2019). Flow-metabolism uncoupling in patients with asymptomatic unilateral carotid artery stenosis assessed by multi-modal magnetic resonance imaging. *Journal of Cerebral Blood Flow & Metabolism*, *39*(11), 2132–2143. https://doi.org/10.1177/0271678X18783369

Graveling, A. J., Deary, I. J., & Frier, B. M. (2013). Acute Hypoglycemia Impairs Executive Cognitive Function in Adults With and Without Type 1 Diabetes. *Diabetes Care*, *36*(10), 3240–3246. https://doi.org/10.2337/dc13-0194

Gusnard, D. A., & Raichle, M. E. (2001). Searching for a baseline: Functional imaging and the resting human brain. *Nature Reviews Neuroscience*, *2*(10), 685–694. https://doi.org/10.1038/35094500

Haggenmüller, B., Kreiser, K., Sollmann, N., Huber, M., Vogele, D., Schmidt, S. A., Beer, M., Schmitz, B., Ozpeynirci, Y., Rosskopf, J., & Kloth, C. (2023). Pictorial Review on

Imaging Findings in Cerebral CTP in Patients with Acute Stroke and Its Mimics: A Primer for General Radiologists. *Diagnostics*, *13*(3), 447. https://doi.org/10.3390/diagnostics13030447

Hasselbalch, S. G., Madsen, P. L., Hageman, L. P., Olsen, K. S., Justesen, N., Holm, S., & Paulson, O. B. (1996). Changes in cerebral blood flow and carbohydrate metabolism during acute hyperketonemia. *American Journal of Physiology-Endocrinology and Metabolism*, *270*(5), E746–E751. https://doi.org/10.1152/ajpendo.1996.270.5.E746

Hechler, A., De Lange, F. P., & Riedl, V. (2023). *The energy metabolic footprint of predictive processing in the human brain* [Preprint]. Neuroscience. https://doi.org/10.1101/2023.12.08.570804

Hedderich, D., Kluge, A., Pyka, T., Zimmer, C., Kirschke, J. S., Wiestler, B., & Preibisch, C. (2019). Consistency of normalized cerebral blood volume values in glioblastoma using different leakage correction algorithms on dynamic susceptibility contrast magnetic resonance imaging data without and with preload. *Journal of Neuroradiology*, *46*(1), 44–51. https://doi.org/10.1016/j.neurad.2018.04.006

Heise, T., Zijlstra, E., Nosek, L., Heckermann, S., Plum-Mörschel, L., & Forst, T. (2016). Euglycaemic glucose clamp: What it can and cannot do, and how to do it. *Diabetes, Obesity and Metabolism*, *18*(10), 962–972. https://doi.org/10.1111/dom.12703

Hernandez-Garzón E, Fernandez AM, Perez-Alvarez A, Genis L, Bascuñana P, Fernandez de la Rosa R, Delgado M, Angel Pozo M, Moreno E, McCormick PJ, Santi A, Trueba Saiz A, Garcia-Caceres C, Tschöp MH, Araque A, Martin ED, Torres Aleman I. The insulin-like growth factor I receptor regulates glucose transport by astrocytes. Glia. 2016 Nov;64(11):1962-71. doi: 10.1002/glia.23035. Epub 2016 Jul 27. PMID: 27462832.

Herrera Moro Chao, D., Kirchner, M. K., Pham, C., Foppen, E., Denis, R. G. P., Castel, J., Morel, C., Montalban, E., Hassouna, R., Bui, L.-C., Renault, J., Mouffle, C., García-Cáceres, C., Tschöp, M. H., Li, D., Martin, C., Stern, J. E., & Luquet, S. H. (2022). Hypothalamic

astrocytes control systemic glucose metabolism and energy balance. *Cell Metabolism*, *34*(10), 1532-1547.e6. https://doi.org/10.1016/j.cmet.2022.09.002

Hertz, L., O'Dowd, B. S., Ng, K. T., & Gibbs, M. E. (2003). Reciprocal changes in forebrain contents of glycogen and of glutamate/glutamine during early memory consolidation in the day-old chick. *Brain Research*, *994*(2), 226–233. https://doi.org/10.1016/j.brainres.2003.09.044

Hirsch, N. M., Toth, V., Förschler, A., Kooijman, H., Zimmer, C., & Preibisch, C. (2014). Technical considerations on the validity of blood oxygenation level-dependent-based MR assessment of vascular deoxygenation: BOLD-BASED ASSESSMENT OF VASCULAR DEOXYGENATION. *NMR in Biomedicine*, *27*(7), 853–862. https://doi.org/10.1002/nbm.3131

Hitze, B., Hubold, C., van Dyken, R., Schlichting, K., Lehnert, H., Entringer, S., Peters, A., 2010. How the Selfish Brain Organizes its 'Supply and Demand'. Front Neuroenerget. 2 https://doi.org/10.3389/fnene.2010.00007.

Iqbal, A., Prince, L. R., Novodvorsky, P., Bernjak, A., Thomas, M. R., Birch, L., Lambert, D., Kay, L. J., Wright, F. J., Macdonald, I. A., Jacques, R. M., Storey, R. F., McCrimmon, R. J., Francis, S., Heller, S. R., & Sabroe, I. (2019). Effect of Hypoglycemia on Inflammatory Responses and the Response to Low-Dose Endotoxemia in Humans. *The Journal of Clinical Endocrinology & Metabolism*, *104*(4), 1187–1199. https://doi.org/10.1210/jc.2018-01168

Kaczmarz, S., Hyder, F., & Preibisch, C. (2020). Oxygen extraction fraction mapping with multi-parametric quantitative BOLD MRI: Reduced transverse relaxation bias using 3D-GraSE imaging. *NeuroImage*, *220*, 117095. https://doi.org/10.1016/j.neuroimage.2020.117095

Kersten, S., Seydoux, J., Peters, J. M., Gonzalez, F. J., Desvergne, B., & Wahli, W. (1999). Peroxisome proliferator–activated receptor α mediates the adaptive response to fasting. *Journal of Clinical Investigation*, *103*(11), 1489–1498. https://doi.org/10.1172/JCI6223

Kind, K. L., Roberts, C. T., Sohlstrom, A. I., Katsman, A., Clifton, P. M., Robinson, J. S., & Owens, J. A. (2005). Chronic maternal feed restriction impairs growth but increases adiposity of the fetal guinea pig. *American Journal of Physiology-Regulatory, Integrative and Comparative Physiology*, *288*(1), R119–R126. https://doi.org/10.1152/ajpregu.00360.2004

Kluge, A., Lukas, M., Toth, V., Pyka, T., Zimmer, C., & Preibisch, C. (2016). Analysis of three leakage-correction methods for DSC-based measurement of relative cerebral blood volume with respect to heterogeneity in human gliomas. *Magnetic Resonance Imaging*, *34*(4), 410–421. https://doi.org/10.1016/j.mri.2015.12.015

Koepsell, H. (2020). Glucose transporters in brain in health and disease. *Pflügers Archiv - European Journal of Physiology*, *472*(9), 1299–1343. https://doi.org/10.1007/s00424-020-02441-x

Kolb, H., Kempf, K., Röhling, M., Lenzen-Schulte, M., Schloot, N. C., & Martin, S. (2021). Ketone bodies: From enemy to friend and guardian angel. *BMC Medicine*, *19*(1), 313. https://doi.org/10.1186/s12916-021-02185-0

Koller, M. (2016). robustlmm: An R Package for Robust Estimation of Linear Mixed-Effects Models. *Journal of Statistical Software*, *75*(6). https://doi.org/10.18637/jss.v075.i06

Kolwicz, S. C. (2021). Ketone Body Metabolism in the Ischemic Heart. *Frontiers in Cardiovascular Medicine*, *8*, 789458. https://doi.org/10.3389/fcvm.2021.789458

Krieger M. (1921). Über die Atrophie der menschlichen Organe bei Inanition [On the atrophy of human organs in inanition]. *Z. Angew. Anat. Konstitutionsl*. 7, 87–134

Kubera, B., Hubold, C., Wischnath, H., Zug, S., & Peters, A. (2014). Rise of ketone bodies with psychosocial stress in normal weight men. *Psychoneuroendocrinology*, *45*, 43–48. https://doi.org/10.1016/j.psyneuen.2014.03.008

Kullmann, S., Fritsche, A., Wagner, R., Schwab, S., Häring, H.-U., Preissl, H., & Heni, M. (2017). Hypothalamic insulin responsiveness is associated with pancreatic insulin

secretion in humans. *Physiology & Behavior*, *176*, 134–138. https://doi.org/10.1016/j.physbeh.2017.03.036

Kullmann, S., Heni, M., Veit, R., Scheffler, K., Machann, J., Häring, H.-U., Fritsche, A., & Preissl, H. (2015). Selective Insulin Resistance in Homeostatic and Cognitive Control Brain Areas in Overweight and Obese Adults. *Diabetes Care*, *38*(6), 1044–1050. https://doi.org/10.2337/dc14-2319

Lee, A., Ader, M., Bray, G. A., & Bergman, R. N. (1992). Diurnal Variation in Glucose Tolerance: Cyclic Suppression of Insulin Action and Insulin Secretion in Normal-Weight, But Not Obese, Subjects. *Diabetes*, *41*(6), 750–759. https://doi.org/10.2337/diab.41.6.750

Lee, J. J., Khoury, N., Shackleford, A. M., Nelson, S., Herrera, H., Antenor-Dorsey, J. A., Semenkovich, K., Shimony, J. S., Powers, W. J., Cryer, P. E., & Arbeláez, A. M. (2017). Dissociation Between Hormonal Counterregulatory Responses and Cerebral Glucose Metabolism During Hypoglycemia. *Diabetes*, *66*(12), 2964–2972. https://doi.org/10.2337/db17-0574

Lima, F. D., Correia, A. L. M., Teixeira, D. da S., Silva Neto, D. V. da, Fernandes, Í. S., Viana, M. B., Petitto, M., Sampaio, R. A., Chaves, S. N., Alves, S. T., Dantas, R. A. E., & Mota, M. R. (2015). Acute metabolic response to fasted and postprandial exercise. *International Journal of General Medicine*, 255. https://doi.org/10.2147/IJGM.S87429

Lubow, J. M., Piñón, I. G., Avogaro, A., Cobelli, C., Treeson, D. M., Mandeville, K. A., Toffolo, G., & Boyle, P. J. (2006). Brain oxygen utilization is unchanged by hypoglycemia in normal humans: Lactate, alanine, and leucine uptake are not sufficient to offset energy deficit. *American Journal of Physiology-Endocrinology and Metabolism*, *290*(1), E149–E153. https://doi.org/10.1152/ajpendo.00049.2005

Ma, Y., Sun, H., Cho, J., Mazerolle, E. L., Wang, Y., & Pike, G. B. (2020). Cerebral OEF quantification: A comparison study between quantitative susceptibility mapping and dual-gas calibrated BOLD imaging. *Magnetic Resonance in Medicine*, *83*(1), 68–82. https://doi.org/10.1002/mrm.27907

Madsen, P. L., Schmidt, J. F., Holm, S., Vorstrup, S., Lassen, N. A., & Wildschiødtz, G. (1991). Cerebral oxygen metabolism and cerebral blood flow in man during light sleep (stage 2). *Brain Research*, *557*(1–2), 217–220. https://doi.org/10.1016/0006-8993(91)90137-K

Maier, N., Nimmrich, V., & Draguhn, A. (2003). Cellular and Network Mechanisms Underlying Spontaneous Sharp Wave–Ripple Complexes in Mouse Hippocampal Slices. *The Journal of Physiology*, *550*(3), 873–887. https://doi.org/10.1113/jphysiol.2003.044602

McAulay, V., Deary, I. J., Ferguson, S. C., & Frier, B. M. (2001). Acute Hypoglycemia in Humans Causes Attentional Dysfunction While Nonverbal Intelligence Is Preserved. *Diabetes Care*, *24*(10), 1745–1750. https://doi.org/10.2337/diacare.24.10.1745

McManus, R., Ioussoufovitch, S., Froats, E., St Lawrence, K., Van Uum, S., & Diop, M. (2020). Dynamic response of cerebral blood flow to insulin-induced hypoglycemia. *Scientific Reports*, *10*(1), 21300. https://doi.org/10.1038/s41598-020-77626-6

McNay, E. C., Fries, T. M., & Gold, P. E. (2000). Decreases in rat extracellular hippocampal glucose concentration associated with cognitive demand during a spatial task. *Proceedings of the National Academy of Sciences*, *97*(6), 2881–2885. https://doi.org/10.1073/pnas.050583697

Miki, T., Liss, B., Minami, K., Shiuchi, T., Saraya, A., Kashima, Y., Horiuchi, M., Ashcroft, F., Minokoshi, Y., Roeper, J., & Seino, S. (2001). ATP-sensitive K+ channels in the hypothalamus are essential for the maintenance of glucose homeostasis. *Nature Neuroscience*, *4*(5), 507–512. https://doi.org/10.1038/87455

Miller, S. L., Green, L. R., Peebles, D. M., Hanson, M. A., & Blanco, C. E. (2002). Effects of chronic hypoxia and protein malnutrition on growth in the developing chick. *American Journal of Obstetrics and Gynecology*, *186*(2), 261–267. https://doi.org/10.1067/mob.2002.119629

Mitrakou A, Ryan C, Veneman T, Mokan M, Jenssen T, Kiss I, Durrant J, Cryer P, Gerich J. Hierarchy of glycemic thresholds for counterregulatory hormone secretion,

symptoms, and cerebral dysfunction. Am J Physiol. 1991 Jan;260(1 Pt 1):E67-74. doi: 10.1152/ajpendo.1991.260.1.E67. PMID: 1987794.

Mulder, A. H., Tack, C. J., Olthaar, A. J., Smits, P., Sweep, F. C. G. J., & Bosch, R. R. (2005). Adrenergic receptor stimulation attenuates insulin-stimulated glucose uptake in 3T3-L1 adipocytes by inhibiting GLUT4 translocation. *American Journal of Physiology-Endocrinology and Metabolism*, *289*(4), E627–E633. https://doi.org/10.1152/ajpendo.00079.2004

Nelder, J. A., & Wedderburn, R. W. M. (2024). *Generalized Linear Models*.

Newman, L. A., Korol, D. L., & Gold, P. E. (2011). Lactate Produced by Glycogenolysis in Astrocytes Regulates Memory Processing. *PLoS ONE*, *6*(12), e28427. https://doi.org/10.1371/journal.pone.0028427

O'Dowd, B. S., Gibbs, M. E., Ng, K. T., Hertz, E., & Hertz, L. (1994). Astrocytic glycogenolysis energizes memory processes in neonate chicks. *Developmental Brain Research*, *78*(1), 137–141. https://doi.org/10.1016/0165-3806(94)90018-3

Öz, G., Seaquist, E. R., Kumar, A., Criego, A. B., Benedict, L. E., Rao, J. P., Henry, P.-G., Van De Moortele, P.-F., & Gruetter, R. (2007). Human brain glycogen content and metabolism: Implications on its role in brain energy metabolism. *American Journal of Physiology-Endocrinology and Metabolism*, *292*(3), E946–E951. https://doi.org/10.1152/ajpendo.00424.2006

Pan, J. W., Rothman, D. L., Behar, K. L., Stein, D. T., & Hetherington, H. P. (2000). Human Brain β-Hydroxybutyrate and Lactate Increase in Fasting-Induced Ketosis. *Journal of Cerebral Blood Flow & Metabolism*, *20*(10), 1502–1507. https://doi.org/10.1097/00004647-200010000-00012

Papatheodoropoulos, C., & Kostopoulos, G. (2002). Spontaneous GABAA-dependent synchronous periodic activity in adult rat ventral hippocampal slices. *Neuroscience Letters*, *319*(1), 17–20. https://doi.org/10.1016/S0304-3940(01)02505-8

Pellerin, L., & Magistretti, P. J. (1997). Glutamate Uptake Stimulates Na ⁺ ,K ⁺ -ATPase Activity in Astrocytes via Activation of a Distinct Subunit Highly Sensitive to Ouabain. *Journal of Neurochemistry*, *69*(5), 2132–2137. https://doi.org/10.1046/j.1471-4159.1997.69052132.x

Peters, A., Bosy-Westphal, A., Kubera, B., Langemann, D., Goele, K., Later, W., Heller, M., Hubold, C., & Müller, M. J. (2011). Why Doesn't the Brain Lose Weight, When Obese People Diet? *Obesity Facts*, *4*(2), 2–2. https://doi.org/10.1159/000327676

Peters, A., Schweiger, U., Pellerin, L., Hubold, C., Oltmanns, K. M., Conrad, M., Schultes, B., Born, J., & Fehm, H. L. (2004). The selfish brain: Competition for energy resources. *Neuroscience & Biobehavioral Reviews*, *28*(2), 143–180. https://doi.org/10.1016/j.neubiorev.2004.03.002

Peters, A., Sprengell, M., & Kubera, B. (2022). The principle of 'brain energy on demand' and its predictive power for stress, sleep, stroke, obesity and diabetes. *Neuroscience & Biobehavioral Reviews*, *141*, 104847. https://doi.org/10.1016/j.neubiorev.2022.104847

Powanda, M. C., & Beisel, W. R. (2003). Metabolic Effects of Infection on Protein and Energy Status. *The Journal of Nutrition*, *133*(1), 322S-327S. https://doi.org/10.1093/jn/133.1.322S

Quirk, C. (2020). PsychopyVisualSearch. GitHub.https://github.com/colinquirk/PsychopyVisualSearch

Qvisth, V., Hagström-Toft, E., Enoksson, S., & Bolinder, J. (2008). Catecholamine Regulation of Local Lactate Production in Vivo in Skeletal Muscle and Adipose Tissue: Role of β-Adrenoreceptor Subtypes. *The Journal of Clinical Endocrinology & Metabolism*, *93*(1), 240–246. https://doi.org/10.1210/jc.2007-1313

Ratter, J. M., Rooijackers, H. M. M., Tack, C. J., Hijmans, A. G. M., Netea, M. G., de Galan, B. E., & Stienstra, R. (2017). Proinflammatory Effects of Hypoglycemia in Humans With or Without Diabetes. *Diabetes*, *66*(4), 1052–1061. https://doi.org/10.2337/db16-1091

Richardson BS, Hohimer AR, Bissonnette JM, Machida CM. Insulin hypoglycemia, cerebral metabolism, and neural function in fetal lambs. Am J Physiol. 1985 Jan;248(1 Pt 2):R72-7. doi: 10.1152/ajpregu.1985.248.1.R72. PMID: 3970187.

Saad, A., Dalla Man, C., Nandy, D. K., Levine, J. A., Bharucha, A. E., Rizza, R. A., Basu, R., Carter, R. E., Cobelli, C., Kudva, Y. C., & Basu, A. (2012). Diurnal Pattern to Insulin Secretion and Insulin Action in Healthy Individuals. *Diabetes*, *61*(11), 2691–2700. https://doi.org/10.2337/db11-1478

Schaefer, A., Kong, R., Gordon, E. M., Laumann, T. O., Zuo, X.-N., Holmes, A. J., Eickhoff, S. B., & Yeo, B. T. T. (2018). Local-Global Parcellation of the Human Cerebral Cortex from Intrinsic Functional Connectivity MRI. *Cerebral Cortex*, *28*(9), 3095–3114. https://doi.org/10.1093/cercor/bhx179

Schreiner, T., Griffiths, B. J., Kutlu, M., Vollmar, C., Kaufmann, E., Quach, S., Remi, J., Noachtar, S., & Staudigl, T. (2023). *Spindle-locked ripples mediate memory reactivation during human NREM sleep*. https://doi.org/10.1101/2023.01.27.525854

Sommerfield, A. J., Deary, I. J., McAulay, V., & Frier, B. M. (2003a). Moderate hypoglycemia impairs multiple memory functions in healthy adults. *Neuropsychology*, *17*(1), 125–132. https://doi.org/10.1037/0894-4105.17.1.125

Sommerfield, A. J., Deary, I. J., McAulay, V., & Frier, B. M. (2003b). Short-Term, Delayed, and Working Memory Are Impaired During Hypoglycemia in Individuals With Type 1 Diabetes. *Diabetes Care*, *26*(2), 390–396. https://doi.org/10.2337/diacare.26.2.390

Spinner, C. D., Kern, K. E., Zink, A., Wolf, E., Balogh, A., Noe, S., Von Werder, A., Schwerdtfeger, C., Schmid, R. M., & Iakoubov, R. (2016). Neither boosted elvitegravir nor darunavir with emtricitabine/tenofovir disoproxil fumarate increase insulin resistance in healthy volunteers: Results from the STRIBILD-IR study. *Antiviral Therapy*, *21*(7), 627–631. https://doi.org/10.3851/IMP3049

Suzuki, A., Stern, S. A., Bozdagi, O., Huntley, G. W., Walker, R. H., Magistretti, P. J., & Alberini, C. M. (2011). Astrocyte-Neuron Lactate Transport Is Required for Long-Term

Memory Formation. *Cell*, *144*(5), 810–823. https://doi.org/10.1016/j.cell.2011.02.018

Teh, M. M., Dunn, J. T., Choudhary, P., Samarasinghe, Y., Macdonald, I., O'Doherty, M., Marsden, P., Reed, L. J., & Amiel, S. A. (2010). Evolution and resolution of human brain perfusion responses to the stress of induced hypoglycemia. *NeuroImage*, *53*(2), 584–592. https://doi.org/10.1016/j.neuroimage.2010.06.033

Teves, D., Videen, T. O., Cryer, P. E., & Powers, W. J. (2004). Activation of human medial prefrontal cortex during autonomic responses to hypoglycemia. *Proceedings of the National Academy of Sciences*, *101*(16), 6217–6221. https://doi.org/10.1073/pnas.0307048101

Thomas, M., Sherwin, R. S., Murphy, J., & Kerr, D. (1997). *Importance of Cerebral Blood Flow to the Recognition of and Physiological Responses to Hypoglycemia*. *46*.

Thomas Yeo, B. T., Krienen, F. M., Sepulcre, J., Sabuncu, M. R., Lashkari, D., Hollinshead, M., Roffman, J. L., Smoller, J. W., Zöllei, L., Polimeni, J. R., Fischl, B., Liu, H., & Buckner, R. L. (2011). The organization of the human cerebral cortex estimated by intrinsic functional connectivity. *Journal of Neurophysiology*, *106*(3), 1125–1165. https://doi.org/10.1152/jn.00338.2011

Wiegers, E. C., Rooijackers, H. M., Tack, C. J., Philips, B. W., Heerschap, A., van der Graaf, M., & de Galan, B. E. (2019). Effect of lactate administration on brain lactate levels during hypoglycemia in patients with type 1 diabetes. *Journal of Cerebral Blood Flow & Metabolism*, *39*(10), 1974–1982. https://doi.org/10.1177/0271678X18775884

Wilcoxon, F. (2024). *Individual Comparisons by Ranking Methods*.

Woods, S.C., Porte Jr., D., 1974. Neural control of the endocrine pancreas. Physiol. Rev. 54, 596–619.

Xu, F., Ge, Y., & Lu, H. (2009). Noninvasive quantification of whole-brain cerebral metabolic rate of oxygen (CMRO $_2$) by MRI: Quantification of CMRO $_2$. *Magnetic Resonance in Medicine*, *62*(1), 141–148. https://doi.org/10.1002/mrm.21994

Yablonskiy, D. A., & Haacke, E. M. (1994). Theory of NMR signal behavior in magnetically inhomogeneous tissues: The static dephasing regime. *Magnetic Resonance in Medicine*, *32*(6), 749–763. https://doi.org/10.1002/mrm.1910320610

Yang, W., Sun, C., Huszár, R., Hainmueller, T., Kiselev, K., & Buzsáki, G. (2024). Selection of experience for memory by hippocampal sharp wave ripples. *Science*, *383*(6690), 1478–1483. https://doi.org/10.1126/science.adk8261

Zhang, K., Herzog, H., Mauler, J., Filss, C., Okell, T. W., Kops, E. R., Tellmann, L., Fischer, T., Brocke, B., Sturm, W., Coenen, H. H., & Shah, N. J. (2014). Comparison of cerebral blood flow acquired by simultaneous [15O]water positron emission tomography and arterial spin labeling magnetic resonance imaging. *Journal of Cerebral Blood Flow and Metabolism*, *34*(8), 1373–1380. https://doi.org/10.1038/jcbfm.2014.92

Zhang, X., Yang, S., Chen, J., & Su, Z. (2019). Unraveling the Regulation of Hepatic Gluconeogenesis. *Frontiers in Endocrinology*, *9*, 802. https://doi.org/10.3389/fendo.2018.00802

Supplementary material

Table S1

Additional subject characteristics.

Variable	**Mean ±std**
Age	24.03 ±2.1 years
Weight	77.34 ±7.15 kg
BMI	22.93 ±2.46 kg/m^2
Body fat	18.22 ±4.61%
Fasting blood glucose	87.33 ±4.8 mg/dl

Note. All subjects were healthy males with no family history of metabolic disorders.

Table S2

Imaging parameters, mean ±SD across subjects and conditions within GM.

CMRO2 [µmol/100g/min]	CBF [ml/100g/min]	OEF [ratio]	CBV [%]
141.68 (19.66)	49.84 (6.82)	0.38 (0.03)	4.79 (0.18)

Note. These values are based on the parameter thresholds mentioned in the methods section.

§*Please note:* Figures S1-S6 depict blood parameters across the experiment per condition. Measurements at t=0 reflect baseline levels, acquired before clamping was initiated. Timepoints t=48 and t=72 are used for assessment of epinephrine differences during the MRI scan. After t=72, clamping was stopped. At t=96, previous hypoglycemia had been restored. At this point, cognitive tests were administered. Significant codes: <0.001: ***, <0.01: **, <0.05: *. Shown are mean values per condition, together with 95% confidence intervals.

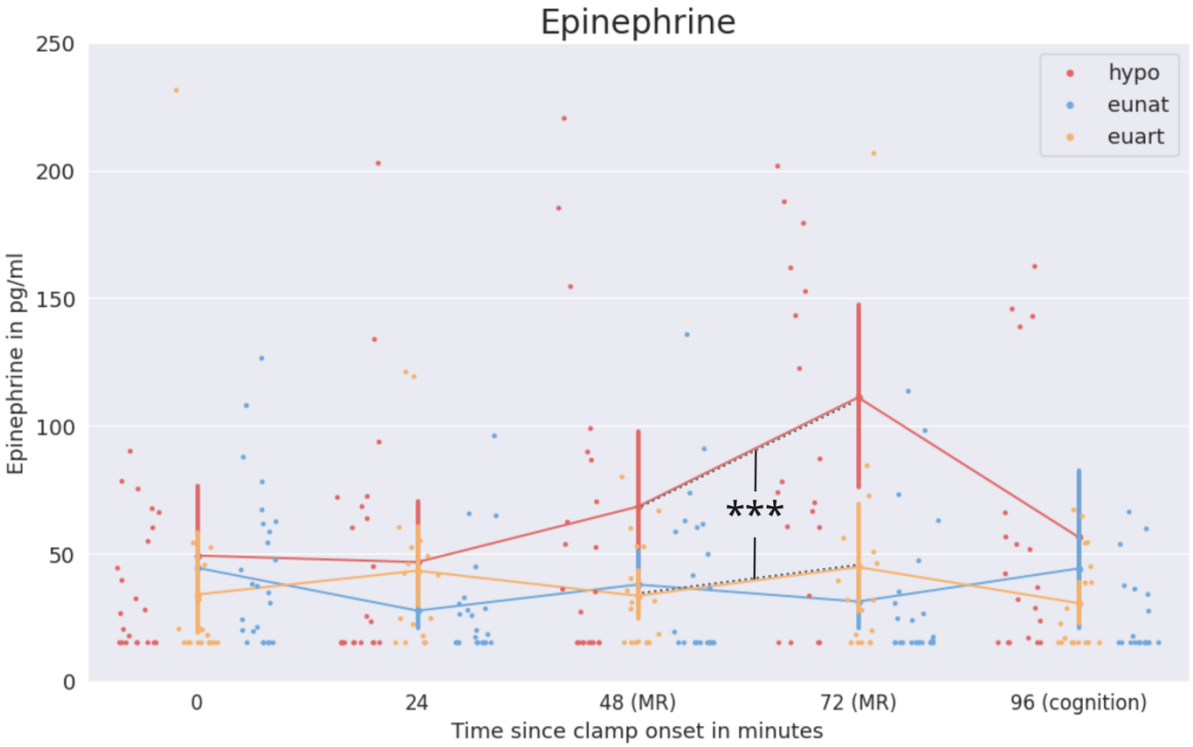

Figure S1. Epinephrine levels across the experiment per condition. During the MR scan, epinephrine levels were significantly higher in hypo vs. eu_{art} ($p<0.001$).§

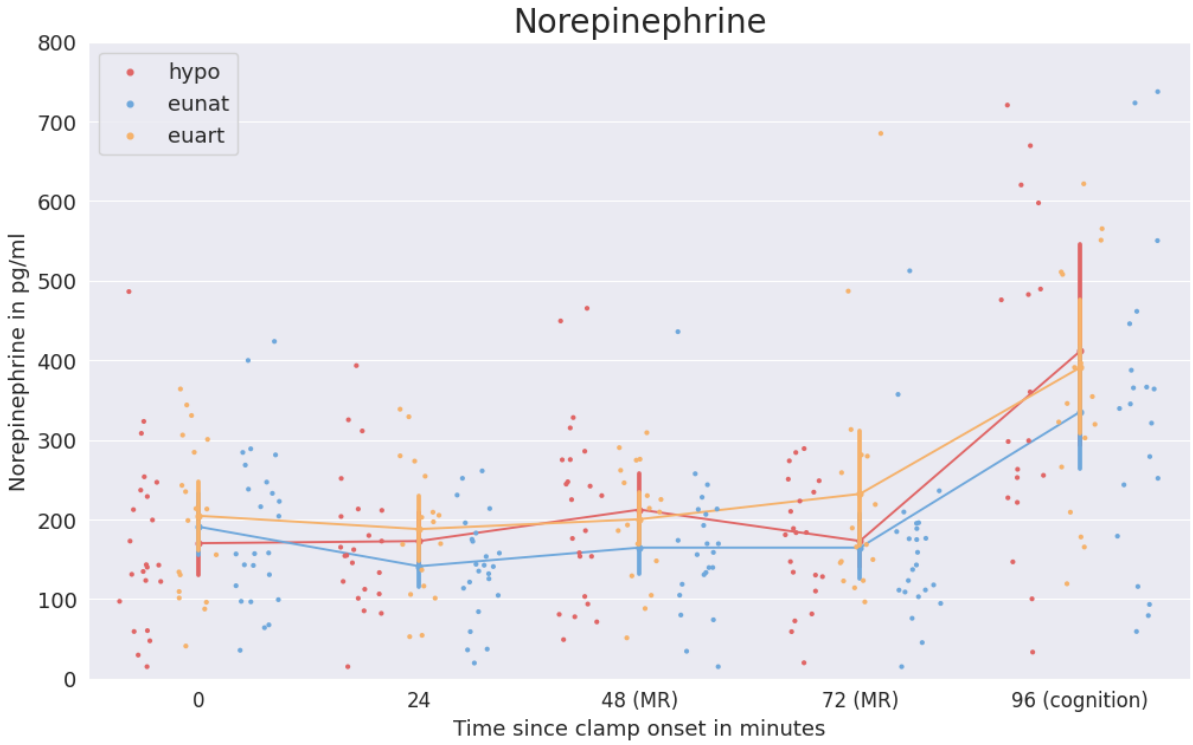

Figure S2. Norepinephrine levels across the experiment per condition. Throughout the experiment, norepinephrine levels never significantly differed between conditions.§

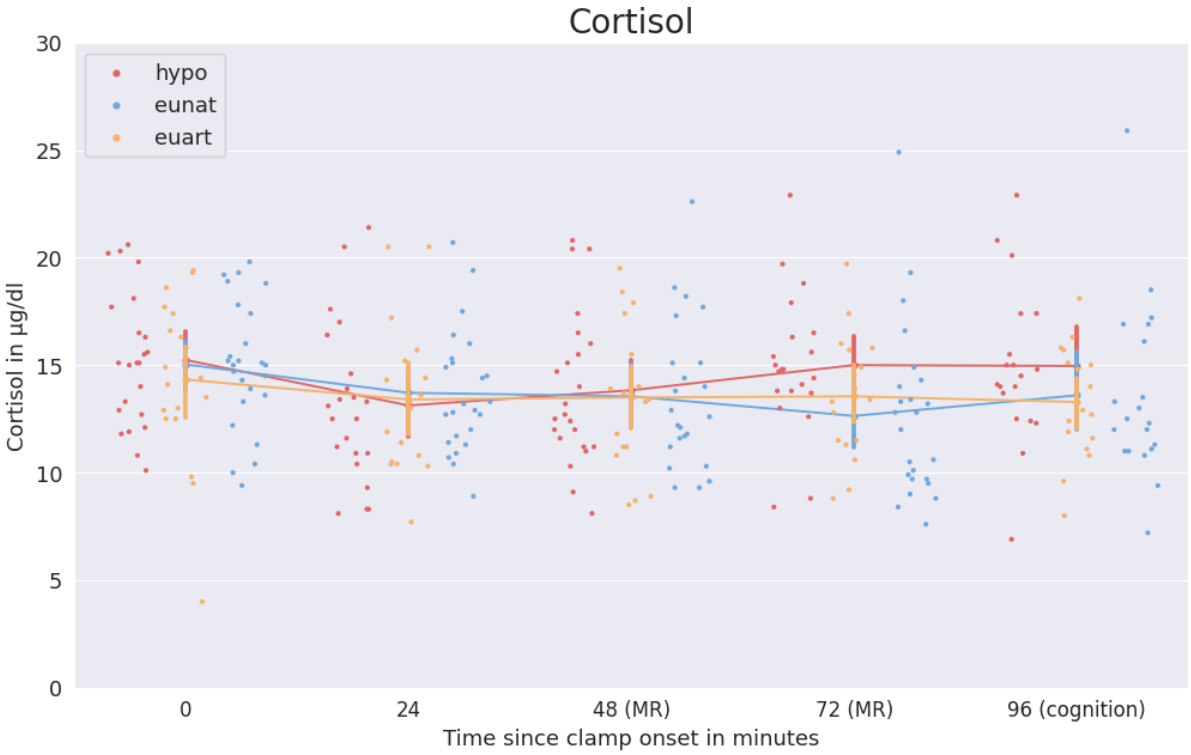

Figure S3. Cortisol levels across the experiment per condition. Throughout the experiment, cortisol levels never significantly differed between conditions.§

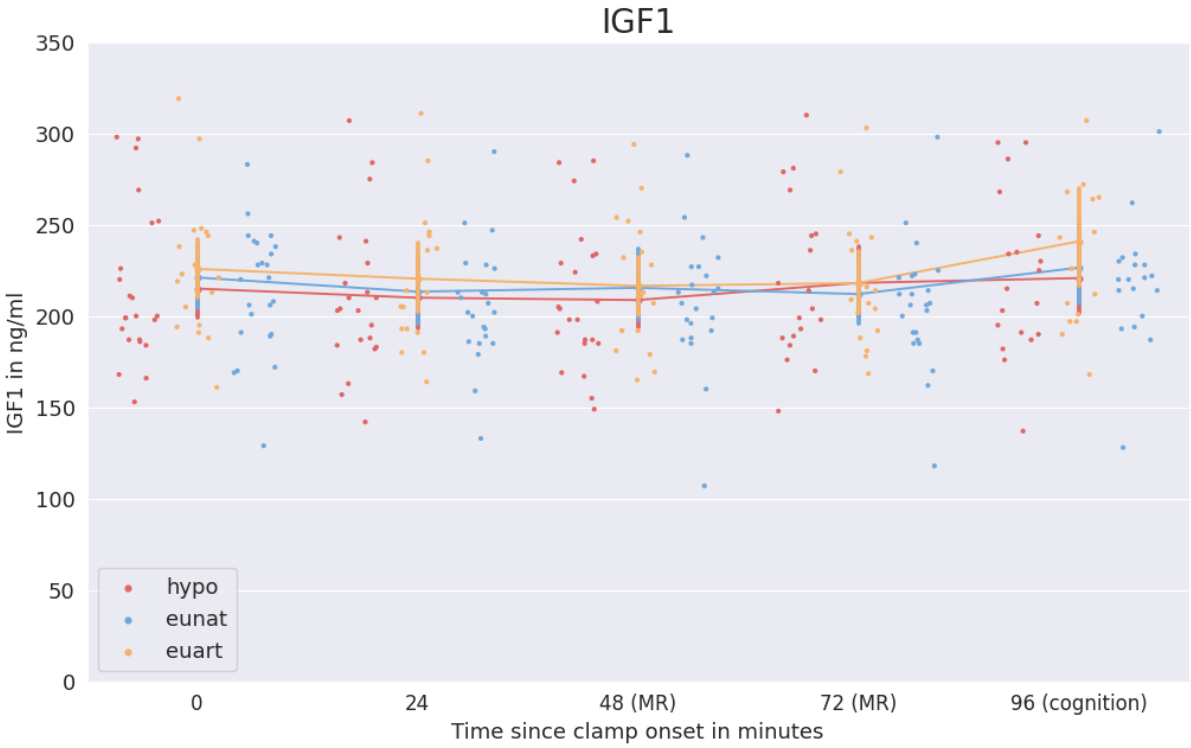

Figure S4. IGF-1 levels across the experiment per condition. Throughout the experiment, IGF-1 levels never significantly differed between conditions.§

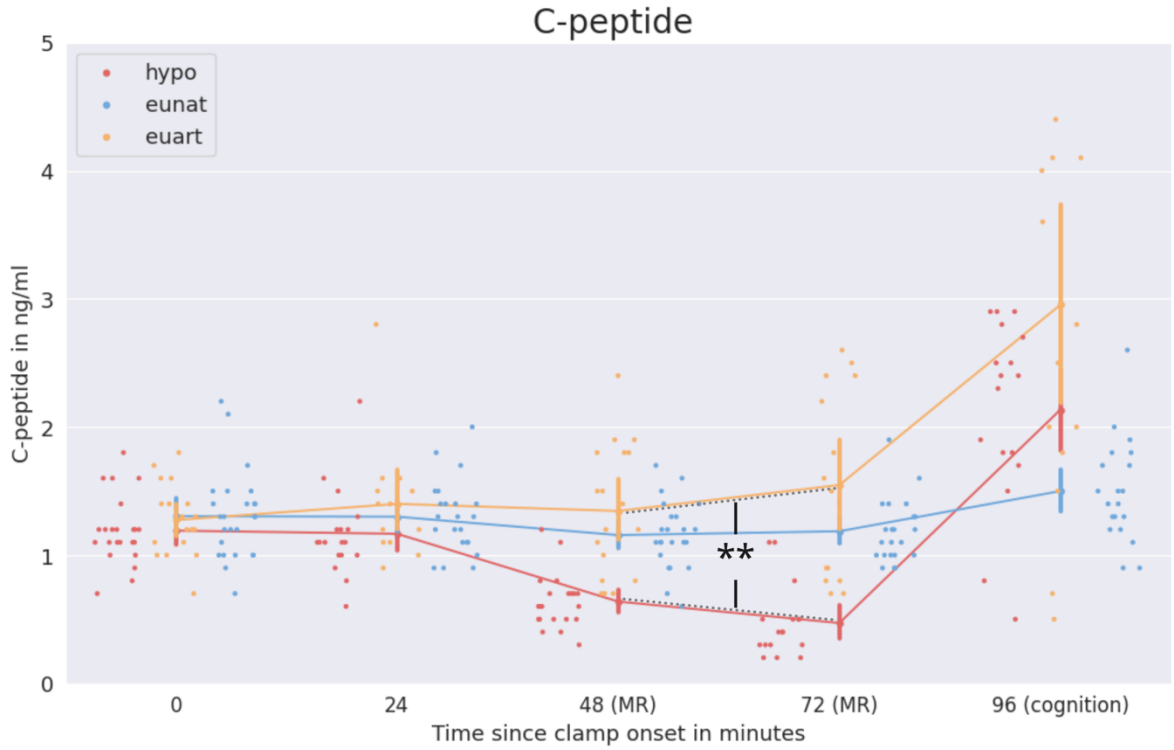

Figure S5. C-peptide levels across the experiment per condition. During MR scanning, c-peptide was significantly lower in hypo than in eu_{art} ($p<0.01$).§

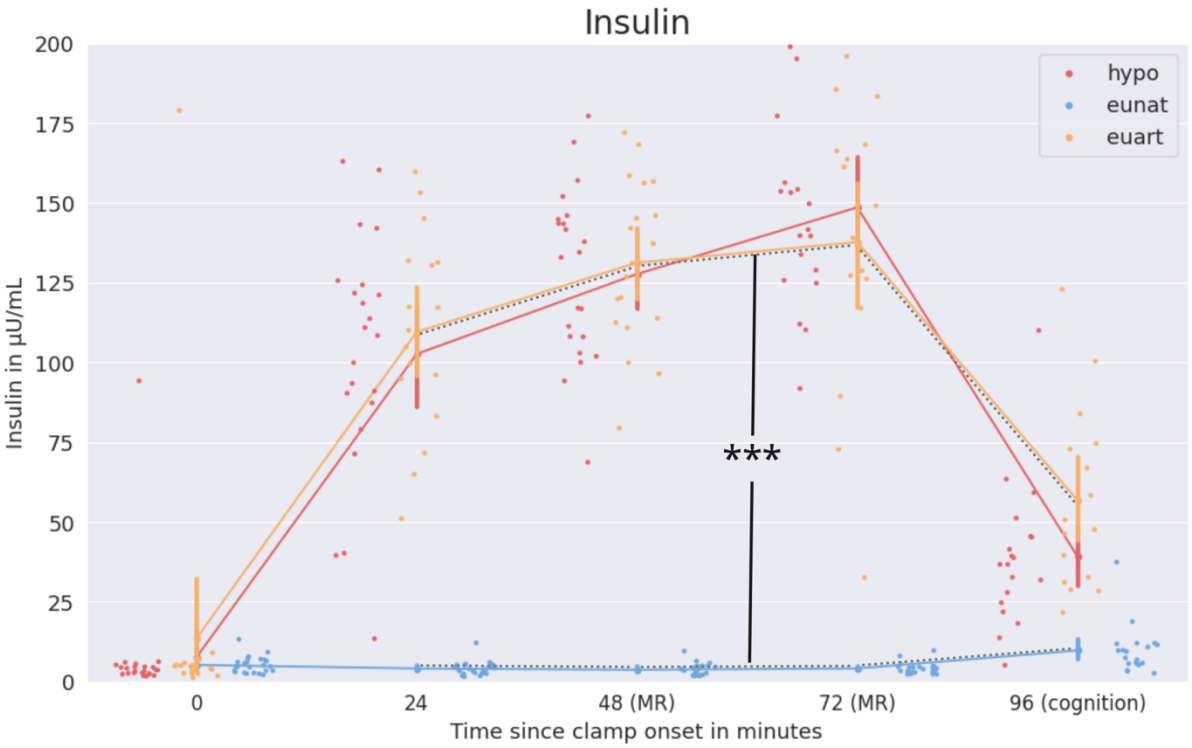

Figure S6. Insulin levels across the experiment per condition. As expected, insulin was significantly higher in eu_{art} than eu_{nat} after clamp start ($p<0.001$). §

Table S3

Results of the linear model predicting CMR_{O2} in the main group.

Fixed effect	Estimate µmol/100g/min	95% CI	p-value
(Intercept)	130.58	121.99 – 139.13	<0.001***
Condition[eunat]	-3.34	-10.49 – 3.79	0.35
Condition[hypo]	-0.73	-8.08 – 6.62	0.84
network[Cont]	19.76	16.26 – 23.26	<0.001***
network[Default]	15.23	12.16 – 18.29	<0.001***
network[DorsAttn]	1.58	-2.03 – 5.18	0.39
network[SalVentAttn]	-9.42	-13.01 – -5.83	<0.001***
yeo_nw[SomMot]	-6.19	-9.35 – -3.02	<0.001***
Condition[eunat]:network[Cont]	0.35	-4.30 – 4.99	0.88
Condition[hypo]:network[Cont]	-0.43	-5.16 – 4.30	0.86
Condition[eunat]:network[Default]	1.39	-2.68 – 5.45	0.50
Condition[hypo]:network[Default]	2.51	-1.63 – 6.65	0.23
Condition[eunat]:network[DorsAttn]	3.14	-1.65 – 7.93	0.20
Condition[hypo]:network[DorsAttn]	-1.76	-6.63 – 3.12	0.48
Condition[eunat]:network[SalVentAttn]	0.94	-3.82 – 5.70	0.70
Condition[hypo]:network[SalVentAttn]	0.23	-4.62 – 5.08	0.93
Condition[eunat]:yeo_nw[SomMot]	1.86	-2.34 – 6.07	0.39
Condition[hypo]: network[SomMot]	0.20	-4.08 – 4.49	0.93

Note. Result parameters for the main group of the following model: CMR_{O2} ~ condition*network + (1|subject/condition). Marginal R^2 / conditional R^2 = 5.33% / 22.51%. Network abbreviations: Cont ≙ Control; Default ≙ Default mode; DorsAttn ≙ Dorsal attention; SalVentAttn ≙ Salience; SomMot ≙ Somatomotor. Significant codes: <0.001: ***; <0.01: **, <0.05: *. Analyses were performed in native space.

Table S4

Results of the linear model predicting CMR_{O2} in the subgroup.

Fixed effect	**Estimate** µmol/100g/min	**95% CI**	**p-value**
(Intercept)	130.29	121.17 – 139.35	<0.001***
Condition[eunat]	-0.67	-7.60 – 6.92	0.93
Condition[hypo]	-0.67	-11.60 – 10.25	0.90
network[Cont]	19.76	16.24 – 23.27	<0.001***
network[Default]	15.23	12.15 – 18.30	<0.001***
network[DorsAttn]	1.58	-2.05 – 5.20	0.39
network[SalVentAttn]	-9.42	-13.02 – -5.82	<0.001***
yeo_nw[SomMot]	-6.19	-9.37 – -3.01	<0.001***
Condition[eunat]:network[Cont]	-2.23	-7.14 – 2.69	0.37
Condition[hypo]:network[Cont]	2.36	-4.39 – 9.12	0.49
Condition[eunat]:network[Default]	-0.82	-5.12 – 3.47	0.71
Condition[hypo]:network[Default]	5.91	-0.01 – 11.83	0.05
Condition[eunat]:network[DorsAttn]	1.02	-4.04 – 6.08	0.69
Condition[hypo]:network[DorsAttn]	0.17	-6.81 – 7.15	0.96
Condition[eunat]:network[SalVentAttn]	-2.43	-7.46 – 2.60	0.34
Condition[hypo]:network[SalVentAttn]	0.43	-6.51 – 7.37	0.90
Condition[eunat]:yeo_nw[SomMot]	-2.00	-6.44 – 2.44	0.38
Condition[hypo]: network[SomMot]	2.85	-3.28 – 8.97	0.36

Note. Result parameters for the subgroup of the following model: CMR_{O2} ~ condition*network + (1|subject/condition). Marginal R^2 / conditional R^2 = 5.49% / 22.26%. Network abbreviations: Cont ≙ Control; Default ≙ Default mode; DorsAttn ≙ Dorsal attention; SalVentAttn ≙ Salience; SomMot ≙ Somatomotor. Significant codes: <0.001: ***; <0.01: **, <0.05: *. Analyses were performed in native space.

Table S5

Results of the linear model predicting CBF in the main group.

Fixed effect	Estimate ml/100g/min	95% CI	p-value
(Intercept)	43.56	40.27 – 46.87	<0.001***
Condition[eunat]	-1.23	-4.23 – 1.80	0.42
Condition[hypo]	0.33	-2.74 – 3.56	0.83
network[Cont]	14.50	13.67 – 15.34	<0.001***
network[Default]	10.11	9.38 – 10.84	<0.001***
network[DorsAttn]	8.31	7.45 – 9.17	<0.001***
network[SalVentAttn]	8.97	8.11 – 9.83	<0.001***
yeo_nw[SomMot]	8.25	7.49 – 9.01	<0.001***
Condition[eunat]:network[Cont]	0.75	-0.36 – 1.85	0.18
Condition[hypo]:network[Cont]	2.29	1.16 – 3.41	<0.001***
Condition[eunat]:network[Default]	0.74	-0.23 – 1.71	0.13
Condition[hypo]:network[Default]	1.94	0.95 – 2.92	<0.001***
Condition[eunat]:network[DorsAttn]	0.94	-0.21 – 2.08	0.11
Condition[hypo]:network[DorsAttn]	0.98	-0.19 – 2.14	0.10
Condition[eunat]:network[SalVentAttn]	0.34	0.79 – 1.48	0.55
Condition[hypo]:network[SalVentAttn]	1.20	0.04 – 2.35	0.04*
Condition[eunat]:yeo_nw[SomMot]	0.45	-0.56 – 1.45	0.38
Condition[hypo]: network[SomMot]	0.99	-0.28 – 2.02	0.06

Note. Result parameters for the main group of the following model: CBF ~ condition*network + (1|subject/condition). Marginal R^2 / conditional R^2 = 12.24% / 44.70%. Network abbreviations: Cont ≙ Control; Default ≙ Default mode; DorsAttn ≙ Dorsal attention; SalVentAttn ≙ Salience; SomMot ≙ Somatomotor. Significant codes: <0.001: ***; <0.01: **, <0.05: *. Analyses were performed in native space.

Table S6

Results of the linear model predicting CBF in the subgroup.

Fixed effect	**Estimate** ml/100g/min	**95% CI**	**p-value**
(Intercept)	43.08	39.83 – 46.33	<0.001***
Condition[eunat]	-0.64	-3.56 – 2.26	0.66
Condition[hypo]	3.12	-1.28 – 7.48	0.16
network[Cont]	14.50	13.65 – 15.35	<0.001***
network[Default]	10.11	9.37 – 10.85	<0.001***
network[DorsAttn]	8.31	7.43 – 9.19	<0.001***
network[SalVentAttn]	8.97	8.10 – 9.84	<0.001***
yeo_nw[SomMot]	8.25	7.48 – 9.02	<0.001***
Condition[eunat]:network[Cont]	-0.14	-1.33 – 1.04	0.81
Condition[hypo]:network[Cont]	4.79	3.15 – 6.42	<0.001***
Condition[eunat]:network[Default]	-0.04	-1.09 – 0.99	0.93
Condition[hypo]:network[Default]	3.89	2.46 – 5.33	<0.001***
Condition[eunat]:network[DorsAttn]	0.16	-1.06 – 1.39	0.79
Condition[hypo]:network[DorsAttn]	2.03	0.34 – 3.72	0.02*
Condition[eunat]:network[SalVentAttn]	-0.46	-1.68 – 0.76	0.46
Condition[hypo]:network[SalVentAttn]	1.93	0.25 – 3.61	0.02*
Condition[eunat]:yeo_nw[SomMot]	-0.70	-1.77 – 0.38	0.20
Condition[hypo]: network[SomMot]	1.63	0.15 – 3.12	0.03*

Note. Result parameters for the subgroup of the following model: CBF ~ condition*network + (1|subject/condition). Marginal R^2 / conditional R^2 = 14.05% / 42.27%. Network abbreviations: Cont ≙ Control; Default ≙ Default mode; DorsAttn ≙ Dorsal attention; SalVentAttn ≙ Salience; SomMot ≙ Somatomotor. Significant codes: <0.001: ***; <0.01: **, <0.05: *. Analyses were performed in native space.

Table S7

Results of the linear model predicting OEF in the main group.

Fixed effect	Estimate ratio	95% CI	p-value
(Intercept)	0.42	0.40 – 0.43	<0.001***
Condition[eunat]	-0.01	-0.02 – 0.00	0.17
Condition[hypo]	-0.01	-0.03 – 0.00	0.15
network[Cont]	-0.07	-0.07 – -0.06	<0.001***
network[Default]	-0.04	-0.05 – -0.03	<0.001***
network[DorsAttn]	-0.07	-0.07 – 0.06	<0.001***
network[SalVentAttn]	-0.10	-0.10 – -0.09	<0.001***
yeo_nw[SomMot]	-0.09	-0.09 – -0.08	<0.001***
Condition[eunat]:network[Cont]	0.00	-0.01 – 0.01	0.76
Condition[hypo]:network[Cont]	-0.01	-0.02 – 0.00	0.10
Condition[eunat]:network[Default]	0.00	-0.01 – 0.01	0.85
Condition[hypo]:network[Default]	0.00	-0.01 – 0.01	0.44
Condition[eunat]:network[DorsAttn]	0.00	-0.01 – 0.01	0.46
Condition[hypo]:network[DorsAttn]	-0.01	-0.02 – 0.00	0.19
Condition[eunat]:network[SalVentAttn]	0.00	-0.01 – 0.01	0.78
Condition[hypo]:network[SalVentAttn]	0.00	-0.01 – 0.01	0.51
Condition[eunat]:yeo_nw[SomMot]	0.01	0.00 – 0.02	0.21
Condition[hypo]: network[SomMot]	0.00	-0.01 – 0.01	0.90

Note. Result parameters for the main group of the following model: OEF ~ condition*network + (1|subject/condition). Marginal R^2 / conditional R^2 = 9.64% / 18.88%. Network abbreviations: Cont ≙ Control; Default ≙ Default mode; DorsAttn ≙ Dorsal attention; SalVentAttn ≙ Salience; SomMot ≙ Somatomotor. Significant codes: <0.001: ***; <0.01: **, <0.05: *. Analyses were performed in native space.

Table S8

Results of the linear model predicting OEF in the subgroup.

Fixed effect	Estimate ratio	95% CI	p-value
(Intercept)	0.42	0.40 – 0.44	<0.001***
Condition[eunat]	-0.01	-0.02 – 0.01	0.39
Condition[hypo]	-0.03	0.05 – -0.01	0.0016**
network[Cont]	-0.06	-0.07 – -0.06	<0.001***
network[Default]	-0.04	-0.05 – -0.03	<0.001***
network[DorsAttn]	-0.07	-0.07 – -0.06	<0.001***
network[SalVentAttn]	-0.10	-0.10 – -0.09	<0.001***
yeo_nw[SomMot]	-0.09	-0.09 – -0.08	<0.001***
Condition[eunat]:network[Cont]	0.00	-4.30 – 4.99	0.79
Condition[hypo]:network[Cont]	0.00	-0.01 – 0.01	0.24
Condition[eunat]:network[Default]	0.00	-0.02 – 0.01	0.94
Condition[hypo]:network[Default]	0.00	-0.01 – 0.01	0.87
Condition[eunat]:network[DorsAttn]	0.00	-0.01 – 0.01	0.70
Condition[hypo]:network[DorsAttn]	0.00	-0.01 – 0.01	0.77
Condition[eunat]:network[SalVentAttn]	0.00	-0.01 – 0.01	0.58
Condition[hypo]:network[SalVentAttn]	0.00	-0.02 – 0.01	0.46
Condition[eunat]:yeo_nw[SomMot]	0.00	-0.01 – 0.01	0.52
Condition[hypo]: network[SomMot]	0.01	0.00 – 0.02	0.10

Note. Result parameters for the subgroup of the following model: OEF ~ condition*network + (1|subject/condition). Marginal R^2 / conditional R^2 = 10.31 % / 20.70%. Network abbreviations: Cont ≙ Control; Default ≙ Default mode; DorsAttn ≙ Dorsal attention; SalVentAttn ≙ Salience; SomMot ≙ Somatomotor. Significant codes: <0.001: ***; <0.01: **, <0.05: *. Analyses were performed in native space.

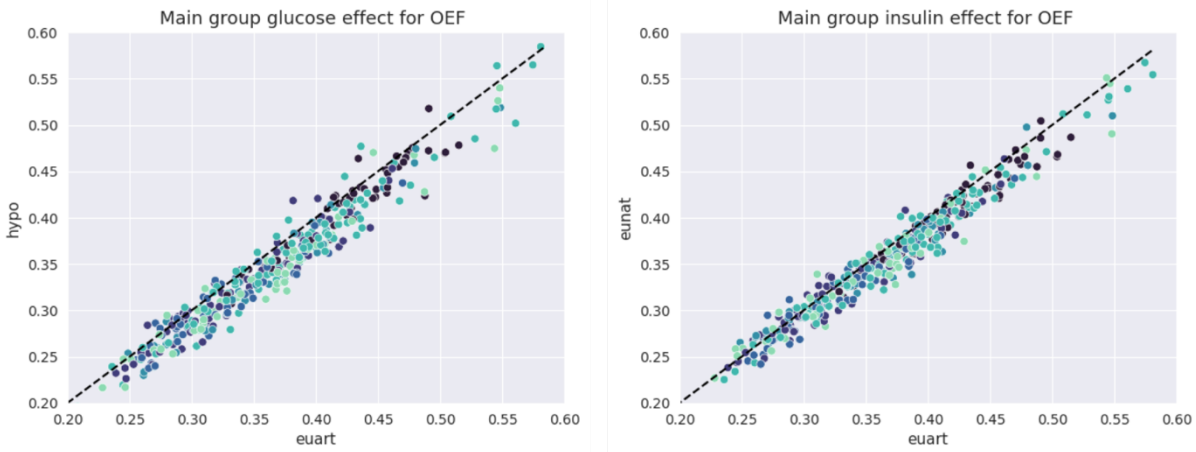

Figure S7. Glucose (left plot) and insulin (right plot) contrasts (main group) for OEF per brain network. Datapoints reflect parameter averages per ROI across subjects. The dashed line represents the angle bisector. OEF does seem to decrease in hypo, but only insignificantly. This effect could also be driven by an OEF increase in euart (see insulin plot on the right). None of the OEF contrasts in the main group were significant. Network abbreviations: Cont ≙ Control; Default ≙ Default mode; DorsAttn ≙ Dorsal attention; SalVentAttn ≙ Salience; SomMot ≙ Somatomotor. Analyses were performed in native space.

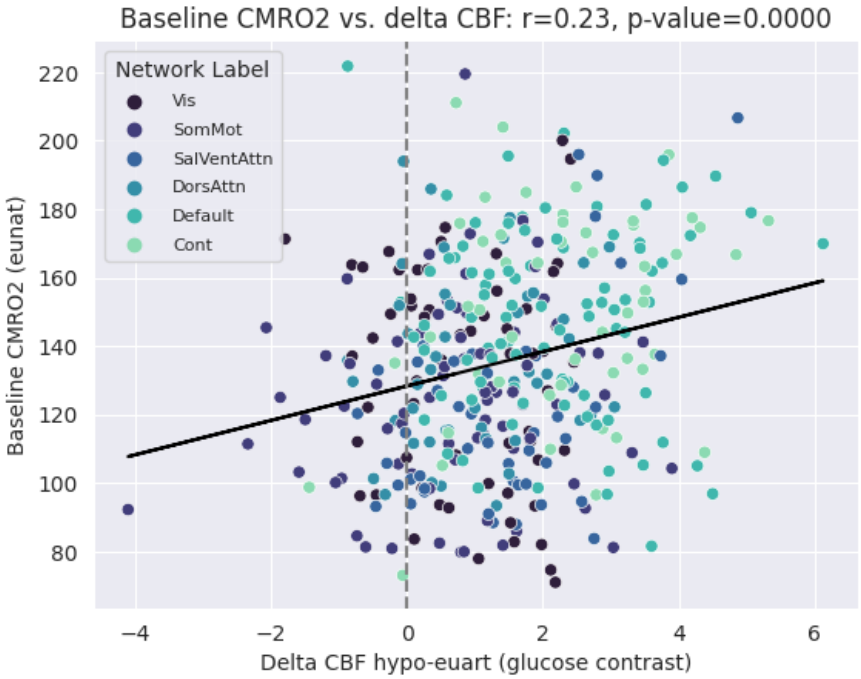

Figure S8. Correlations between baseline metabolism (CMRO2 in eunat) and CBF increase in the glucose contrast (hypo-euart) per ROI, color-coded per network. The black line represents the line of best fit. CBF increase in hypo correlates significantly and positively with baseline metabolism. Network abbreviations: Cont ≙ Control; Default ≙ Default mode; DorsAttn ≙ Dorsal attention; SalVentAttn ≙ Salience; SomMot ≙ Somatomotor. Analyses were performed in native space.

3 Manuscript II: Simultaneous quantification of oxygen and glucose consumption during visual stimulation in the human cortex

Antonia Bose[1,2] & Samira Maria Epp[1,2,7], Roman Belenya[1,2], Katarzyna Kurcyus[1], Eric Ceballos Dominguez[1], Andreas Ranft[3], Eliana Salas Villa[4], Moritz Bursche[1], Christine Preibisch[1], Gabriel Castrillón[1,6,7] & Valentin Riedl[1,7]

1 Department of Neuroradiology, Neuroimaging Center, Technical University of Munich, Munich, Germany

2 Graduate School of Systemic Neurosciences, Ludwig-Maximilians-Universität, Munich, Germany

3 Department of Anesthesiology and Intensive Care Medicine, Technical University of Munich, Germany

4 Department of Bioengineering, Universidad de Antioquia, Medellín, Colombia

6 Research Group in Medical Imaging, SURA Ayudas Diagnósticas, Medellín, Colombia

7 Department of Neuroradiology, Friedrich-Alexander-Universität, Erlangen, Germany

Abstract

The brain relies on oxidized glucose as its primary fuel. Despite robust coupling of cerebral oxygen and glucose consumption during rest, the oxygen to glucose index (OGI) has been suggested to drop significantly during neuronal activation. However, empirical evidence regarding the extent of this uncoupling is scarce, mainly due to the inability of previous studies to measure CMR_{O2} and CMR_{glc} concurrently during tasks. Therefore, in the present study, we integrated multiparametric quantitative BOLD (mqBOLD) with functional PET (fPET) to simultaneously quantify cerebral oxygen and glucose metabolism during visual stimulation and rest within a single scan. Results show increases in both CMR_{O2} and CMR_{glc} in visual areas, concomitant with focal blood flow increases. Moreover, OGI values during rest were close to the theoretical value of 6 which is in line with previous literature. In response to visual stimulation, the OGI decreased by 6.6-21.6%. For the first time, the present study demonstrates feasibility of combining mqBOLD and fPET to study CMR_{O2} and CMR_{glc} simultaneously. This setup has the potential to be applied to various experimental settings, providing valuable information about the extent of oxidative glucose metabolism in the human brain under different conditions in health and disease.

Introduction

The human brain, while accounting for only 2% of our body weight, consumes about 20% of our energy, making it one of the energetically most expensive organs relative to its mass (Padamsey & Rochefort, 2023). The brain predominantly relies on oxidized glucose as its fuel and thus, due to limited energy storage capacities, depends on a constant supply of oxygen and glucose. Typically, cerebral metabolic rates of oxygen and glucose (CMR_{O2} and CMR_{glc}, respectively) are tightly coupled, with 6 moles of oxygen required to fully oxidize 1 mole of glucose. This process of aerobic cellular respiration eventually generates 32 molecules of adenosine triphosphate (ATP), the universal currency for cellular energy. However, under certain conditions, the molar ratio between CMR_{O2} and CMR_{glc}, also known as the oxygen-to-glucose index (OGI), can deviate from its expected value of ~6 (Fox et al., 1988). An OGI of <6 indicates increased rates of nonoxidative glucose metabolism, where, instead of being further metabolized, glucose is converted into lactate, a process that produces only 2 ATP. Conversely, an OGI of >6 suggests the oxidation of energy substrates other than glucose, such as lactate or fatty acids, as observed during prolonged fasting (Kersten et al., 1999; Kolb et al., 2021; Pan et al., 2000). Generally, with oxygen and glucose being the primary fuels, understanding their dynamics is crucial for further insights into neuroenergetics. Therefore, in the present study, we integrated recent advances in functional neuroimaging, simultaneously acquiring multiparametric quantitative BOLD (mqBOLD) and functional ^{18}F-FDG-PET (fPET) data. This allowed us, for the first time, to measure CMR_{O2} and CMR_{glc} at the same time and under different conditions in one scanning session.

In previous studies, CMR_{O2} and CMR_{glc} were acquired separately in different sessions, typically using $^{15}O_2$-PET and ^{18}F-FDG-PET (Fox et al., 1988; Fox & Raichle, 1986; Leenders et al., 1990; Vafaee et al., 2012), impeding comparability across modalities, and thus potentially introducing inaccuracies in OGI calculation. While FDG-PET is still the gold standard to measure glucose metabolism, it typically involves a bolus injection of the radiotracer FDG prior to scan initiation, followed by a waiting period to enable FDG to distribute throughout the body and accumulate in cells. Thereby, conventional FDG-PET does not allow for dynamic imaging of glucose metabolism over time. If one were interested in alterations in glucose metabolism induced by interventions or tasks, one would need to acquire multiple PET scans on separate days, increasing the amount of radiation exposure for patients, as well as financial and time investments. Additionally,

inter-session variations can cause inaccuracies in result interpretation. More recently, researchers have developed functional FDG-PET (fPET), involving a bolus administration followed by a continuous infusion of the radiotracer instead of a single bolus injection (Hahn et al., 2016; Jamadar et al., 2019; Rischka et al., 2018; Villien et al., 2014). The constant infusion maintains a steady-state level of tracer in the bloodstream, allowing for dynamic imaging of glucose metabolism over time. In this way, fPET enables the measurement of multiple conditions within a single scanning session, as successfully applied in previous studies (Hahn et al., 2016, 2017; Jamadar et al., 2021; Villien et al., 2014).

Originally, CMR_{O2} was measured via $^{15}O_2$-PET (Mintun et al., 1984), involving inhalation of $^{15}O_2$-labeled gas and the injection of $[^{15}O]H_2O$ to cerebral blood volume (CBV), the oxygen extraction fraction (OEF) and cerebral blood flow (CBF) separately (Herscovitch et al., 1983; Raichle et al., 1983). CBF increases in response to heightened energy demand upon neuronal activation. This is called neurovascular coupling. However, the elevated CBF rate overcompensates for required nutrients, thereby ultimately reducing the relative amount of oxygen being extracted from the blood for the oxidation of energy substrates. Combining CBF and OEF, one can calculate CMR_{O2} in µmol/100g/min via Fick's principle (Fick, 1870):

$$CMR_{O2} = Ca_{O2} * CBF * OEF$$

where Ca_{O2} denotes the arterial oxygen content. However, $^{15}O_2$-PET has its drawbacks, such as a short radiotracer decay time of approximately two minutes. It thus requires multiple injections within a single session and consequently higher total tracer doses to ensure sufficient tracer availability for imaging. Moreover, again, this method would not allow for multiple conditions to be scanned within one session, let alone to be simultaneously employed with FDG-fPET. Using hybrid PET-MR scanners, however, fPET can be combined with MR techniques for CMR_{O2} measurements. In this context, calibrated BOLD imaging, an MRI technique involving gas challenges (hypoxia/hypercapnia) and CBF acquisition, has been used to measure CMR_{O2} (Kim et al., 1999). Calibrated BOLD experiments do, however, not measure CBV directly, but estimate it from CBF, which has been found to be an important confounding variable (Blockley et al., 2013; Liu et al.,

2019). Moreover, these experiments follow a complex setup involving air masks for the application of gas challenges.

An alternative approach is multiparametric quantitative BOLD (mqBOLD) imaging, which involves separate measurements of the transverse relaxation rate R2' and CBV that can be combined into a more direct assessment of the OEF, as well as the measurement of CBF (Christen et al., 2012; Hirsch et al., 2014; Kaczmarz et al., 2020). A more detailed description on mqBOLD acquisition and data processing will be provided below. The advancement of mqBOLD avoids previous limitations of both calibrated BOLD imaging as well as $^{15}O_2$-PET. In the present study, we combined mqBOLD with the aforementioned advances in fPET to simultaneously quantify oxygen and glucose metabolism under different conditions in one single scanning session.

Given the methodological focus of this study, we chose a visual stimulation task contrasted with a rest condition to validate our approach. During rest, CMR_{O2} and CMR_{glc} are robustly coupled, with studies reporting an OGI close to the theoretical value of 6 (Blazey, Snyder, Goyal, et al., 2018; Hyder et al., 2016; Shulman et al., 2001). In response to increased energy demand during visual stimulation, CBF typically increases in the visual cortex (Attwell et al., 2010; Attwell & Iadecola, 2002), enhancing the supply of glucose and oxygen to active regions. Accordingly, early PET studies noted a CBF increase of ~50% (Fox et al., 1988). However, while CMR_{glc} showed similar increases, reported CMR_{O2} increases were substantially smaller (~5%), resulting in an OGI of 0.4 during visual stimulation in one study (Fox et al., 1988). This uncoupling between CMR_{O2} and CMR_{glc} suggests that, despite sufficient oxygen availability, not all of the additionally delivered glucose is oxidized to produce 32 ATP. Instead, some glucose is converted to lactate, thereby producing merely 2 ATP per mole of glucose. The underlying mechanisms of this preference for lactate fermentation over oxidative phosphorylation are not fully understood. One theory is that lactate fermentation is faster (Pfeiffer, 2001). Consequently, despite it only generating 2 ATP per mole of glucose, it might eventually be more efficient and better suited for supporting rapid bursts of activity in neurons. In their study, Fox et al. (1988) further demonstrate that, despite significant increases in CBF and CMR_{glc} of ~50%, the disproportionately smaller increase in CMR_{O2} results in a mere increase of 8% in ATP production during visual stimulation. Thereby, they underline the importance of considering both oxygen and glucose dynamics, as reliance on just one parameter may not yield sufficient information about alterations in ATP production. It

remains unclear whether the drop in OGI is as substantial as described by Fox et al. (1988), though. Calibrated BOLD studies found larger increases in CMR_{O2} in response to visual stimulation, ranging from 12-30% (Davis et al., 1998; Donahue et al., 2009; Fujita et al., 2006; Hoge & Pike, 2001; Kim et al., 1999). One study even reported a 15.1% increase alongside a 21.4% rise in CBF (Germuska et al., 2019), resulting in a $\Delta CBF:\Delta CMR_{O2}$ ratio of 1.42, contrasted to previously found ratio of 10 (Fox et al., 1988). Moreover, other studies reported a lower increase in CMR_{glc}, ranging from 22-28% (W. Chen et al., 1993; Newberg et al., 2005; Vlassenko et al., 2006) instead of previously reported ~50% (Fox et al., 1988). Evidently, there is huge variance in past results. None of these studies, however, measured changes in CMR_{O2} and CMR_{glc} concurrently. To accurately evaluate OGI alterations in response to increased neuronal activity, it is crucial to acquire within-subject data on glucose and oxygen changes at the same time and within a single session.

Despite remaining questions regarding the exact extent to which CMR_{O2} and CMR_{glc} are uncoupled during neuronal activation, in the present study we still expect larger increases in CMR_{glc} than CMR_{O2} in response to visual stimulation. We assume that these increases will be accompanied by an increase in CBF. With this study we aim to demonstrate the simultaneous applicability of mqBOLD and fPET, thereby fully quantifying CMR_{O2} and CMR_{glc} at the same time. Additionally, we aim to provide further insights into OGI alterations during neuronal activation.

Methods

Participants

A total of 25 healthy, right-handed participants was recruited for this study. Four subjects had to be excluded entirely, two due to artifacts in anatomical images (most likely due to signals from the camera, see below), and one each due to large motion artifacts, and errors in accurately timing the onset of visual stimulation, scanning and tracer injections. Moreover, we had to discard five MR datasets due to image artifacts, mainly in T2* data. This resulted in a final MR sample size of 16 (mean age: 37 years ±11.32; 9 females, 7 males). Four participants were excluded from PET analyses: one due to difficulties in arterial sampling and three due to insufficient FDG doses. This resulted in a final PET sample size of 17 (mean age: 33.29 years ±9.79; 9 females, 8 males). 13

participants overlapped, contributing both MR and PET data to the final analyses. The study was approved by the ethics board of the university hospital of the Technical University of Munich and all participants gave written informed consent prior to study initiation.

Experimental protocol

Participants arrived at the study site following an overnight fast. After measuring baseline parameters (body weight, baseline blood glucose, blood pressure, arterial oxygen saturation), an anesthesiologist placed two catheters: an intravenous catheter in the participant's left forearm for the administration of the radiotracer and contrast agent, and an arterial catheter in the right radial artery for arterial blood sampling. Prior to scanning, venous blood samples were collected and sent to the in-house clinical chemistry laboratory for analysis of creatinine and hematocrit values, both required for the mqBOLD analysis. Subjects were then transferred into the scanner and imaging data acquisition was initiated. A detailed description of image acquisition parameters can be found below. During PET-MR scanning, the subject was presented with blocks of full-field visual stimulation (STIM, checkerboard moving with 8Hz), alternating with resting-state blocks (REST, white fixation cross on black background) at approximately 6-minute intervals. PET scanning, visual presentation and the radiotracer infusion pump (Harvard Apparatus, Cambridge, Massachusetts, United States) were started simultaneously. For the ^{18}F-FDG, participants received a decay-corrected total dose of 3.6 MBq per kg body weight. 20% of the total syringe volume were injected as a bolus (flow rate: 1ml/s) to increase signal-to-noise ratio (SNR) (Rischka et al., 2018). The remaining 80% were infused continuously over the total PET duration of 70 minutes (flow rate: 0.2ml/min). Throughout these 70 minutes, arterial blood was sampled continuously via a Twilite blood sampling system (Swisstrace, Zurich, Switzerland). It was crucial for participants to keep their eyes open during the entire experiment, as previous studies showed significant reductions in metabolic activity in the visual cortex under closed eyes compared to open eyes (Uludağ et al., 2004). Given the rather tedious nature of the tasks, we installed a camera (MRC Systems GmbH, Heidelberg, Germany) on top of the head coil to closely monitor participants' wakefulness. Figure 1A shows a schematic depiction of the experimental protocol.

Image acquisition

All data were acquired on a 3T Biograph PET-MR scanner (Siemens, Erlangen, Germany), using a 12-channel phase-array head neck coil. Anatomical images served anatomical reference and exclusion of brain lesions. This included a T1-weighted 3D MPRAGE pre- and post-gadolinium (TI=900 ms, TR=2300 ms, TE=2.98 ms, α=9°; 160 slices, voxel size: 1.0x1.0x1.0 mm^3; acquisition time: 5:03 minutes) and a T2-weighted 3D fluid-attenuated inversion recovery (FLAIR) image (TR = 5000 ms; TE = 394 ms, α=40°; 140 slices, voxel size: 0.5x0.5x1 mm^3 EPI factor: 130, acquisition time: 3:27 minutes).

mqBOLD

The mqBOLD (Christen et al., 2012, p. 0; Hirsch et al., 2014; Kaczmarz et al., 2020) protocol consisted of the following MR sequences:

- T2: 6:16 min 2D Turbo spin echo acquired only in REST (8 echoes, TE1 = ΔTE = 16 ms, TR=4870 ms, α=90°, voxel size 2x2x3 mm^3, 36 slices).
- T2* (Hirsch et al., 2014; Kaczmarz et al., 2020): 7:32 min multi-echo gradient-echo mapping acquired in STIM and REST (12 echoes, TE1 = 6ms, ΔTE = 5 ms, TR=2340 ms, α=30°, voxel size 2x2x3 mm^3, gap 0.3 mm, 36 slices (32 slices in one subject); 1 concatenation (4 concatenations in one subject)). The images were corrected for magnetic background gradients with a standard exponential excitation pulse (Baudrexel et al., 2009; Hirsch & Preibisch, 2013) half-resolution data acquisition of the k-space center (Nöth et al., 2014).
- ASL (Alsop et al., 2015): 5:09 min pseudo-continuous arterial spin labelling (pCASL) acquired in STIM and REST (post-labeling delay (PLD): 1800 ms, label duration: 1800 ms, 4 background suppression pulses, 2D EPI readout, TE=22.12 ms, TR=4600 ms, α=180°, 24 slices, EPI factor: 31, acquisition voxel size: 3x3x6.6 mm^3, gap: 0.6 mm, 30 dynamic scans, including a proton density weighted M0 scan).
- Dynamic susceptibility contrast (DSC) (Hedderich et al., 2019): 2.38 min single-shot GRE-EPI acquired after the injection of a gadolinium-based contrast agent (CA) as a bolus after 5 dynamic scans in both conditions (EPI factor: 128, 80 dynamic scans, TE=40 ms, TR=1890 ms, α=70°, acquisition voxel size: 2x2x3.5 mm^3, 27 slices (26 slices in one subject)) Dosage: 0.2ml/kg body weight, split into two injections of 0.1ml/kg body weight (min. 6ml, max. 8ml) for two conditions

(for the first five subjects only in REST). Flow rate: 4ml/s, plus 20 ml NaCl. Prior to CA administration, healthy kidney function was ensured. The CA was only injected at creatinine levels of ≤ 1.2mg/dl.

fMRI

We also acquired a 4:08min BOLD fMRI task-localizer using single-shot EPI (EPI factor: 64, voxel size = 3.0x3.0.3.0 mm^3, FOV: 192x192x192mm^3, TE=30 ms, TR=2.0 s, α=90°, 120 dynamic scans plus 2 dummy scans, 36 slices, interleaved acquisition together with a 0:54 min B0 field mapping scan (2 echoes, TR=400 ms, TE1=4.92 ms,TE2=7.38 ms, α=60°, voxel size: 3x3x3 mm^3, 36 slices, interleaved acquisition).

Data processing & statistical analyses

mqBOLD processing and CMR_{O2} calculation

Quantitative MR parameter maps were calculated with in-house scripts, using MATLAB and SPM12 (Wellcome Trust Centre for Human Neuroimaging, UCL, London, UK). Quantitative T2 and T2* maps were obtained by mono-exponential fits of the multi-echo spin and gradient echo data (Hirsch et al., 2014; Kaczmarz et al., 2020; Preibisch et al., 2008). Corrections were performed for macroscopic magnetic background fields (Hirsch & Preibisch, 2013) and motion using redundant acquisitions of k-space center (Nöth et al., 2014). R2', the transverse, reversible relaxation rate, was calculated via

$$R2' = \frac{1}{T2*} - \frac{1}{T2}$$

R2' depends on the vascular deoxygenated hemoglobin (deoxy-Hb) content (Blockley et al., 2013, 2015; Bright et al., 2019). However, confounds from uncorrectable strong magnetic field inhomogeneities at air-tissue boundaries, iron deposition in deep grey matter (GM) as well as white matter structures needed to be considered (Hirsch & Preibisch, 2013; Kaczmarz et al., 2020). The cerebral blood volume (CBV) was derived from DSC maps via full integration of leakage-corrected ΔR2*-curves (Boxermann, J.L., Schmainda, K.M., Weisskoff, R.M., 2006) and normalization to a white matter value of

2.5% (Hedderich et al., 2019; Kluge et al., 2016; Leenders et al., 1990). Combining CBV and R2' subsequently yielded the OEF via

$$OEF = \frac{R2'}{c \cdot CBV}$$

(Christen et al., 2012; Hirsch et al., 2014; Yablonskiy & Haacke, 1994), where $c = \gamma \cdot \frac{4}{3} \cdot \pi \cdot \Delta\chi 0 \cdot hct \cdot B0$, the gyromagnetic ration $\gamma = 2.675 \cdot 10^8\ s^{-1}\ T^{-1}$, the susceptibility difference between fully deoxygenated and oxygenated hemoglobin $\Delta\chi_0 = 0.264 \cdot 10^{-6}$, the magnetic field strength B0 = 3T and the small-vessel hematocrit hct, which was estimated as 85% of subject-specific (large-vessel) hematocrit levels (Eichling et al., 1975; Hirsch et al., 2014). CBF maps were obtained from pCASL data as in Alsop et al. (2015) to calculate CBF from averaged, pairwise differences of motion-corrected label and control images and a proton-density weighted image. Finally, for each subject and condition, we calculated the voxelwise CMR_{O2} by combining all parameter maps via Fick's principle (Fick, 1870):

$$CMR_{O2} = OEF \cdot CBF \cdot Ca_{O2}$$

where Ca_{O2} is the arterial oxygen content, calculated as $Ca_{O2} = 0.334 \cdot hct \cdot 55.6 \cdot O2sat$, with O2sat being the arterial oxygen saturation measured by pulse oximetry and hct the subject-specific hematocrit value (Bright et al., 2019; Ma et al., 2020). All parameter maps of each individual subject were registered to the first echo of their respective multi echo T2 data. Figure 1E summarizes calculation steps and shows examples of parameter maps in native space.

Case-specific adjustments. For some subjects, we had to make specific adjustments due to missing data. For three subjects, we acquired T2* data only in full resolution instead of additional acquisitions in half-resolution for motion correction. This affected the T2* value range, resulting in values that were too low. These subjects' T2* parameter maps were consequently upscaled so that their GM median matched that of the other 13 mqBOLD subjects. Results are based on the upscaled T2* maps. For five subjects, we only acquired one DSC in REST. For them, we estimated their respective CBV maps in STIM based subject-averaged CBV increases from the rest of the cohort (n=11).

Venous versus arterial CBV increases. CBV measurements based on the intravascular injection of contrast agents measure total CBV, including arterial as well as venous blood volume within each voxel (Hua et al., 2019). For stimuli shorter than 40s, CBV increases may be ignored due to the passive, slow increase of venous CBV (Simon & Buxton, 2015). However, for prolonged stimulation, as applied in the present study, venous CBV increase only accounts for 29% (Huber et al., 2014) to 50% (Kim & Ogawa, 2012) of total CBV increase. Thus, considering total CBV increase might underestimate CMR_{O2} changes, specifically during visual or somatosensory stimulation, where large total CBV increases are usually observed. As our visual stimulation persisted over a few minutes, we measured changes in CBV by acquiring two DSC scans, one per condition. DSC is a measure of total CBV, therefore, we calculated CMR_{O2} group results assuming 30% of total CBV changes being venous, based on results on 7T during visual stimulation in human subjects (Huber et al., 2014).

Artifacts and GM masking. To exclude voxels from brain areas affected by artifacts, we calculated the temporal signal-to-noise ratio (tSNR) from fMRI BOLD images per subject and voxel in standard 2mm MNI space. Voxels in the lowest 15th percentile across more than 66% of participants were masked out, primarily localized in susceptibility-prone regions, like fronto- and temporo-basal areas. Additionally, we masked out the cerebellum and considered only voxels with a GM probability >0.5. The resulting SNR-GM mask in standard space was applied to the input matrices for partial least squares analyses.

For native space analyses, we further masked out areas influenced by cerebrospinal fluid (T2>150ms), susceptibility artifacts (R2'>11 s^{-1}), voxels with elevated blood volume (CBV>12%, probably driven by large vessels) and voxels with physiologically unexpected values (T2*>90ms, OEF>1, CBF>120). These masking parameters were applied for calculations of baseline parameters (see Table 1). Here, per imaging parameter, we calculated a whole-brain median across voxels per subject in native space and subsequently computed the mean and standard deviation. Similarly, for calculations of delta and percent change values, we computed median values across voxels within the respective ROI mask (see Table 2 and Figure 2), with all thresholds applied in native space as previously described and subsequently normalized to standard space. We then took the mean and standard deviation across subjects. Delta and percent change were calculated per subject as the within-ROI median STIM value minus within-

ROI median REST value (and divided by median REST for percent change values). These values are shown in Table 2.

PET processing and CMR_{glc} calculation

For PET data processing, we reconstructed the raw long-listmode data offline, using the ordered subsets expectation maximization (OSEM) algorithm. The data were divided into 93 frames of 45 seconds each, with an additional frame of 15 seconds at the end (matrix: 344, 3D iterative reconstruction method, zoom: 2.0, filter: allpass, iterations: 4, subsets: 21, scatter correction: relative). Subsequently, the reconstructed PET images were motion corrected, spatially smoothed (Gaussian filter, FWHM = 6 mm) and low-pass filtered (360s).

For CMR_{glc} calculation, subject specific arterial input functions (AIF) were derived from arterial blood data. Preprocessing was performed with in-house Python scripts (Python Software Foundation, version 3.8). Initially, we estimated the blood delay by determining the time between injection start and peak in the blood data. Next, background radioactivity was estimated and the blood TAC were modelled by fitting a sum of three exponential functions to the raw blood data (Feng et al., 1993). Blood TAC were then converted to plasma TAC, using the reference FDG plasma-to-blood ratio function (Phelps et al., 1979) along with subject-specific hematocrit values. For two subjects with erroneous arterial blood sampling, we calculated a population-based AIF by averaging across remaining participants' AIFs, as previously described (Castrillon et al., 2023; Vriens et al., 2009). Addressing the delay of measurable FDG uptake, we shifted the task onsets by two minutes as recommended by previous literature (Stiernman et al., 2021). Subsequently, we calculated CMR_{glc} separately for STIM and REST by dividing the PET time-series data into four REST and four STIM periods. We calculated the net uptake rate constant (Ki) using the Patlak plot model (Patlak & Blasberg, 1985) based on (shifted) STIM and REST frames of the preprocessed PET images and the individual, preprocessed, AIF. Next, we calculated voxel-wise CMR_{glc} separately for each STIM and REST period by multiplying the Ki map with the plasma glucose concentration value of each subject, multiplied by 100 to get values per 100g, and then divided it by a lumped constant of 0.65 (Wu, 2003). Finally, the average CMR_{glc} maps across all four STIM and REST blocks were calculated and normalized to standard 2mm MNI (Montreal Neurological Institute, McGill University) space via the mean PET and anatomical images.

Oxygen-to-glucose index (OGI)

The oxygen-to-glucose index is an indicator for the underlying mechanisms of energy metabolism. In aerobic cellular respiration, 6 moles of oxygen are required to fully oxidize 1 mole of glucose, finally yielding 32 ATP (Byrne et al., 2014). Consequently, the OGI in aerobic cellular respiration amounts to 6. An OGI of >6 indicates the oxidation of other substrates than glucose for ATP production (e.g. lactate, fatty acids), while an OGI of <6 suggests non-oxidative glucose metabolism, hence glucose being converted to lactate, yielding 2 ATP. Here, the OGI was calculated voxelwise as

$$\mathrm{OGI} = \frac{\mathrm{CMRO2}}{\mathrm{CMRglc}}$$

in native space per subject and condition. We thresholded all OGI maps as suggested by previous literature (Blazey, Snyder, Su, et al., 2018). To this end, we took the median GM OGI (median=5.02), calculated the median absolute deviation (MAD=2.41) and subsequently thresholded the maps at GM median + 5*MAD = 17.07. Subsequently, the OGI maps were registered into standard space (interpolation method: nearest neighbor), where we calculated the mean OGI across all GM voxels within the respective group masks (see Figure 3A) per subject and condition. For functional network comparisons (see Figure 3B, we took the mean OGI across GM voxels within the respective network in native space, per subject. The limbic network was excluded due to its proneness to susceptibility artifacts. OGI comparisons between conditions (see Figure 3A) or networks (see Figure 3B) were conducted using paired t-tests, correcting for multiple comparisons (FDR-corrected for 15 tests in Figure 3B).

fMRI BOLD processing and task analysis

The BOLD fMRI localizer data was preprocessed using fMRIPrep 20.2.4 (Esteban, 2019) in a docker container, based on Nipype 1.6.1 (Gorgolewski et al., 2011). This included segmentation, estimation of motion parameters and other confounds, susceptibility distortion correction, coregistration in native T1w space and normalization to MNI152 ICBM 2mm Non-linear 6th Generation Asymmetric Average Brain Stereotaxic Registration Model (Montreal Neurological Institute, McGill University). fMRIPrep utilizes FSL 5.0.9 (Jenkinson et al., 2012; Smith et al., 2004) boundary-based registration (BBR)

to register BOLD fMRI EPI time series data to T1w data, FSL FAST for brain tissue segmentation and ANTs 2.3.3 for spatial normalization to standard space (Avants et al., 2008), a multiscale, mutual-information based, nonlinear registration, concatenating all transforms and applying all registration steps at once. This final normalization matrix was then also applied to all quantitative mqBOLD parameter maps, after 6-dof (degrees of freedom) coregistration to native T1w space, to transform all images to MNI 2mm standard space. Further, task analysis was done following recent recommendations (Esteban et al., 2020), setting up a general linear model (GLM) with CSF and white-matter signal, dvars, framewise-displacement and translations and rotations in x-, y- and z-axis as confounds, high-pass filter of 120s and 6mm smoothing. For analyses based on native GLM masks, we used individual 1st level z-maps, z>3.1.

Partial least squares analysis

To detect differences between STIM and REST in our parameter maps, we ran partial least squares (PLS) analyses, using the Python pyls library (Python Software Foundation, version 3.8). Mean-centered PLS is a data-reduction method that computes latent variables and corresponding brain patterns, which optimally relate brain signals to experimental design factors, such as groups or conditions (McIntosh & Lobaugh, 2004). In the present study, the input data matrix consisted of one row per subject containing all voxels within the SNR-GM-mask in standard 2mm space, and stacked STIM and REST conditions. For BOLD fMRI data, median values of percent signal change (relative to the median REST value) across 20 seconds (10 TRs) per task condition were used, with the initial 10 seconds per task block excluded to account for the hemodynamic response lag. For non-quantitative PET data, median values of percent signal change (relative to the median REST value) across the entire duration of the condition blocks were used, but shifted by 6 TRs to ensure that 'peaks' and 'valleys' in the time-course did not cancel out during median calculation. For quantitative data, OEF, CBF, CMR_{O2} or CMR_{glc} values per voxel and subject were used and stacked for both REST and STIM conditions. Using a dummy-coding matrix, the pyls library computes within-condition averages, mean-centering them columnwise (Krishnan et al., 2011). The resulting matrix, Rmean-centered (q x p), comprising q conditions and p voxels, is then subjected to singular value decomposition. This results in:

$$R'_{\text{mean-centered}} = USV'$$

$U_{p \times q}$ are the voxel weights (brain saliences), one row per latent variable (LV) i which reflects how much this voxel contributes to the effect captured by LV_i. $V_{q \times q}$ are the task saliences (one row per LV) that indicate how each condition contributes to the spatial pattern identified by LV_i. $S_{q \times q}$ are the singular values per LV that reflect the strength of the relationship extracted by LV_i (McIntosh & Mišić, 2013). The significance of the latent variables, i.e., the entire multivariate pattern, is tested via permutation tests (here: 2000 permutations), the reliability of the brain saliences, i.e., the voxel's contribution to the latent variables, is deduced via bootstrap resampling (here: 2000 samples). Brain regions showing significant effects are identified via the ratio of the brain saliences to the bootstrap standard error (bootstrap ratio ≙ BSR), where a BSR >2/<-2 is analogical to a confidence interval of 95%, if the bootstrap distribution is normal (Krishnan et al., 2011; McIntosh & Mišić, 2013).

In the present paper, we performed PLS analyses on a group level to identify brain regions that differentiate between the STIM versus the REST condition. Application of the same analyses to BOLD fMRI, fPET and quantitative MR data enabled comparison across all modalities. Statistical maps were thresholded with a BSR of ±2 and only clusters with more than 30 voxels were included in the visual masks. For correct interpretation, BSR maps must be compared to the design scores (design variables multiplied by brain saliences) of each condition within each LV to yield the direction of task differences that is captured within the BSR pattern. In the present work, BSRs are depicted using a blue-red color gradient, with red indicating higher voxel values in STIM than in REST and, conversely, blue indicating higher voxel values in REST than in STIM.

Other statistical analyses

Most statistical analyses, except the ones in native space, were based on median voxel values within a group visual region of interest (ROI) in standard space, by taking the across-subjects median value per voxel in STIM and in REST. Delta values for OEF, CBF, CMR_{O2} and $CMR_{glc,}$ as shown in Table 2 and in the boxplots in Figure 2, were calculated for each voxel (STIM minus REST), and then averaged (median) across voxels within the respective ROI or mask per subject. Subsequently, we tested for significant differences in REST compared to STIM via paired-samples t-tests, across subjects. For native space

analyses, as shown in Figure 2, we calculated median values within each native-space activation ROI (output of the first level GLM, thresholded with z>3.1) per subject.

Results

In the present study, we integrated FDG-fPET with mqBOLD for simultaneous quantification of cerebral oxygen und glucose metabolism in healthy participants during a visual stimulation task, involving alternating blocks (~6 minutes) of a moving checkerboard (STIM) and fixation cross (REST) (Figure 1A). Due to neurovascular coupling, we expected to see increases in CBF and, consequently, reductions in OEF in visual regions in response to visual stimulation (see physiological model in Figure 1B). This is due to the large increase in CBF overcompensating the rise in oxygen consumption, resulting in a relative decrease in oxygen extraction. This mechanism is reflected in an increased BOLD signal. Similarly, we expected increases in both oxygen and glucose metabolism (CMR_{O2} and CMR_{glc}, respectively), albeit with less prominent increases in CMR_{O2}. This is based on previous literature demonstrating an uncoupling of cerebral oxygen and glucose metabolism during increased neuronal activation (Fox et al., 1988). Additionally, we acquired a BOLD fMRI task-localizer, consisting of eight 30-second task blocks, alternating between REST and STIM. Mean values at baseline of all quantitative parameter maps were in physiologically plausible ranges (see Table 1).

Table 1

Baseline (REST) values, mean (SD) across subjects, within GM.

R2' [1/s]	CBV [%]	OEF [ratio]	CBF [ml/100g/min]	CMRO2 [μmol/100g/min]	CMRglc [μmol/100g/min]
8.1 (2.2)	5.5 (0.3)	0.51 (0.17)	54.1 (8.9)	172.5 (30.7)	32.8 (6.4)

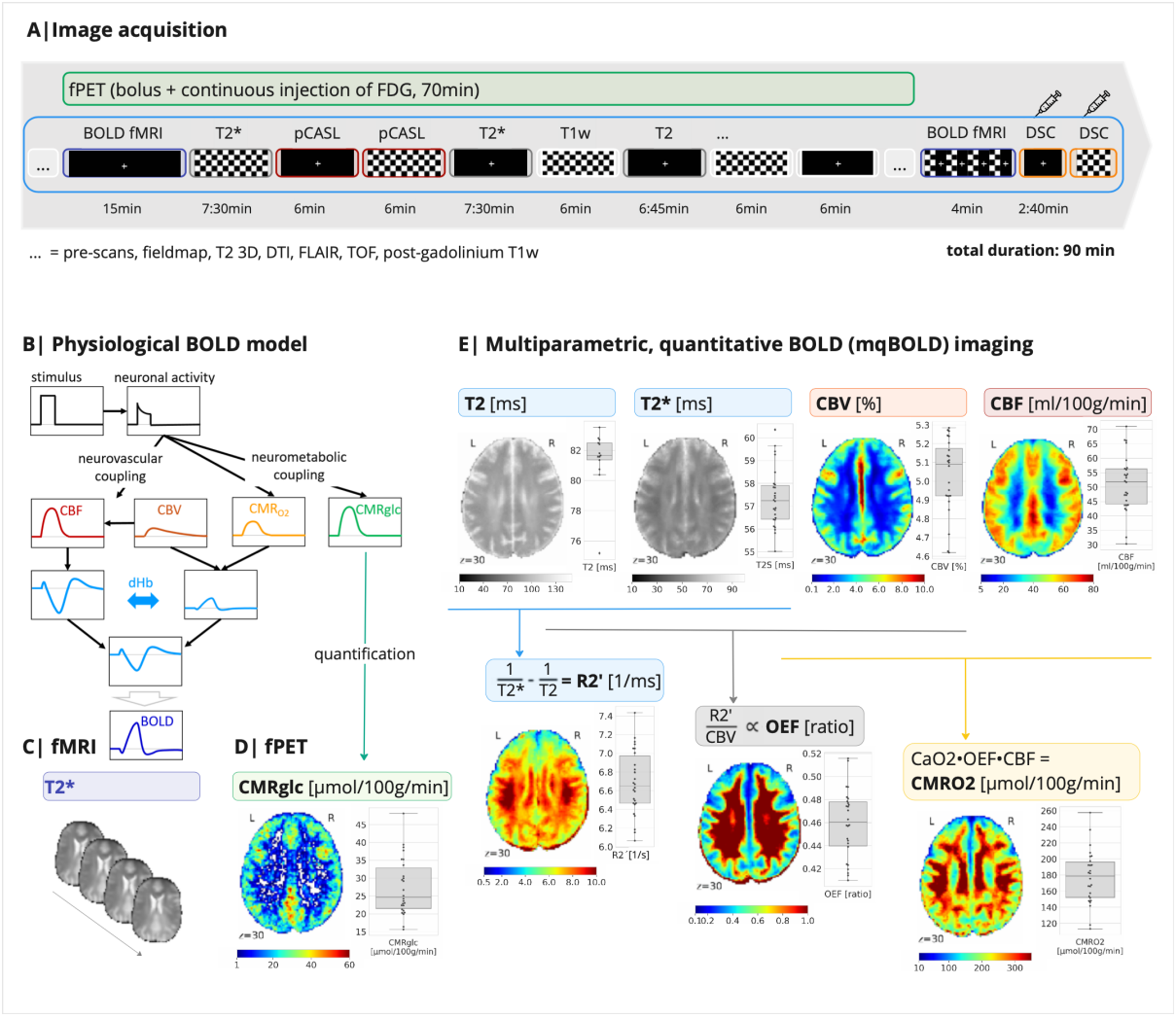

Figure 1. Data acquisition and underlying physiological parameters. **A.** Image acquisition protocol. PET and MR data were acquired simultaneously. Following the FDG bolus injection, the radiotracer was continuously infused at a constant rate throughout the entire duration of the PET scan (green box). Concurrent MR acquisition (blue box) included mqBOLD sequences. Participants were presented with alternating blocks of a moving checkerboard and a fixation cross. Finally, we acquired BOLD localizer data as well as the two DSC scans, involving the administration of a gadolinium-based contrast agent. The entire imaging protocol took approximately 90 minutes. **B & C.** The physiological BOLD model. Heightened neuronal activation results in an increase in energy demand. In response, CBF and CBV are increased, with large, overcompensating CBF increases eventually leading to a reduction in OEF and deoxy-Hb. The reductions in deoxy-Hb can be detected as changes in the BOLD signal. CMRO2 and CMRglc typically increase in response to neuronal activity, albeit to different extents. This relationship is known as neurometabolic coupling. **D.** The fPET signal, being independent of changes in oxygenation, reflects glucose consumption. Shown here is the CMRglc median map averaged across 17 participants in standard space. **E.** Multiparametric quantitative BOLD (mqBOLD). Quantification of transverse relaxation times T2 and T2*, combined with measurements of cerebral blood volume (CBV) and cerebral blood flow (CBF) allow for full quantification of CMRO2. Resulting parameter maps yield voxelwise CMRO2 values in µmol/100g/min. Using these calculation steps in the present study, we are able to quantify CMRO2 in REST and STIM. Axial slices show parameter maps in REST, averaged across 16 subjects in standard space, non-thresholded. Boxplots show median GM values per subject in standard space.

Significant group level changes in response to visual stimulation

In all parameters of interest, PLS analyses revealed significant changes in response to visual stimulation, indicated by a significant first latent variable for BOLD, CBF, OEF, CMR_{O2} ($p<0.001$) and CMR_{glc} ($p<0.01$). We found significant increases in visual regions (both visual regions from the 17 network parcellation atlas (Thomas Yeo et al., 2011)) in BOLD, CBF, CMR_{O2} and CMR_{glc}, while the OEF was reduced in these areas (see Figure 2A). Hence, the directions of change were as expected. OEF decreases were most likely due to an overcompensation of CBF, thereby delivering more oxygen than required to active regions. Consequently, the relative amount of oxygen extracted from the blood decreases. Within the visual areas, changes in BOLD, CBF and OEF were more extended compared to the rather focal increases in CMR_{O2} and CMR_{glc}. Furthermore, the first latent variable of the CBF data indicated significant flow decreases across the cortex outside of visual ROIs, suggesting a flow redistribution towards visual areas upon visual stimulation. A similar pattern, although less pronounced, can be observed in the CMR_{O2} data, probably driven by the aforementioned CBF alterations. In some isolated regions, we also observed OEF reductions across the cortex. Changes in BOLD and CMR_{glc} are restricted to the examined visual regions, outlined by the black contour (see Figure 2A, right column).

Next, we created BOLD and PET masks (containing 2833 and 237 voxels, respectively) from the respective significant activation voxels and used them to mask the parameter maps. Figure 2B depicts the distribution across these masks, with median across subjects, alongside median delta and percent-change values. To test for significant changes across subjects in all parameters during STIM, we calculated median values per subject within each ROI, based on the individually thresholded parameter maps, see Table 2 and Methods. In response to visual stimulation, we found BOLD increases of 1.2% and 2.5% in the BOLD and PET group ROIs, respectively. Within the same ROIs we tested whether there were concomitant changes in CBF, CMR_{O2} and CMR_{glc}. We found significant increases in CBF and CMR_{glc} in both ROIs (see Table 2). CMR_{O2} increases were not statistically significant across subjects within the depicted ROIs ($p=0.09$ and $p=0.06$ for BOLD and PET ROIs, respectively, see Table 2).

Table 2

Mean values (SD) across subjects within BOLD and PET ROIs.

ROI	BOLD [%]	CBF [ml/100g/min]		CMRO2 [µmol/100g/min]		CMRglc [µmol/100g/min]	
		REST	ΔCBF	REST	ΔCMR_{O2}	REST	ΔCMR_{glc}
BOLD -ROI	1.2%	50.4 (10.9)	6.9** (4.6)	183.8 (43.7)	7.5 (16.2) (p=0.09)	34.7 (8.9)	6.5** (4.1)
			14.5%		4.3%		19.4%
PET-ROI	2.5%	53.7 (12.2)	14.3** (8.6)	193.6 (49.1)	17.8 (34.3) (p=0.06)	35.0 (8.5)	14.7 (9.6)
			26.7%		9.0%		40.5%

Note. This table shows mean and SD values across subjects within both group ROIs during REST (baseline), as well as absolute delta and percent change values for STIM minus REST). The exact calculations are outlined above. Significance was tested on REST vs. STIM median subject values with paired t-tests. Significance of ΔCMRglc within the PET-ROI was not tested, as this would be circular reasoning. **p<0.001.

Across subjects, in native space ROIs obtained from first level GLM results, in contrast to group ROIs derived from PLS in Table 2, the BOLD signal increased on average (median) by 1.67%. CMR_{glc} increased on average by 19.2% in STIM vs. REST (p<0.001) and CBF increased about 14.38% (p<0.001). However, despite CMR_{O2} increasing by 4.3% on average within these ROIs, the magnitude was not statistically significant (p=0.1). Lastly, OEF decreased by 8.23% (p<0.001).

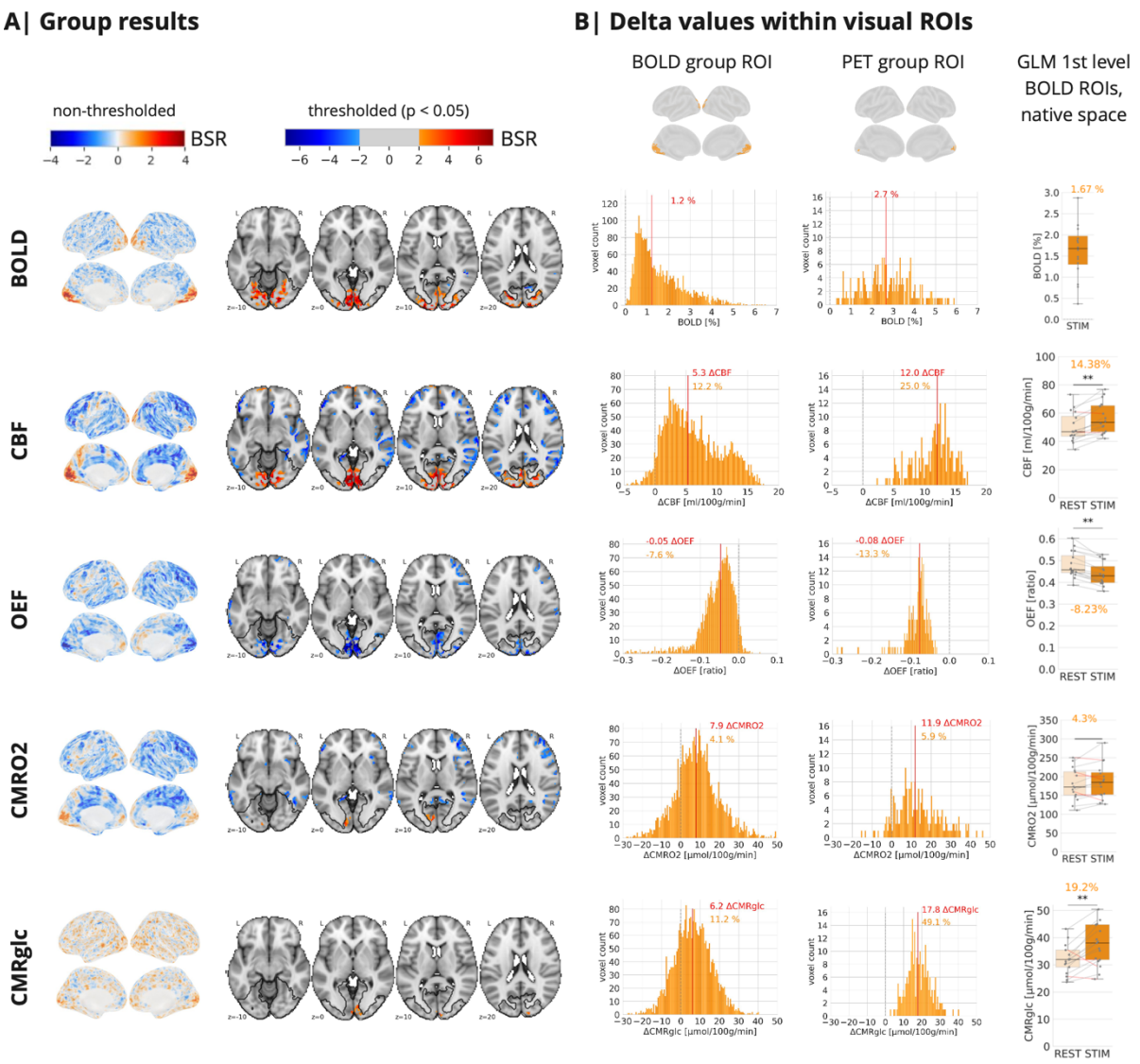

Figure 2. Group level results for REST vs. STIM. **A.** Statistical maps of the PLS results for the 1st latent variable per imaging parameter contrasting STIM to REST conditions. The 1st latent variable was significant for all parameters (CMRglc: p<0.01, else: p<0.001). The color gradient denotes the bootstrap ratio (BSR), with red voxels indicating STIM > REST and blue voxels REST > STIM. Left column: Non-thresholded BSR maps per parameter. Right: Axial slices showing statistical maps with BSR thresholded at ±2, corresponding to p<0.05. The black contour marks visual regions A and B from the 17 network parcellation according to Yeo et al. (2011). Within visual areas, we found significant effects in all parameters, with increases in BOLD, CBF, CMRO2 and CMRglc, and decreases in OEF. **B.** Absolute and percent change (delta values) for all parameters across subject-averaged voxels within the BOLD and PET group visual ROIs (containing 2833 and 237 voxels, respectively) as well as across subjects within native-space BOLD visual ROIs, resulting from a GLM 1st level analysis. Within these masks, CBF and CMRglc showed significant increases in STIM compared to REST, while OEF decreased. CMRO2 increased, too, but not significantly.

Significant reductions in OGI in response to visual stimulation

As a next step, we calculated the oxygen-to-glucose index (OGI) in REST and STIM. The OGI serves as a measure of oxidative and non-oxidative glucose metabolism. In theory, 6 moles of oxygen are required to fully oxidize 1 mole of glucose. Thus, an OGI of approximately 6 implies oxidative glucose metabolism, whereas an OGI of <6 suggests the presence of non-oxidative glucose metabolism. We calculated the OGI in native space, as described in the methods section. Results are based on one median value per subject within whole-brain GM as well as within the BOLD and PET group masks (see Figure 3A). Intriguingly, in all three masks (whole-brain GM, BOLD, PET), the mean OGI across subjects in REST equals 6.0. This corresponds exactly to the theoretical value of oxidative glucose metabolism, where 6 moles of oxygen oxidize 1 mole of glucose. Moreover, in all three masks, we find significant OGI decreases in STIM compared to REST (OGI_{STIM} = 5.6, $p<0.05$; OGI_{STIM} = 5.3, $p<0.01$; OGI_{STIM} = 4.7, $p<0.001$ for whole-brain, BOLD and PET masks, respectively) (see Figure 3A). The largest drop occurs, as expected, in the PET mask and amounts to a decrease of 21.6%.

Uniform OGI across networks

Additionally, we calculated the OGI per brain network as described above. Previous studies examining the uniformity of the OGI across brain networks reported discrepant results. While some results suggest uniform OGI distributions across GM (Hyder et al., 2016), other researchers analyzing the same data, but accounting for within-subject effects, report differences between brain networks, particularly between the visual and default mode network (Blazey, Snyder, Su, et al., 2018). In the present data, we find no differences in mean OGI between networks, both in REST and in STIM (see Figure 3B). This is in favor of the idea of a uniform OGI across GM. However, our data show quite large variance, necessitating caution in ultimate result interpretation.

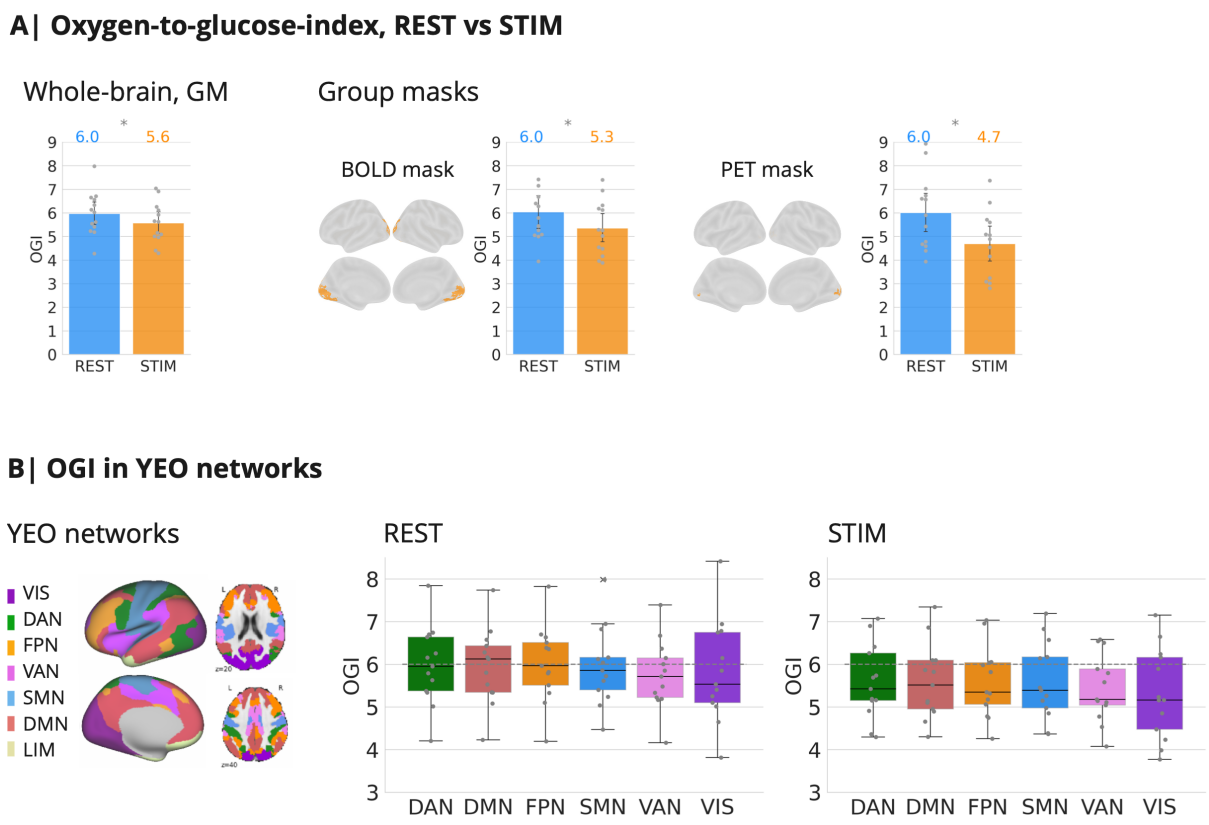

Figure 3. Oxygen-to-glucose index (OGI) across conditions. OGI was calculated in native space and corrected for outliers, as described previously. For analyses within group masks, native OGI maps were registered into standard space. Analyses on network level were entirely performed in native space. **A.** OGI in REST and STIM for whole-brain GM as well as within BOLD and PET group masks. In REST, the OGI was equal to 6.0 in each of the three masks, corresponding exactly to the theoretical value expected from oxidative glucose metabolism. In all three masks, the OGI dropped significantly during STIM compared to REST ($p<0.05$, $p<0.01$, $p<0.001$, respectively). **B.** OGI within brain networks (Yeo et al., 2011). Our results do not suggest any differences in mean OGI between networks in both REST and STIM. In all networks, the OGI drops from REST to STIM. Network abbreviations: VIS ≙ visual, DAN ≙ dorsal attention, FPN ≙ fronto-parietal/control, VAN ≙ ventral attention/salience, SMN ≙ somatomotor, DMN ≙ default mode, LIM ≙ limbic (excluded here).

As described in the methods section, CBV values were corrected for arterial CBV increase. This means we only considered 30% of CBV increase for OEF and CMRO2 calculations. The results shown here are all based on this correction.

Discussion

In the present study we combined multiparametric quantitative BOLD (mqBOLD) and ^{18}F-FDG functional PET (fPET) on a hybrid PET-MR scanner to simultaneously acquire cerebral metabolic rates of oxygen and glucose (CMR_{O2} and CMR_{glc}, respectively) during visual stimulation (STIM) and rest (REST) within a single scanning session. For the first

time, we showed that it is possible to measure CMR_{O2} and CMR_{glc} concurrently. Validating this, results showed significant increases in both parameters in visual areas during STIM compared to REST (see Figure 2A). These increases were accompanied by focal increases in CBF and the BOLD signal as well as OEF decreases in visual ROIs. Further, we found widespread reductions of CBF across the cortex (except for visual areas), suggesting a redirection of blood flow towards visual regions during STIM.

Within the group masks, we do not find significant increases of CMR_{O2} during STIM. With 4-9% change, CMR_{O2} increases are smaller than we expected based on literature (Davis et al., 1998; Donahue et al., 2009; Kim et al., 1999). Similarly, CBF increases (15-27%) were also smaller than expected (Kim et al., 1999; Mintun et al., 2001; Newberg et al., 2005), suggesting that CBF could be the limiting factor in weak CMR_{O2} increases. We suspect our CBF data to be too noisy, primarily resulting from the 12-channel coil used in our study. OEF, BOLD and CMR_{glc} alterations are well within ranges reported in previous literature (W. Chen et al., 1993; Davis et al., 1998; Mintun et al., 2001; Newberg et al., 2005; Vlassenko et al., 2006).

Our baseline CMR_{O2} value of 172.5 µmol/100g/min (see Table 1) is in the upper range compared to other studies finding baseline CMR_{O2} medians of ~130 µmol/100g/min (Epp et al., 2023; Raichle et al., 2001). Here, the key factor seems to be the chosen method for T2-mapping. Initially for mqBOLD, 2D turbo spin echo sequences were utilized, leading to a GM CMR_{O2} mean value of 174.94 µmol/100g/min (Christen et al., 2012, p. 201), which matches well with our data. However, a 2D TSE sequence has been suggested to introduce stimulated echoes that distort T2 relaxation, leading to too high T2, R2' and, ultimately, inflated CMR_{O2} values. More recently, it has been suggested to employ a 3D GRASE sequence for T2-mapping to reduce this transverse relaxation bias (Kaczmarz et al., 2020). Studies reporting baseline CMR_{O2} values around 130 µmol/100g/min usually use T2-GRASE imaging (Epp et al., 2023). Thus, our CMR_{O2} values might be slightly inflated due to the TSE sequence.

Next to alterations in individual imaging parameters, we calculated the oxygen-to-glucose index (OGI) in both REST and STIM within group masks as well as per network. The OGI represents the molar ratio of oxygen and glucose consumption, thereby providing information about oxidative and non-oxidative glucose metabolism. Purely oxidative glucose metabolism leads to an OGI of 6, while values below 6 suggest the presence of non-oxidative glucose metabolism. The latter has been found during

increased neuronal activity, with first studies suggesting an OGI drop of 90% during stimulation (Fox et al., 1988). Subsequent studies still suggested an OGI decrease upon increased energy demand but not as large as previously reported (Davis et al., 1998; Donahue et al., 2009; Kim et al., 1999).

Our results showed a baseline OGI of 6.0, both on a whole-brain level as well as within visual ROIs. This corresponds exactly to the theoretical value of 6 for purely oxidative glucose metabolism. Past studies reported a resting OGI of around 5.5 (Blazey, Snyder, Goyal, et al., 2018; Hyder et al., 2016; Shulman et al., 2001). Considering our slightly inflated CMR_{O2} values, it is likely that our true baseline OGI values are slightly below 6 and thus within the range of previously reported numbers. Moreover, we observed a significant reduction in OGI in response to visual stimulation, again both on a whole-brain level (6.6%) as well as within visual ROIs (11.6-21.6%). As percent values normalized by baseline CMR_{O2}, these numbers are not affected by the inflation of CMR_{O2} values. Further, our results suggest uniform OGI values across networks, both in rest as well as under visual stimulation. This is in line with a previous study (Hyder et al., 2016) but contradicts another (Blazey, Snyder, Su, et al., 2018). Our data show large across-subject variance with medium sample size, though, necessitating caution in ultimate result interpretation.

Limitations

While our study offers interesting insights into the brain's oxygen and glucose dynamics as well as promising results for future studies, some limitations must be noted. First of all, as mentioned before, even though we measured CBV directly, we had to estimate venous CBV changes. We estimated them to be 30% of total CBV changes, as suggested by a previous ultrahigh field MRI study (Huber et al., 2014). For future studies, we encourage researchers to measure venous CBV, for instance via specific multi-echo VASO (vascular space occupancy) techniques such as SS-SI-VASO (Huber et al., 2014), the VERVE technique (venous refocusing for volume estimation) (J. J. Chen & Pike, 2010), or by combining LL-FAIR (Look-Locker flow-sensitive alternating inversion recovery) with contrast-agent techniques to measure both total and arterial CBV (Wesolowski et al., 2019). Second, while we were able to employ both mqBOLD and fPET on a simultaneous PET-MR scanner, the SNR was limited by a 12-channel coil. We strongly recommend using a 32-channel coil if possible. It must be noted that changes in (total) CBV and CBF within

the BOLD ROI in our data are both around 12%. Yet, the CBV and CBF increases exert opposite effects on the direction of CMR_{O2} changes, thus diminishing CMR_{O2} effects. We assume that measuring venous CBV changes together with a pCASL sequence with higher sensitivity for task-induced changes, would have resulted in higher delta CMR_{O2} values, comparable to values reported in the literature. Third, as discussed, using a TSE sequence for T2 mapping leads to inflated CMR_{O2} values. There are corrections for these inflations (Nöth et al., 2017), requiring additional acquisition of B1 and B0 grefield mapping.

Conclusion

In the present study, we were able to quantify cerebral oxygen and glucose metabolism simultaneously and dynamically. Validating this, we found changes in CMR_{glc}, CMR_{O2}, CBF, OEF and BOLD in visual areas during visual stimulation. Further, we observed decreases in OGI upon visual stimulation of 11.6-21.6% in visual ROIs, suggesting an increase in non-oxidative glucose metabolism during increased neuronal activity. The complex setup of the study comes with some methodological hurdles to which we provided possible solutions in order to avoid them in the future. The unique combination of mqBOLD and fPET described here has the potential to be applied to various studies, furthering knowledge about underlying mechanisms of energy metabolism in the human brain.

References

Alsop, D. C., Detre, J. A., Golay, X., Günther, M., Hendrikse, J., Hernandez-Garcia, L., Lu, H., MacIntosh, B. J., Parkes, L. M., Smits, M., van Osch, M. J. P., Wang, D. J. J., Wong, E. C., & Zaharchuk, G. (2015). Recommended implementation of arterial spin-labeled perfusion MRI for clinical applications: A consensus of the ISMRM perfusion study group and the European consortium for ASL in dementia: Recommended Implementation of ASL for Clinical Applications. *Magnetic Resonance in Medicine*, *73*(1), 102–116. https://doi.org/10.1002/mrm.25197

Attwell, D., Buchan, A. M., Charpak, S., Lauritzen, M., MacVicar, B. A., & Newman, E. A. (2010). Glial and neuronal control of brain blood flow. *Nature*, *468*(7321), 232–243. https://doi.org/10.1038/nature09613

Attwell, D., & Iadecola, C. (2002). The neural basis of functional brain imaging signals. *Trends in Neurosciences*, *25*(12), 621–625.

Avants, B., Epstein, C., Grossman, M., & Gee, J. (2008). Symmetric diffeomorphic image registration with cross-correlation: Evaluating automated labeling of elderly and neurodegenerative brain. *Medical Image Analysis*, *12*(1), 26–41. https://doi.org/10.1016/j.media.2007.06.004

Baudrexel, S., Volz, S., Preibisch, C., Klein, J. C., Steinmetz, H., Hilker, R., & Deichmann, R. (2009). Rapid single-scan T2*-mapping using exponential excitation pulses and image-based correction for linear background gradients: T2* Mapping With Field Gradient Correction. *Magnetic Resonance in Medicine*, *62*(1), 263–268. https://doi.org/10.1002/mrm.21971

Blazey, T., Snyder, A. Z., Goyal, M. S., Vlassenko, A. G., & Raichle, M. E. (2018). A systematic meta-analysis of oxygen-to-glucose and oxygen-to-carbohydrate ratios in the resting human brain. *PLOS ONE*, *13*(9), e0204242. https://doi.org/10.1371/journal.pone.0204242

Blazey, T., Snyder, A. Z., Su, Y., Goyal, M. S., Lee, J. J., Vlassenko, A. G., Arbeláez, A. M., & Raichle, M. E. (2018). Quantitative positron emission tomography reveals regional differences in aerobic glycolysis within the human brain. *Journal of Cerebral Blood*

Flow & Metabolism, 0271678X1876700. https://doi.org/10.1177/0271678X18767005

Blockley, N. P., Griffeth, V. E. M., Simon, A. B., & Buxton, R. B. (2013). A review of calibrated blood oxygenation level-dependent (BOLD) methods for the measurement of task-induced changes in brain oxygen metabolism: A REVIEW OF CALIBRATED BOLD METHODS. *NMR in Biomedicine*, *26*(8), 987–1003. https://doi.org/10.1002/nbm.2847

Blockley, N. P., Griffeth, V. E. M., Simon, A. B., Dubowitz, D. J., & Buxton, R. B. (2015). Calibrating the BOLD response without administering gases: Comparison of hypercapnia calibration with calibration using an asymmetric spin echo. *NeuroImage*, *104*, 423–429. https://doi.org/10.1016/j.neuroimage.2014.09.061

Boxermann, J.L., Schmainda, K.M., Weisskoff, R.M. (2006). Relative Cerebral Blood Volume Maps Corrected for Contrast Agent Extravasation Significantly Correlate with Glioma Tumor Grade, Whereas Uncorrected Maps Do Not. *Amercian Journal of Neuroradiology*, *27*(4), 859–867.

Bright, M. G., Croal, P. L., Blockley, N. P., & Bulte, D. P. (2019). Multiparametric measurement of cerebral physiology using calibrated fMRI. *NeuroImage*, *187*, 128–144. https://doi.org/10.1016/j.neuroimage.2017.12.049

Byrne, J. H., Heidelberger, R., & Waxham, M. N. (Eds.). (2014). *From molecules to networks: An introduction to cellular and molecular neuroscience* (Third edition). Elsevier/AP, Academic Press is an imprint of Elsevier.

Castrillon, G., Epp, S., Bose, A., Fraticelli, L., Hechler, A., Belenya, R., Ranft, A., Yakushev, I., Utz, L., Sundar, L., Rauschecker, J., Preibisch, C., Kurcyus, K., & Riedl, V. (2023). The energetic costs of the human connectome. *OpenNeuro*. https://doi.org/10.18112/openneuro.ds004513.v1.0.0

Chen, J. J., & Pike, G. B. (2010). MRI measurement of the BOLD-specific flow–volume relationship during hypercapnia and hypocapnia in humans. *NeuroImage*, *53*(2), 383–391. https://doi.org/10.1016/j.neuroimage.2010.07.003

Chen, W., Novotny, E. J., Zhu, X. H., Rothman, D. L., & Shulman, R. G. (1993). Localized 1H NMR measurement of glucose consumption in the human brain during visual stimulation. *Proceedings of the National Academy of Sciences*, *90*(21), 9896–9900. https://doi.org/10.1073/pnas.90.21.9896

Christen, T., Schmiedeskamp, H., Straka, M., Bammer, R., & Zaharchuk, G. (2012). Measuring brain oxygenation in humans using a multiparametric quantitative blood oxygenation level dependent MRI approach. *Magnetic Resonance in Medicine*, *68*(3), 905–911. https://doi.org/10.1002/mrm.23283

Davis, T. L., Kwong, K. K., Weisskoff, R. M., & Rosen, B. R. (1998). Calibrated functional MRI: Mapping the dynamics of oxidative metabolism. *Proceedings of the National Academy of Sciences*, *95*(4), 1834–1839. https://doi.org/10.1073/pnas.95.4.1834

Donahue, M. J., Blicher, J. U., Østergaard, L., Feinberg, D. A., MacIntosh, B. J., Miller, K. L., Günther, M., & Jezzard, P. (2009). Cerebral blood flow, blood volume, and oxygen metabolism dynamics in human visual and motor cortex as measured by whole-brain multi-modal magnetic resonance imaging. *Journal of Cerebral Blood Flow and Metabolism*, *29*(11), 1856–1866. https://doi.org/10.1038/jcbfm.2009.107

Eichling, J. O., Raichle, M. E., Grubb, R. L., Larson, K. B., & Ter-Pogossian, M. M. (1975). In vivo determination of cerebral blood volume with radioactive oxygen-15 in the monkey. *Circulation Research*, *37*(6), 707–714. https://doi.org/10.1161/01.RES.37.6.707

Epp, S. M., Castrillón, G., Yuan, B., Andrews-Hanna, J., Preibisch, C., & Riedl, V. (2023). *Two distinct modes of hemodynamic responses in the human brain* [Preprint]. Neuroscience. https://doi.org/10.1101/2023.12.08.570806

Esteban, O. (2019). fMRIPrep: A robust preprocessing pipeline for functional MRI. *Nature Methods*, *16*, 14.

Esteban, O., Ciric, R., Finc, K., Blair, R. W., Markiewicz, C. J., Moodie, C. A., Kent, J. D., Goncalves, M., DuPre, E., Gomez, D. E. P., Ye, Z., Salo, T., Valabregue, R., Amlien, I. K., Liem, F., Jacoby, N., Stojić, H., Cieslak, M., Urchs, S., … Gorgolewski, K. J. (2020).

Analysis of task-based functional MRI data preprocessed with fMRIPrep. *Nature Protocols*, *15*(7), 2186–2202. https://doi.org/10.1038/s41596-020-0327-3

Feng, D., Huang, S.-C., & Wang, X. (1993). Models for computer simulation studies of input functions for tracer kinetic modeling with positron emission tomography. *International Journal of Bio-Medical Computing*, *32*(2), 95–110. https://doi.org/10.1016/0020-7101(93)90049-C

Fick, A. (1870). Ueber die Messung des Blutquantums in den Herzventrikeln. *Sitzungsberichte Der Physikalisch-Medizinischen Gesellschaft Zu Würzburg*, 16.

Fox, P., & Raichle, M. E. (1986). Focal physiological uncoupling of cerebral blood flow and oxidative metabolism during somatosensory stimulation in human subjects. *Proceedings of the National Academy of Sciences*, *83*(4), 1140–1144. https://doi.org/10.1073/pnas.83.4.1140

Fox, P., Raichle, M., Mintun, M., & Dence, C. (1988). Nonoxidative glucose consumption during focal physiologic neural activity. *Science*, *241*(4864), 462–464. https://doi.org/10.1126/science.3260686

Fujita, N., Matsumoto, K., Tanaka, H., Watanabe, Y., & Murase, K. (2006). Quantitative study of changes in oxidative metabolism during visual stimulation using absolute relaxation rates. *NMR in Biomedicine*, *19*(1), 60–68. https://doi.org/10.1002/nbm.1001

Germuska, M., Chandler, H. L., Stickland, R. C., Foster, C., Fasano, F., Okell, T. W., Steventon, J., Tomassini, V., Murphy, K., & Wise, R. G. (2019). Dual-calibrated fMRI measurement of absolute cerebral metabolic rate of oxygen consumption and effective oxygen diffusivity. *NeuroImage*, *184*, 717–728. https://doi.org/10.1016/j.neuroimage.2018.09.035

Gorgolewski, K., Burns, C. D., Madison, C., Clark, D., Halchenko, Y. O., Waskom, M. L., & Ghosh, S. S. (2011). Nipype: A Flexible, Lightweight and Extensible Neuroimaging Data Processing Framework in Python. *Frontiers in Neuroinformatics*, *5*. https://doi.org/10.3389/fninf.2011.00013

Göttler, J., Kaczmarz, S., Kallmayer, M., Wustrow, I., Eckstein, H.-H., Zimmer, C., Sorg, C., Preibisch, C., & Hyder, F. (2019). Flow-metabolism uncoupling in patients with asymptomatic unilateral carotid artery stenosis assessed by multi-modal magnetic resonance imaging. *Journal of Cerebral Blood Flow & Metabolism*, *39*(11), 2132–2143. https://doi.org/10.1177/0271678X18783369

Hahn, A., Gryglewski, G., Nics, L., Hienert, M., Rischka, L., Vraka, C., Sigurdardottir, H., Vanicek, T., James, G. M., Seiger, R., Kautzky, A., Silberbauer, L., Wadsak, W., Mitterhauser, M., Hacker, M., Kasper, S., & Lanzenberger, R. (2016). Quantification of Task-Specific Glucose Metabolism with Constant Infusion of 18F-FDG. *Journal of Nuclear Medicine*, *57*(12), 1933–1940. https://doi.org/10.2967/jnumed.116.176156

Hahn, A., Gryglewski, G., Nics, L., Rischka, L., Ganger, S., Sigurdardottir, H., Vraka, C., Silberbauer, L., Vanicek, T., Kautzky, A., Wadsak, W., Mitterhauser, M., Hartenbach, M., Hacker, M., Kasper, S., & Lanzenberger, R. (2017). Task-relevant brain networks identified with simultaneous PET/MR imaging of metabolism and connectivity. *Brain Structure and Function*. https://doi.org/10.1007/s00429-017-1558-0

Hedderich, D., Kluge, A., Pyka, T., Zimmer, C., Kirschke, J. S., Wiestler, B., & Preibisch, C. (2019). Consistency of normalized cerebral blood volume values in glioblastoma using different leakage correction algorithms on dynamic susceptibility contrast magnetic resonance imaging data without and with preload. *Journal of Neuroradiology*, *46*(1), 44–51. https://doi.org/10.1016/j.neurad.2018.04.006

Herscovitch, P., Markham, J., & Raichle, M. E. (n.d.). *BrainBloodFlow Measuredwith IntravenousH2'50. I. TheoryandErrorAnalysis*. *24*(9).

Hirsch, N. M., & Preibisch, C. (2013). T2* Mapping with Background Gradient Correction Using Different Excitation Pulse Shapes. *American Journal of Neuroradiology*, *34*(6), E65–E68. https://doi.org/10.3174/ajnr.A3021

Hirsch, N. M., Toth, V., Förschler, A., Kooijman, H., Zimmer, C., & Preibisch, C. (2014). Technical considerations on the validity of blood oxygenation level-dependent-based MR assessment of vascular deoxygenation: BOLD-BASED ASSESSMENT OF

VASCULAR DEOXYGENATION. *NMR in Biomedicine*, *27*(7), 853–862. https://doi.org/10.1002/nbm.3131

Hoge, R. D., & Pike, G. B. (2001). Oxidative metabolism and the detection of neuronal activation via imaging. *Journal of Chemical Neuroanatomy*, *22*(1–2), 43–52. https://doi.org/10.1016/S0891-0618(01)00114-4

Hua, J., Liu, P., Kim, T., Donahue, M., Rane, S., Chen, J. J., Qin, Q., & Kim, S.-G. (2019). MRI techniques to measure arterial and venous cerebral blood volume. *NeuroImage*, *187*, 17–31. https://doi.org/10.1016/j.neuroimage.2018.02.027

Huber, L., Goense, J., Kennerley, A. J., Ivanov, D., Krieger, S. N., Lepsien, J., Trampel, R., Turner, R., & Möller, H. E. (2014). Investigation of the neurovascular coupling in positive and negative BOLD responses in human brain at 7T. *NeuroImage*, *97*, 349–362. https://doi.org/10.1016/j.neuroimage.2014.04.022

Hyder, F., Herman, P., Bailey, C. J., Møller, A., Globinsky, R., Fulbright, R. K., Rothman, D. L., & Gjedde, A. (2016). Uniform distributions of glucose oxidation and oxygen extraction in gray matter of normal human brain: No evidence of regional differences of aerobic glycolysis. *Journal of Cerebral Blood Flow & Metabolism*, *36*(5), 903–916. https://doi.org/10.1177/0271678X15625349

Jamadar, S. D., Ward, P. GD., Li, S., Sforazzini, F., Baran, J., Chen, Z., & Egan, G. F. (2019). Simultaneous task-based BOLD-fMRI and [18-F] FDG functional PET for measurement of neuronal metabolism in the human visual cortex. *NeuroImage*, *189*, 258–266. https://doi.org/10.1016/j.neuroimage.2019.01.003

Jamadar, S. D., Zhong, S., Carey, A., McIntyre, R., Ward, P. G. D., Fornito, A., Premaratne, M., Jon Shah, N., O'Brien, K., Stäb, D., Chen, Z., & Egan, G. F. (2021). Task-evoked simultaneous FDG-PET and fMRI data for measurement of neural metabolism in the human visual cortex. *Scientific Data*, *8*(1), 267. https://doi.org/10.1038/s41597-021-01042-2

Jenkinson, M., Beckmann, C. F., Behrens, T. E. J., Woolrich, M. W., & Smith, S. M. (2012). FSL. *NeuroImage*, *62*(2), 782–790. https://doi.org/10.1016/j.neuroimage.2011.09.015

Kaczmarz, S., Hyder, F., & Preibisch, C. (2020). Oxygen extraction fraction mapping with multi-parametric quantitative BOLD MRI: Reduced transverse relaxation bias using 3D-GraSE imaging. *NeuroImage*, *220*, 117095. https://doi.org/10.1016/j.neuroimage.2020.117095

Kersten, S., Seydoux, J., Peters, J. M., Gonzalez, F. J., Desvergne, B., & Wahli, W. (1999). Peroxisome proliferator–activated receptor α mediates the adaptive response to fasting. *Journal of Clinical Investigation*, *103*(11), 1489–1498. https://doi.org/10.1172/JCI6223

Kim, S.-G., & Ogawa, S. (2012). Biophysical and Physiological Origins of Blood Oxygenation Level-Dependent fMRI Signals. *Journal of Cerebral Blood Flow & Metabolism*, *32*(7), 1188–1206. https://doi.org/10.1038/jcbfm.2012.23

Kim, S.-G., Rostrup, E., Larsson, H. B. W., Ogawa, S., & Paulson, O. B. (1999). Determination of relative CMRO2 from CBF and BOLD changes: Significant increase of oxygen consumption rate during visual stimulation. *Magnetic Resonance in Medicine*, *41*(6), 1152–1161. https://doi.org/10.1002/(SICI)1522-2594(199906)41:6<1152::AID-MRM11>3.0.CO;2-T

Kluge, A., Lukas, M., Toth, V., Pyka, T., Zimmer, C., & Preibisch, C. (2016). Analysis of three leakage-correction methods for DSC-based measurement of relative cerebral blood volume with respect to heterogeneity in human gliomas. *Magnetic Resonance Imaging*, *34*(4), 410–421. https://doi.org/10.1016/j.mri.2015.12.015

Kolb, H., Kempf, K., Röhling, M., Lenzen-Schulte, M., Schloot, N. C., & Martin, S. (2021). Ketone bodies: From enemy to friend and guardian angel. *BMC Medicine*, *19*(1), 313. https://doi.org/10.1186/s12916-021-02185-0

Krishnan, A., Williams, L. J., McIntosh, A. R., & Abdi, H. (2011). Partial Least Squares (PLS) methods for neuroimaging: A tutorial and review. *NeuroImage*, *56*(2), 455–475. https://doi.org/10.1016/j.neuroimage.2010.07.034

Leenders, K. L., Perani, D., Lammertsma, A. A., Heather, J. D., Buckingham, P., Jones, T., Healy, M. J. R., Gibbs, J. M., Wise, R. J. S., Hatazawa, J., Herold, S., Beaney, R. P., Brooks, D. J., Spinks, T., Rhodes, C., & Frackowiak, R. S. J. (1990). CEREBRAL BLOOD FLOW,

BLOOD VOLUME AND OXYGEN UTILIZATION: NORMAL VALUES AND EFFECT OF AGE. *Brain*, *113*(1), 27–47. https://doi.org/10.1093/brain/113.1.27

Liu, E. Y., Guo, J., Simon, A. B., Haist, F., Dubowitz, D. J., & Buxton, R. B. (2019). The potential for gas-free measurements of absolute oxygen metabolism during both baseline and activation states in the human brain. *NeuroImage*, 116342. https://doi.org/10.1016/j.neuroimage.2019.116342

Ma, Y., Sun, H., Cho, J., Mazerolle, E. L., Wang, Y., & Pike, G. B. (2020). Cerebral OEF quantification: A comparison study between quantitative susceptibility mapping and dual-gas calibrated BOLD imaging. *Magnetic Resonance in Medicine*, *83*(1), 68–82. https://doi.org/10.1002/mrm.27907

McIntosh, A. R., & Lobaugh, N. J. (2004). Partial least squares analysis of neuroimaging data: Applications and advances. *NeuroImage*, *23*, S250–S263. https://doi.org/10.1016/j.neuroimage.2004.07.020

McIntosh, A. R., & Mišić, B. (2013). Multivariate Statistical Analyses for Neuroimaging Data. *Annual Review of Psychology*, *64*(1), 499–525. https://doi.org/10.1146/annurev-psych-113011-143804

Mintun, M. A., Lundstrom, B. N., Snyder, A. Z., Vlassenko, A. G., Shulman, G. L., & Raichle, M. E. (2001). Blood flow and oxygen delivery to human brain during functional activity: Theoretical modeling and experimental data. *Proceedings of the National Academy of Sciences*, *98*(12), 6859–6864. https://doi.org/10.1073/pnas.111164398

Mintun, M. A., Raichle, M. E., & Martin, W. R. W. (1984). Brain Oxygen Utilization Measured with 0- 15 Radiotracers and Positron Emission Tomography. *The Journal of Nuclear Medicine*, *25*(2).

Newberg, A. B., Wang, J., Rao, H., Swanson, R. L., Wintering, N., Karp, J. S., Alavi, A., Greenberg, J. H., & Detre, J. A. (2005). Concurrent CBF and CMRGlc changes during human brain activation by combined fMRI – PET scanning. *NeuroImage*, *28*(2), 500–506. https://doi.org/10.1016/j.neuroimage.2005.06.040

Nöth, U., Shrestha, M., Schüre, J.-R., & Deichmann, R. (2017). Quantitative in vivo T2 mapping using fast spin echo techniques – A linear correction procedure. *NeuroImage*, *157*, 476–485. https://doi.org/10.1016/j.neuroimage.2017.06.017

Nöth, U., Volz, S., Hattingen, E., & Deichmann, R. (2014). An improved method for retrospective motion correction in quantitative T2* mapping. *NeuroImage*, *92*, 106–119. https://doi.org/10.1016/j.neuroimage.2014.01.050

Padamsey, Z., & Rochefort, N. L. (2023). Paying the brain's energy bill. *Current Opinion in Neurobiology*, *78*, 102668. https://doi.org/10.1016/j.conb.2022.102668

Pan, J. W., Rothman, D. L., Behar, K. L., Stein, D. T., & Hetherington, H. P. (2000). Human Brain β-Hydroxybutyrate and Lactate Increase in Fasting-Induced Ketosis. *Journal of Cerebral Blood Flow & Metabolism*, *20*(10), 1502–1507. https://doi.org/10.1097/00004647-200010000-00012

Patlak, C. S., & Blasberg, R. G. (1985). Graphical Evaluation of Blood-to-Brain Transfer Constants from Multiple-Time Uptake Data. Generalizations. *Journal of Cerebral Blood Flow & Metabolism*, *5*(4), 584–590. https://doi.org/10.1038/jcbfm.1985.87

Pfeiffer T, Schuster S, Bonhoeffer S. Cooperation and competition in the evolution of ATP producing pathways. Science. 2001 Apr 20;292(5516):504-7. doi: 10.1126/science.1058079. Epub 2001 Mar 29. Erratum in: Science 2001 Aug 24;293(5534):1436. PMID: 11283355.

Phelps, M. E., Huang, S. C., Hoffman, E. J., Selin, C., Sokoloff, L., & Kuhl, D. E. (1979). Tomographic measurement of local cerebral glucose metabolic rate in humans with (F-18)2-fluoro-2-deoxy-D-glucose: Validation of method. *Annals of Neurology*, *6*(5), 371–388. https://doi.org/10.1002/ana.410060502

Preibisch, C., Volz, S., Anti, S., & Deichmann, R. (2008). Exponential excitation pulses for improved water content mapping in the presence of background gradients. *Magnetic Resonance in Medicine*, *60*(4), 908–916. https://doi.org/10.1002/mrm.21730

Raichle, M. E., MacLeod, A. M., Snyder, A. Z., Powers, W. J., Gusnard, D. A., & Shulman, G. L. (2001). A default mode of brain function. *Proceedings of the National Academy of Sciences*, *98*(2), 676–682. https://doi.org/10.1073/pnas.98.2.676

Raichle, M. E., Martin, W. R. W., Herscovltch, P., Mintun, M. A., & Markham, J. (n.d.). *BrainBlOOdFlowMeasuredwith IntravenousH2150. II. ImplementationandValidation*. *24*(9).

Rischka, L., Gryglewski, G., Pfaff, S., Vanicek, T., Hienert, M., Klöbl, M., Hartenbach, M., Haug, A., Wadsak, W., Mitterhauser, M., Hacker, M., Kasper, S., Lanzenberger, R., & Hahn, A. (2018). Reduced task durations in functional PET imaging with [18F]FDG approaching that of functional MRI. *NeuroImage*, *181*(June), 323–330. https://doi.org/10.1016/j.neuroimage.2018.06.079

Shulman, R. G., Hyder, F., & Rothman, D. L. (2001). Lactate efflux and the neuroenergetic basis of brain function. *NMR in Biomedicine*, *14*(7–8), 389–396. https://doi.org/10.1002/nbm.741

Simon, A. B., & Buxton, R. B. (2015). Understanding the dynamic relationship between cerebral blood flow and the BOLD signal: Implications for quantitative functional MRI. *NeuroImage*, *116*, 158–167. https://doi.org/10.1016/j.neuroimage.2015.03.080

Smith, S. M., Jenkinson, M., Woolrich, M. W., Beckmann, C. F., Behrens, T. E. J., Johansen-Berg, H., Bannister, P. R., De Luca, M., Drobnjak, I., Flitney, D. E., Niazy, R. K., Saunders, J., Vickers, J., Zhang, Y., De Stefano, N., Brady, J. M., & Matthews, P. M. (2004). Advances in functional and structural MR image analysis and implementation as FSL. *NeuroImage*, *23*, S208–S219. https://doi.org/10.1016/j.neuroimage.2004.07.051

Stiernman, L. J., Grill, F., Hahn, A., Rischka, L., Lanzenberger, R., Panes Lundmark, V., Riklund, K., Axelsson, J., & Rieckmann, A. (2021). Dissociations between glucose metabolism and blood oxygenation in the human default mode network revealed by simultaneous PET-fMRI. *Proceedings of the National Academy of Sciences*, *118*(27), e2021913118. https://doi.org/10.1073/pnas.2021913118

Thomas Yeo, B. T., Krienen, F. M., Sepulcre, J., Sabuncu, M. R., Lashkari, D., Hollinshead, M., Roffman, J. L., Smoller, J. W., Zöllei, L., Polimeni, J. R., Fischl, B., Liu, H., & Buckner, R. L. (2011). The organization of the human cerebral cortex estimated by intrinsic functional connectivity. *Journal of Neurophysiology*, *106*(3), 1125–1165. https://doi.org/10.1152/jn.00338.2011

Uludağ, K., Dubowitz, D. J., Yoder, E. J., Restom, K., Liu, T. T., & Buxton, R. B. (2004). Coupling of cerebral blood flow and oxygen consumption during physiological activation and deactivation measured with fMRI. *NeuroImage*, *23*(1), 148–155. https://doi.org/10.1016/j.neuroimage.2004.05.013

Vafaee, M. S., Vang, K., Bergersen, L. H., & Gjedde, A. (2012). Oxygen consumption and blood flow coupling in human motor cortex during intense finger tapping: Implication for a role of lactate. *Journal of Cerebral Blood Flow & Metabolism*, *32*, 1859–1868. https://doi.org/10.1038/jcbfm.2012.89

Villien, M., Wey, H.-Y., Mandeville, J. B., Catana, C., Polimeni, J. R., Sander, C. Y., Zürcher, N. R., Chonde, D. B., Fowler, J. S., Rosen, B. R., & Hooker, J. M. (2014). Dynamic functional imaging of brain glucose utilization using fPET-FDG. *NeuroImage*, *100*, 192–199. https://doi.org/10.1016/j.neuroimage.2014.06.025

Vlassenko, A. G., Rundle, M. M., & Mintun, M. A. (2006). Human brain glucose metabolism may evolve during activation: Findings from a modified FDG PET paradigm. *NeuroImage*, *33*(4), 1036–1041. https://doi.org/10.1016/j.neuroimage.2006.06.065

Vriens, D., de Geus-Oei, L.-F., Oyen, W. J. G., & Visser, E. P. (2009). A Curve-Fitting Approach to Estimate the Arterial Plasma Input Function for the Assessment of Glucose Metabolic Rate and Response to Treatment. *Journal of Nuclear Medicine*, *50*(12), 1933–1939. https://doi.org/10.2967/jnumed.109.065243

Wesolowski, R., Blockley, N. P., Driver, I. D., Francis, S. T., & Gowland, P. A. (2019). Coupling between cerebral blood flow and cerebral blood volume: Contributions of different vascular compartments. *NMR in Biomedicine*, *32*(3), e4061. https://doi.org/10.1002/nbm.4061

Wu, H. (2003). Measurement of the Global Lumped Constant for 2-Deoxy-2-[18F]Fluoro-D-Glucose in Normal Human Brain Using [15O]Water and 2-Deoxy-2-[18F]Fluoro-D-Glucose Positron Emission Tomography Imaging A Method with Validation Based on Multiple Methodologies. *Molecular Imaging & Biology*, *5*(1), 32–41. https://doi.org/10.1016/S1536-1632(02)00122-1

Yablonskiy, D. A., & Haacke, E. M. (1994). Theory of NMR signal behavior in magnetically inhomogeneous tissues: The static dephasing regime. *Magnetic Resonance in Medicine*, *32*(6), 749–763. https://doi.org/10.1002/mrm.1910320610

4 General discussion

In the present thesis, I examined the dynamics of oxygen and glucose metabolism in the human brain. As one of the energetically most expensive organs, the brain primarily relies on oxidized glucose as its fuel. Given that it does not possess large energy storage capacities, it depends on a constant supply of oxygen and glucose. To further understand the implications of this dependency, the first project investigated how reduced availability of glucose affects cerebral metabolism of oxygen. Subsequently, the second project aimed to expand on current methodologies by introducing a novel possibility to concurrently measure glucose and oxygen consumption dynamically, thereby providing opportunities for future studies to investigate oxidative glucose metabolism more reliably. In the following, I will discuss implications of the individual projects as well as how their respective findings interconnect.

4.1 Implications

Given its heavy reliance on ATP production for sustaining healthy functioning, the body has developed several fallback systems to ensure energy homeostasis even if its primary fuel, oxidized glucose, is insufficiently available. In cases of prolonged glucose deficiency, it can, for instance, synthesize new glucose (gluconeogenesis), consume glucose storages (glycogenolysis) or utilize alternative substrates, such as ketone bodies and fatty acids for ATP production (Bartlett & Eaton, 2004; Exton et al., 1972; Krebs, 1966; X. Zhang et al., 2019). What was unknown, though, is whether the brain, in the face of glucose deficiency, utilizes similar mechanisms to maintain energy balance, whether it maintains glucose metabolism entirely or whether it decreases its energy metabolism, at least in part. According to the Selfish Brain Theory, the brain prioritizes its own energy requirements, often coming at the expense of other bodily systems (Peters et al., 2004, 2022). In this context, studies examining brain glucose uptake during hypoglycemia found decreases of cerebral metabolic rates of glucose (CMR_{glc}) under low blood glucose levels (T. M. Blazey & Raichle, 2019; Boyle et al., 1994). It was unclear whether this finding implies a general reduction in brain glucose metabolism, possibly as an energy-saving measure, or whether the brain utilizes alternate energy substrates for ATP production. The first manuscript presented in this thesis addressed this exact question: Does cerebral energy metabolism decrease during hypoglycemia or is it maintained, most likely by the

utilization of other substrates? To this end, we measured cerebral oxygen metabolism during hypoglycemia and euglycemia, using mqBOLD, a novel MR technique to quantify the cerebral metabolic rate of oxygen (CMR_{O2}) by acquiring data on blood oxygenation, cerebral blood volume (CBV) and cerebral blood flow (CBF) separately (Christen et al., 2012; Hirsch et al., 2014; Kaczmarz et al., 2020). Results showed steady levels of CMR_{O2} during hypoglycemia, suggesting maintained cerebral energy metabolism via alternate energy substrates. This conclusion can be drawn because alternate substrates (e.g. ketone bodies, fatty acids, astrocytic glycogen) still need to be oxidized for ATP production. Decreased levels of CMR_{glc} together with steady levels of CMR_{O2} thus imply the oxidation of different substrates.

4.1.1 Alternative oxidative energy pathways

While our results suggest that cerebral energy metabolism is maintained by the utilization of alternative substrates, our data cannot provide information on which specific substrates are metabolized to which extent. In response to periods of starvation, the body typically uses fatty acids, ketone bodies and glycogen in addition to the limited levels of glucose as fuels for energy production.

Fatty acids (FAs) are released from triglycerides in adipose tissue and then undergo beta-oxidation, thereby producing acetyl-CoA, which enters the TCA cycle for ATP production. Some organs with high energetic costs, such as the heart, largely rely on beta-oxidation for energy provision (Lopaschuk et al., 2010). The brain, being one of the energetically most expensive organ, has been found to be able to oxidize and even synthesize FAs in its glial cells (Aizawa et al., 2016; Garcia Corrales et al., 2021). However, relative to other organs with high energetic turnovers, the brain relies on FAs to a smaller extent (Schönfeld & Reiser, 2013). This is in part due to the slow transportation of FAs across the blood brain barrier (BBB) (Alberghina et al., 1993) and relatively slow rates of beta-oxidation, implying an inability of FA metabolism to quickly adapt to the rapidly changing energy requirements of the central nervous system caused by sudden bursts of activity in neurons. Also, beta-oxidation requires more oxygen to produce one molecule of ATP than any other energy substrate, making them unfavorable for the brain.

Under prolonged fasting, in addition to beta-oxidation, the liver converts FAs into ketone bodies, which are highly efficient energy suppliers. Ketone bodies are water-

soluble and can readily cross the BBB. Neural cells are able to take up ketone bodies and convert them into acetyl-CoA, which is subsequently fed into the TCA cycle. While the majority of ketone bodies are produced in the liver (Krebs, 1966), astrocytes have been found to synthesize ketone bodies from FAs as well (Auestad et al., 1991; Blázquez et al., 1998). While only accounting for approximately 5% of cerebral energy metabolism after an overnight fast (Cunnane et al., 2016), ketone bodies can cover up to 60% of the brain's energy requirements during starvation (Cahill, 2006). Even though glucose remains the brain's primary fuel, research showed a preference of the brain to use ketone bodies over glucose when both substrates are available (Hasselbalch et al., 1996). Considering the brain's seemingly high affinity for ketone bodies as a metabolic fuel, it comes naturally to wonder why they are not utilized as a primary source of energy. This is due to continuously high levels of ketone bodies leading to ketoacidosis, an overacidification of the body (Ghimire, 2023). This is a known difficulty in diabetes mellitus and leads to a variety of adverse symptoms reaching from headaches and vomiting to coma (Nyenwe & Kitabchi, 2016). Therefore, while ketone bodies can be a highly efficient source of energy for a limited period of time, the brain still relies on glucose as its primary and default fuel.

In addition to the utilization of FAs and ketone bodies, lactate is another valuable source of energy. As a byproduct of anaerobic cellular respiration, lactate was long considered a mere waste product. More recently, however, it has been found to not only fuel increased energy demand during exercise (van Hall et al., 2009) but also to be utilized during insufficient energy supply (Lima et al., 2015). Lactate is produced from glucose and can be shuttled between cells to ensure energy homeostasis. As such, it is shuttled from astrocytes to neurons in order to adjust to rapidly changing energy demands of neuronal activity (Pellerin & Magistretti, 1994). While astrocytes can produce lactate acutely, they can also store glycogen which, in the face of insufficient energy supply, is released in the form of lactate (Brunet et al., 2010; Suzuki et al., 2011). In line with the theory that the brain uses up glycogen storages under hypoglycemia (Öz et al., 2007), a study found significantly higher levels of lactate in the extracellular fluid in neuronal tissue under hypoglycemia compared to plasma lactate levels (Abi-Saab et al., 2002). With respect to amounts of glycogen stored in astrocytes, a study approximated storages to last only a few minutes in case of aglycemia (Brown, 2004). Under hypoglycemia, however, an experiment in rats found glycogen to last for more than two hours, with glycogen replenishment overcompensating upon restoration of euglycemia (Choi et al., 2003).

Most likely, during acute hypoglycemia, the brain utilizes each of the aforementioned energy substrates (glycogen, lactate, fatty acids, ketone bodies, spare glucose) but it is unclear to which degree exactly. The subjective extent to which each metabolite is used would probably depend on various factors, like metabolic health, physical condition, age or body composition as well as hypoglycemia severity and duration. It must be noted that elevated insulin levels have been found to inhibit ketogenesis (Laffel, 1999). Under normal circumstances, that makes sense since increased insulin secretion is a consequence of increased blood glucose levels. Consequently, there would be no need to provide additional energy substrates. In our study, however, hypoglycemia was induced by hyperinsulinemia, meaning that insulin levels were increased despite low blood glucose levels. From our data, we cannot answer whether the presence of hypoglycemia would disinhibit alternative energy pathways even under hyperinsulinemia but previous data shows energy supply to shift from glucose to ketones in the face of insulin resistance and prolonged hyperinsulinemia (S. Yang et al., 2015). It is quite likely that (astrocytic) glycogen is utilized during acute hypoglycemia since glucagon, the hormone promoting glycogen consumption, is increasingly secreted during hypoglycemia (Gerich et al., 1975). Moreover, due to their proximity, it seems logical for on-site energy storages (i.e. astrocytic glycogen) to be among the first alternate energy sources. Also, cerebral glycogen has been suggested to be consumed even during increased energy demand caused by cognitive processes (Christie & Schrater, 2015). Ketone bodies are likely to be utilized due to their rapid metabolism (Edmond et al., 1987), particularly in comparison to fatty acids. Moreover, intravenous injections of ketone bodies have shown to increase CBF (Hasselbalch et al., 1996; Svart et al., 2018), which fits our further imaging results. Taken together, even though we cannot definitely conclude which alternate substrates are utilized during hypoglycemia, it seems most likely that the brain uses astrocytic glycogen storages and lactate, as well as local and peripheral ketone bodies in addition to the remaining glucose to fuel its ATP production. Future studies are required to determine the exact extent to which each of these substrates is metabolized in the face of hypoglycemia.

4.1.2 Effects of hypoglycemia on neurovasculature

In response to hypoglycemia, we found increased levels of CBF, particularly in higher cognitive brain networks. In the more severely hypoglycemic subgroup (<49mg/dl; defined as a threshold for neuroglycopenic symptoms by Mitrakou et al. (1991)) we found CBF increases in all but the visual network. The exact underlying mechanisms of increased blood flow rates are unknown but they could be attributed to increased levels of stress hormones, ketone bodies and inflammatory markers. Stress hormones, like epinephrine, have been shown to increase blood flow (Thomas et al., 1997) and in our study epinephrine increased significantly in response to hypoglycemic glucose clamping. Further, elevated levels of ketone bodies are known to increase blood flow (Hasselbalch et al., 1996). Lastly, blood flow rates rise in response to inflammation (Fassbender et al., 1996). Even acute hypoglycemic periods have been shown to induce inflammatory processes (Iqbal et al., 2019; Ratter et al., 2017), suggesting them to, at least in part, cause the CBF increases. One alternative explanation that was mentioned only briefly in the manuscript is that the CBF enhancement could compensate for low blood glucose levels. That would mean that, due to less milligram glucose available per deciliter of blood, the brain increases the flow rate. This explanation may seem the most intuitive at first. However, there are two counterarguments. First of all, if blood flow increases served the provision with additional glucose, CMR_{glc} levels would not drop to the extent they do (T. M. Blazey & Raichle, 2019). Secondly, CBF increases resulting from hypoglycemia (in our case maximally ~6%) are weaker than CBF increases caused by increased neuronal activity (~30-50%) (Davis et al., 1998; Fox et al., 1988; Kim et al., 1999; Liu et al., 2020). In case of neuronal activation, higher flow rates partly serve the provision of tissues with nutrients, like oxygen and glucose, required to fuel the heightened energy demand. Although these CBF increments are usually larger than necessary, it seems unlikely that a flow increase of merely 6% would primarily serve the provision with additional glucose, compensating for lower blood glucose levels with faster flow. Thus, while increased CBF surely provides more glucose, this does not seem to be the primary reason for the observed CBF increases.

Next to CBF alterations, we observed reductions in OEF in the more severely hypoglycemic subgroup. These OEF decreases most likely reflect the increases in CBF, which supply the brain with more oxygen. Consequently, the relative amount of oxygen being extracted from the blood decreases, a process that is reflected in the BOLD contrast.

Our significant changes in CBF and OEF, concomitant with no changes in CMR_{O2}, illustrate that, while BOLD fMRI may be a valid method for estimating blood oxygenation changes in response to neuronal activation, one should be careful applying it to investigations of metabolism. Our data suggest OEF to reflect counterregulatory mechanisms in response to hypoglycemia rather than changes in neuronal activity or oxygen consumption.

4.1.3 Effects of restored euglycemia on cognitive function

Even though the brain seems able to keep its energy metabolism stable during hypoglycemic rest, it is important to note that hypoglycemia still impacts brain function. Acute hypoglycemia has consistently been found to impair various domains of cognition, with memory being impaired in particular (Sommerfield et al., 2003a, 2003b). This might be due to memory processes being especially energetically expensive, with glucose shuttling from glial cells to neurons playing a key role (McNay et al., 2000). Possibly, these processes are inhibited during low glucose availability (de Tredern et al., 2021). Further, the hippocampus, one of the most crucial brain areas for memory processing (Dickerson & Eichenbaum, 2010), has been found to be particularly vulnerable to hypoglycemia (Auer 1984; Auer, 2004).

In our study, we were interested in whether these cognitive impairments only pertain to acute hypoglycemic episodes or are more enduring, while controlling for potential confounding effects of decreased attention. It is known that people with recurrent hypoglycemic episodes (as especially observed in diabetics) show general cognitive deficits even during euglycemia (Chen et al., 2017). What remained unclear, though, was whether hypoglycemia, when induced onetime and rather briefly, would impair cognition also in healthy people once they returned to normal glucose levels. Therefore, in our study, once MR scanning was completed, we restored or maintained subjects' euglycemia (depending on whether they were hypoglycemic or euglycemic beforehand) and subsequently started cognitive testing. Here, we tested for deficits in attention as well as memory in *restored* euglycemia compared to *maintained* euglycemia. Our data showed no impairments in attention or learning under restored euglycemia. However, 24 hours post intervention, subjects performed significantly worse on the memory test when euglycemia was restored rather than maintained. This suggests that previous hypoglycemia has an isolated effect on memory consolidation even though

learning occurred under restored euglycemia. This is most likely caused by a glycogen deficits post hypoglycemia (Öz et al., 2007) since the breakdown of astrocytic glycogen has been shown to be crucial for memory formation (Boury-Jamot et al., 2016). Glycogen is also involved in de novo synthesis of glutamate, a neurotransmitter that is essential for sharp wave ripples (SWRs) (Behrens et al., 2005; Colgin et al., 2004; Maier et al., 2003; Papatheodoropoulos & Kostopoulos, 2002). As oscillatory patterns of neural activity in the hippocampus during rest, SWRs are the underyling mechanism of memory replay and, with that, of memory consolidation. It was found that memories tagged by SWRs during wakefulness are more likely to be replayed during sleep (W. Yang et al., 2024). Subsequently, these are the memories most likely to be consolidated since it has been shown that memory replay during sleep, particularly mediated by ripples, is crucial for memory consolidation (Schreiner et al., 2023). This is one potential explanation of how acutely low levels of glycogen/glutamate can impair long-term memory consolidation. Our findings imply that altered brain function, as previously demonstrated during acute hypoglycemia, does not end once glycemic levels are returned to baseline. This poses the question of what happens in the brain after hypoglycemia and further validates our decision to perform different clamping conditions on separate days. Contrasting data that has been acquired on different days can introduce confounds due to intersession variability. However, our data suggest that, due to enduring effects of hypoglycemia, acquiring data of different conditions on separate days is inevitable. The only alternative would be to always acquire hypoglycemic data last, but that introduces order effects, that have been suggested to be problematic in metabolism research (Stapleton et al., 1997; Tyler et al., 1988).

In this first project, we found steady levels of cerebral oxygen metabolism and interpreted these findings as an uncoupling between oxygen and glucose consumption during hypoglycemia. However, it must be noted that our interpretations are entirely based on previous literature showing substantial drops in CMR_{glc} on a whole-brain level. In the present study, we did not measure cerebral glucose metabolism in response to hypoglycemia. For more reliable data as well as information about the extent of this potential CMR_{O2}/CMR_{glc} uncoupling, it would be necessary to measure CMR_{O2} and CMR_{glc} simultaneously. The second manuscript in this thesis demonstrates how this could be accomplished in future studies.

4.1.4 Simultaneous measurements of oxygen and glucose metabolism

The second study presented in this thesis is rather a methodological and proof-of-concept study. Here, we combined novel neuroimaging techniques to acquire CMR_{O2} and CMR_{glc} simultaneously within a single scanning session. Just like in the first study, we used mqBOLD to measure CMR_{O2} (Christen et al., 2012, p. 201; Hirsch et al., 2014; Kaczmarz et al., 2020). For acquisition of CMR_{glc} data, we applied ^{18}F-FDG functional PET (fPET) (Hahn et al., 2016; Jamadar, Ward, Carey, et al., 2019; Jamadar, Ward, Li, et al., 2019; Rischka et al., 2018; Villien et al., 2014). In PET imaging of glucose metabolism, the radiotracer FDG is injected, which closely mimics glucose. FDG then accumulates in those cells with increased glucose metabolism and its decay can be picked up by the PET scanner. In the past, investigating alterations in CMR_{glc} between conditions involved separate PET scans on separate days. This is because a PET tracer is typically injected as a bolus and PET images are then averaged across the scanning session. In fPET, however, after an initial bolus, the tracer is infused continuously at a constant rate, thereby maintaining a steady-state level of tracer in the bloodstream, allowing for dynamic imaging of glucose metabolism over an extended period. In this way, we were able to simultaneously measure CMR_{O2} and CMR_{glc} in different conditions in a single scanning session. To the best of our knowledge, this is the first time, these neuroimaging techniques were combined for concurrent quantifications of cerebral oxygen and glucose consumption. Given the methodological focus of the study, we chose to contrast the rest condition with a visual stimulation paradigm, where we presented a moving checkerboard to the participants. Results demonstrated that we successfully measured CMR_{O2} and CMR_{glc} at the same time and under different tasks, indicated by significant increases of both parameters in visual regions during stimulation. CMR_{O2} changes were lower than we had expected, probably due to noise in the data caused in part by the utilization of a 12 channel head coil instead of, as in the first project, a 32 channel head coil.

The simultaneous acquisition of CMR_{O2} and CMR_{glc} allowed for reconsideration of the oxygen-to-glucose index (OGI), the molar ratio between oxygen and glucose consumption. In fully oxidative glucose metabolism, the OGI equals 6, as 6 moles of oxygen are required to oxidize one mole of glucose for ATP production. During rest, we found an OGI of exactly 6, which is most likely slightly too high due to potentially inflated absolute CMR_{O2} values. These are probably due to the utilization of a turbo spin echo sequence for T2-mapping opposed to a GRASE sequence. These resulting CMR_{O2} values are still in the

range of previously reported data (Christen et al., 2012), though, and are not to be confused with the aforementioned rather low levels of CMR_{O2} *change*. Given these circumstances, we expect true CMR_{O2} values to be slightly lower, resulting in an OGI <6 as reported by literature (T. Blazey, Snyder, Goyal, et al., 2018; Shulman et al., 2001). The previously described methodological issues do not, however, affect evaluations of OGI changes in response to visual stimulation. Here, we found significant decreases in OGI of ~12-22% in visual areas, hence an increase of non-oxidative glucose metabolism despite sufficient oxygen available. This drop, albeit significant, is not as large as the assumed 90% decrease in OGI found in an earlier study integrating CMR_{O2} and CMR_{glc} measured in different subjects (Fox et al., 1988). The underlying mechanisms of the increase in non-oxidative glucose metabolism in response to increased neuronal activity are not well understood. At first glance, it seems counterintuitive that the brain would increase an energy pathway (i.e. non-oxidative conversion of glucose into lactate) that only yields 2 ATP in contrast to oxidative phosphorylation resulting in 32 ATP. However, non-oxidative glucose metabolism also has some advantages. Firstly, it is faster than oxidative phosphorylation (Pfeiffer, 2001), so even though it yields less ATP, it might eventually be more efficient in meeting the rapid and localized increases in energy demands of active neurons. Secondly, non-oxidative glucose metabolism does not only produce 2 ATP but also lactate, which was long considered to be a mere waste product. More recently, however, lactate has been found to be an alternate fuel source and signaling molecule, mediating metabolic coupling between neurons and glial cells (van Hall et al., 2009). Through the production and subsequent shuttling of lactate, astrocytes are able to support neuronal function during periods of increased activity.

Despite some methodological difficulties in this second study, we were successful in demonstrating that concurrent quantification of oxygen and glucose metabolism during different tasks is possible. We offered realistic solutions to a number of methodological issues, so that in the future, this setup can be applied to various experimental settings.

4.2 Limitations

Both studies presented in this thesis came with some limitations, some of which have already been mentioned and discussed. In the first project, the biggest limitation is

that we only measured oxygen metabolism during hypoglycemia but not CMR_{glc}. Therefore, our interpretations of the data are entirely based on the assumption that past studies were correct in finding CMR_{glc} to decrease in response to hypoglycemia (T. M. Blazey & Raichle, 2019; Boyle et al., 1994). Conversely, if CMR_{glc} levels are, just like CMR_{O2} levels, kept stable during hypoglycemia, this would imply no utilization of alternate substrates. However, this would still be in line with the Selfish Brain Theory (Peters et al., 2004), assuming the brain to prioritize its own energy demand even under adverse circumstances, such as hypoglycemia. Of course, simultaneous measurements of CMR_{O2} and CMR_{glc}, as presented in the second project, would have been beneficial but we first needed to validate the approach of combining fPET with mqBOLD. Moreover, both studies require complex experimental setups and combining these would imply constant infusions of insulin, glucose and the radiotracer, injections of the contrast agent, performing arterial blood sampling continuously and venous blood sampling at 6-minute intervals – all while the subject lies in the scanner. Additionally, the continuous acquisition of PET data would cause time pressure in performing venous sampling which, as we can say from experience, can take some time due to restricted accessibility of the catheters within the scanner bore as well as blood in syringes. I still think that these two setups can be integrated in the future but one needs to be aware of the high complexity that comes along with combining them.

Another limiting factor in the first study is that we interpret stable CMR_{O2} levels as stable rates of cerebral energy metabolism. However, while energy substrates like glucose ketone bodies, fatty acids or lactate are all oxidized, they have different ATP yields. The phosphate to oxygen (p/o) ratio reflects the efficiency of oxidative phosphorylation (Hinkle, 2005). The p/o ratio of fatty acids, for instance, is lower (~2.33) than that of ketone bodies (~2.50), and the p/o ratio of glucose is still higher (~2.58), although only marginally relative to ketones (Kolwicz, 2021). Hence, to generate the same amount of ATP as glucose, one would need slightly more oxygen if the energy substrates are ketones and considerably more oxygen if the alternate energy substrates are fatty acids. The process is, however, even more complex since the rates of metabolism are significantly different between energy substrates, with ketone bodies, for instance, having a 7-9 times faster rate of energetic turnover than glucose (Edmond et al., 1987). Thus, for future studies, it might be insightful to acquire more information on which substrates are metabolized to which extent. To this end, one could, as previously described, measure

CMR_{glc} concurrently to evaluate the extent of reduction in glucose metabolism, but, additionally, one could draw blood samples for analyses of peripheral glucagon, fatty acids and ketone bodies. It must be noted, however, that these may involve advanced analysis techniques. Moreover, these measurements would not provide information about cerebral substrate utilization.

Limitations of the second manuscript have been discussed extensively, with the biggest limiting factor probably being the estimation, instead of direct measurement, of venous CBV increase during visual stimulation. While literature implies that our estimations are justified (Huber et al., 2014), future studies can avoid this issue by measuring venous CBV directly, which is possible e.g. via VASO techniques (Huber et al., 2014). The other main limitation of that manuscript, the 12 channel coil, can easily be fixed by the utilization of a 32 channel coil, if available at the study site.

5 Conclusion and outlook

In the present thesis, I presented two manuscripts that investigate cerebral oxygen and glucose dynamics. Further understanding the relationship between these two metabolites yields valuable information about the underlying nature of cerebral energy metabolism, with oxidized glucose being the predominant fuel. The first project examined how glucose deficiency affects the brain's oxygen metabolism and found stable CMR_{O2} rates. This suggests that the brain is indeed *selfish*, as suggested by the Selfish Brain Theory. However, the brain does not seem to be unaffected by hypoglycemia. In fact, it seems to be affected more enduringly than previously assumed, demonstrated by impaired memory consolidation even when learning took place during restored euglycemia. The second project demonstrated the feasibility of acquiring quantitative data on glucose and oxygen consumption concurrently, thereby providing a basis for future studies to apply simultaneous measurements of CMR_{O2} and CMR_{glc} to different experimental settings. Additionally, in that study, we reported a drop in the oxygen-to-glucose index upon increased neuronal activity. With this, we found an uncoupling of oxygen and glucose metabolism in both projects: There seems to be decreased oxidative glucose metabolism during hypoglycemia and increased non-oxidative glucose metabolism during visual stimulation.

Ideally, future studies could combine the two projects presented here and in addition to CMR_{O2} simultaneously measure CMR_{glc} during hypoglycemia. As described before, there is a range of technical and organizational aspects that need to be considered before study initiation, but I do think that it is possible. This would offer a unique chance to validate the decrease in oxidative glucose metabolism during hypoglycemia. Hypoglycemic and euglycemic conditions should, as previously mentioned, not be scanned within the same scanning session due to longer lasting effects of hypoglycemia on brain function. However, the opportunity to measure multiple conditions within a singular scanning session provided by fPET could be used to investigate how brain energy metabolism changes after hypoglycemia, once euglycemic levels have been restored. Hence, data on restored euglycemia could be acquired. Moreover, while studying the basis of cerebral energy metabolism under rest offers interesting insights already, future studies could investigate whether CMR_{O2} levels are still kept stable during hypoglycemia when engaging in cognitive tasks. Previous fMRI studies suggested increased neuronal activity upon visual stimulation under euglycemia but when repeating the same stimulation under hypoglycemia, neuronal activity was reported not to increase (Anderson et al., 2006). As put forward before, BOLD fMRI is not the ideal method for studying alterations in energy metabolism. But it would be interesting to apply our aforementioned imaging methods and examine whether the brain also behaves selfishly during cognitive tasks or whether it is merely capable of maintaining normal metabolic rates during rest. This would be particularly interesting for cognitive processes that are known to be energetically expensive, like memory formation. There is a lot of potential for the methods and experimental setups I described in this work, and I hope with this thesis to have contributed to the knowledge about cerebral energy metabolism under metabolically challenging conditions as well as provoked curiosity to study this topic further in the future.

References

Abel, E., Dale. (2004). Glucose transport in the heart. *Frontiers in Bioscience*, *9*(1–3), 201. https://doi.org/10.2741/1216

Abi-Saab, W. M., Maggs, D. G., Jones, T., Jacob, R., Srihari, V., Thompson, J., Kerr, D., Leone, P., Krystal, J. H., Spencer, D. D., During, M. J., & Sherwin, R. S. (2002). Striking Differences in Glucose and Lactate Levels between Brain Extracellular Fluid and Plasma in Conscious Human Subjects: Effects of Hyperglycemia and Hypoglycemia. *Journal of Cerebral Blood Flow & Metabolism*, *22*(3), 271–279. https://doi.org/10.1097/00004647-200203000-00004

Adzovic, L., Lynn, A. E., D'Angelo, H. M., Crockett, A. M., Kaercher, R. M., Royer, S. E., Hopp, S. C., & Wenk, G. L. (2015). Insulin improves memory and reduces chronic neuroinflammation in the hippocampus of young but not aged brains. *Journal of Neuroinflammation*, *12*(1), 63. https://doi.org/10.1186/s12974-015-0282-z

Aizawa, F., Nishinaka, T., Yamashita, T., Nakamoto, K., Koyama, Y., Kasuya, F., & Tokuyama, S. (2016). Astrocytes Release Polyunsaturated Fatty Acids by Lipopolysaccharide Stimuli. *Biological & Pharmaceutical Bulletin*, *39*(7), 1100–1106. https://doi.org/10.1248/bpb.b15-01037

Alam, U., Asghar, O., Azmi, S., & Malik, R. A. (2014). General aspects of diabetes mellitus. In *Handbook of Clinical Neurology* (Vol. 126, pp. 211–222). Elsevier. https://doi.org/10.1016/B978-0-444-53480-4.00015-1

Alberghina, M., Lupo, G., Anfuso, C. D., & Moro, F. (1993). Palmitate transport through the blood-retina and blood-brain barrier of rat visual system during aging. *Neuroscience Letters*, *150*(1), 17–20. https://doi.org/10.1016/0304-3940(93)90097-5

Allaman I, Magistretti PJ: Brain energy metabolism; in Fundamental Neuroscience. 4th ed. Edited by Squire LR, Berg D, Bloom FE, et al.. San Diego, *Academic Press*, 2013, pp 261–284

Anderson, A. W., Heptulla, R. A., Driesen, N., Flanagan, D., Goldberg, P. A., Jones, T. W., Rife, F., Sarofin, H., Tamborlane, W., Sherwin, R., & Gore, J. C. (2006). Effects of hypoglycemia on human brain activation measured with fMRI. *Magnetic Resonance Imaging*, *24*(6), 693–697. https://doi.org/10.1016/j.mri.2006.03.013

Attwell, D., & Iadecola, C. (2002). The neural basis of functional brain imaging signals. *Trends in Neurosciences*, *25*(12), 621–625.

Auer RN, Wieloch T, Olsson Y, Siesjö BK. The distribution of hypoglycemic brain damage. Acta Neuropathol. 1984;64(3):177-91. doi: 10.1007/BF00688108. PMID: 6496035.

Auer RN. Hypoglycemic brain damage. Metab Brain Dis. 2004 Dec;19(3-4):169-75. doi: 10.1023/b:mebr.0000043967.78763.5b. PMID: 15554413.

Auestad, N., Korsak, R. A., Morrow, J. W., & Edmond, J. (1991). Fatty Acid Oxidation and Ketogenesis by Astrocytes in Primary Culture. *Journal of Neurochemistry*, *56*(4), 1376–1386. https://doi.org/10.1111/j.1471-4159.1991.tb11435.x

Bak, L. K., Walls, A. B., Schousboe, A., & Waagepetersen, H. S. (2018). Astrocytic glycogen metabolism in the healthy and diseased brain. *Journal of Biological Chemistry*, *293*(19), 7108–7116. https://doi.org/10.1074/jbc.R117.803239

Bangsbo, J. (2000). Muscle oxygen uptake in humans at onset of and during intense exercise. *Acta Physiologica Scandinavica*, *168*(4), 457–464. https://doi.org/10.1046/j.1365-201x.2000.00697.x

Barañano, K. W., & Hartman, A. L. (2008). The ketogenic diet: Uses in epilepsy and other neurologic illnesses. *Current Treatment Options in Neurology*, *10*(6), 410–419. https://doi.org/10.1007/s11940-008-0043-8

Bartlett, K., & Eaton, S. (2004). Mitochondrial beta-oxidation. *European Journal of Biochemistry*, *271*(3), 462–469. https://doi.org/10.1046/j.1432-1033.2003.03947.x

Behrens, C. J., van den Boom, L. P., de Hoz, L., Friedman, A., & Heinemann, U. (2005). Induction of sharp wave–ripple complexes in vitro and reorganization of

hippocampal networks. *Nature Neuroscience*, *8*(11), 1560–1567. https://doi.org/10.1038/nn1571

Berger, S., Raman, G., Vishwanathan, R., Jacques, P. F., & Johnson, E. J. (2015). Dietary cholesterol and cardiovascular disease: A systematic review and meta-analysis. *The American Journal of Clinical Nutrition*, *102*(2), 276–294. https://doi.org/10.3945/ajcn.114.100305

Bernardin, C. P., & Moller, A. (2013). Recommended Daily Caloric Intake. *The FASEB Journal*, *27*(S1). https://doi.org/10.1096/fasebj.27.1_supplement.854.2

Blazey, T. M., & Raichle, M. E. (2019). *Brain Blood Flow and Metabolism: Variable Relationships in Altered Metabolic States*.

Blazey, T., Snyder, A. Z., Goyal, M. S., Vlassenko, A. G., & Raichle, M. E. (2018). A systematic meta-analysis of oxygen-to-glucose and oxygen-to-carbohydrate ratios in the resting human brain. *PLOS ONE*, *13*(9), e0204242. https://doi.org/10.1371/journal.pone.0204242

Blazey, T., Snyder, A. Z., Su, Y., Goyal, M. S., Lee, J. J., Vlassenko, A. G., Arbeláez, A. M., & Raichle, M. E. (2018). Quantitative positron emission tomography reveals regional differences in aerobic glycolysis within the human brain. *Journal of Cerebral Blood Flow & Metabolism*, 0271678X1876700. https://doi.org/10.1177/0271678X18767005

Blázquez, C., Sánchez, C., Velasco, G., & Guzmán, M. (1998). Role of Carnitine Palmitoyltransferase I in the Control of Ketogenesis in Primary Cultures of Rat Astrocytes. *Journal of Neurochemistry*, *71*(4), 1597–1606. https://doi.org/10.1046/j.1471-4159.1998.71041597.x

Borghouts, L. B., & Keizer, H. A. (2000). Exercise and Insulin Sensitivity: A Review. *International Journal of Sports Medicine*, *21*(1), 1–12. https://doi.org/10.1055/s-2000-8847

Boury-Jamot, B., Carrard, A., Martin, J. L., Halfon, O., Magistretti, P. J., & Boutrel, B. (2016). Disrupting astrocyte–neuron lactate transfer persistently reduces conditioned

responses to cocaine. *Molecular Psychiatry*, *21*(8), 1070–1076. https://doi.org/10.1038/mp.2015.157

Boyle, P. J., Nagy, R. J., O'Connor, A. M., Kempers, S. F., Yeo, R. A., & Qualls, C. (1994). Adaptation in brain glucose uptake following recurrent hypoglycemia. *Proceedings of the National Academy of Sciences*, *91*(20), 9352–9356. https://doi.org/10.1073/pnas.91.20.9352

Brady, T., Siegel, G. J., Albers, R. W., Price, D. L., & Benjamins, J. (Eds.). (2012). *Basic neurochemistry: Principles of molecular, cellular, and medical neurobiology* (8th ed). Elsevier/Academic Press.

Brierley, J. B. (1977). Experimental hypoxic brain damage. *Journal of Clinical Pathology*, *s3-11*(1), 181–187. https://doi.org/10.1136/jcp.s3-11.1.181

Brocchi, A., Rebelos, E., Dardano, A., Mantuano, M., & Daniele, G. (2022). Effects of Intermittent Fasting on Brain Metabolism. *Nutrients*, *14*(6), 1275. https://doi.org/10.3390/nu14061275

Brown, A. M. (2004). Brain glycogen re-awakened. *Journal of Neurochemistry*, *89*(3), 537–552. https://doi.org/10.1111/j.1471-4159.2004.02421.x

Brown, A. M., & Ransom, B. R. (2007). Astrocyte glycogen and brain energy metabolism. *Glia*, *55*(12), 1263–1271. https://doi.org/10.1002/glia.20557

Browning, J. D., Baxter, J., Satapati, S., & Burgess, S. C. (2012). The effect of short-term fasting on liver and skeletal muscle lipid, glucose, and energy metabolism in healthy women and men. *Journal of Lipid Research*, *53*(3), 577–586. https://doi.org/10.1194/jlr.P020867

Brunet, J., Allaman, I., Magistretti, P., & Pellerin, L. (2010). Glycogen Metabolism as a Marker of Astrocyte Differentiation. *Journal of Cerebral Blood Flow & Metabolism*, *30*(1), 51–55. https://doi.org/10.1038/jcbfm.2009.207

Buxton, R. B. (2010). Interpreting oxygenation-based neuroimaging signals: The importance and the challenge of understanding brain oxygen metabolism. *Frontiers in Neuroenergetics*. https://doi.org/10.3389/fnene.2010.00008

Byrne, J. H., Heidelberger, R., & Waxham, M. N. (Eds.). (2014). *From molecules to networks: An introduction to cellular and molecular neuroscience* (Third edition). Elsevier/AP, Academic Press is an imprint of Elsevier.

Cahill, G. F. (2006). Fuel Metabolism in Starvation. *Annual Review of Nutrition*, *26*(1), 1–22. https://doi.org/10.1146/annurev.nutr.26.061505.111258

Catalano, F., De Vito, F., Cassano, V., Fiorentino, T. V., Sciacqua, A., & Hribal, M. L. (2022). Circadian Clock Desynchronization and Insulin Resistance. *International Journal of Environmental Research and Public Health*, *20*(1), 29. https://doi.org/10.3390/ijerph20010029

Chen, Y., Liu, Z., Yu, Y., Yao, E., Liu, X., & Liu, L. (2017). Effect of recurrent severe hypoglycemia on cognitive performance in adult patients with diabetes: A meta-analysis. *Current Medical Science*, *37*(5), 642–648. https://doi.org/10.1007/s11596-017-1784-y

Choi, I., Seaquist, E. R., & Gruetter, R. (2003). Effect of hypoglycemia on brain glycogen metabolism in vivo. *Journal of Neuroscience Research*, *72*(1), 25–32. https://doi.org/10.1002/jnr.10574

Christen, T., Schmiedeskamp, H., Straka, M., Bammer, R., & Zaharchuk, G. (2012). Measuring brain oxygenation in humans using a multiparametric quantitative blood oxygenation level dependent MRI approach. *Magnetic Resonance in Medicine*, *68*(3), 905–911. https://doi.org/10.1002/mrm.23283

Christie, S. T., & Schrater, P. (2015). Cognitive cost as dynamic allocation of energetic resources. *Frontiers in Neuroscience*, *9*. https://doi.org/10.3389/fnins.2015.00289

Colgin, L. L., Kubota, D., Jia, Y., Rex, C. S., & Lynch, G. (2004). Long-term potentiation is impaired in rat hippocampal slices that produce spontaneous sharp waves. *The Journal of Physiology*, *558*(3), 953–961. https://doi.org/10.1113/jphysiol.2004.068080

Cunnane, S. C., Courchesne-Loyer, A., Vandenberghe, C., St-Pierre, V., Fortier, M., Hennebelle, M., Croteau, E., Bocti, C., Fulop, T., & Castellano, C.-A. (2016). Can Ketones Help Rescue Brain Fuel Supply in Later Life? Implications for Cognitive Health during Aging and the Treatment of Alzheimer's Disease. *Frontiers in Molecular Neuroscience*, *9*. https://doi.org/10.3389/fnmol.2016.00053

Dappert, A., Guenther, R. S., & Peyrard, S. (Eds.). (1992). *In-vivo magnetic resonance spectroscopy*. Springer-Verlag.

Davis, T. L., Kwong, K. K., Weisskoff, R. M., & Rosen, B. R. (1998). Calibrated functional MRI: Mapping the dynamics of oxidative metabolism. *Proceedings of the National Academy of Sciences*, *95*(4), 1834–1839. https://doi.org/10.1073/pnas.95.4.1834

de Tredern, E., Rabah, Y., Pasquer, L., Minatchy, J., Plaçais, P.-Y., & Preat, T. (2021). Glial glucose fuels the neuronal pentose phosphate pathway for long-term memory. *Cell Reports*, *36*(8), 109620. https://doi.org/10.1016/j.celrep.2021.109620

Dickerson, B. C., & Eichenbaum, H. (2010). The Episodic Memory System: Neurocircuitry and Disorders. *Neuropsychopharmacology*, *35*(1), 86–104. https://doi.org/10.1038/npp.2009.126

Dienel, G. A. (2017). The metabolic trinity, glucose–glycogen–lactate, links astrocytes and neurons in brain energetics, signaling, memory, and gene expression. *Neuroscience Letters*, *637*, 18–25. https://doi.org/10.1016/j.neulet.2015.02.052

Dinan, T. G., & Cryan, J. F. (2013). Melancholic microbes: A link between gut microbiota and depression? *Neurogastroenterology & Motility*, *25*(9), 713–719. https://doi.org/10.1111/nmo.12198

Dinan TG, Stanton C, Cryan JF. Psychobiotics: a novel class of psychotropic. Biol Psychiatry. 2013 Nov 15;74(10):720-6. doi: 10.1016/j.biopsych.2013.05.001. Epub 2013 Jun 10. PMID: 23759244.

Donahue, M. J., Blicher, J. U., Østergaard, L., Feinberg, D. A., MacIntosh, B. J., Miller, K. L., Günther, M., & Jezzard, P. (2009). Cerebral blood flow, blood volume, and oxygen metabolism dynamics in human visual and motor cortex as measured by whole-

brain multi-modal magnetic resonance imaging. *Journal of Cerebral Blood Flow and Metabolism*, *29*(11), 1856–1866. https://doi.org/10.1038/jcbfm.2009.107

Drew, P. J. (2019). Vascular and neural basis of the BOLD signal. *Current Opinion in Neurobiology*, *58*, 61–69. https://doi.org/10.1016/j.conb.2019.06.004

Du, Y., Zhang, Q., Zhang, X., Song, Y., Zheng, J., An, Y., & Lu, Y. (2023). Correlation between inflammatory biomarkers, cognitive function and glycemic and lipid profiles in patients with type 2 diabetes mellitus: A systematic review and meta-analysis. Clinical Biochemistry, Volumes 121–122, 110683. https://doi.org/10.1016/j.clinbiochem.2023.110683

Edmond, J., Robbins, R. A., Bergstrom, J. D., Cole, R. A., & de Vellis, J. (1987). Capacity for substrate utilization in oxidative metabolism by neurons, astrocytes, and oligodendrocytes from developing brain in primary culture. *Journal of Neuroscience Research*, *18*(4), 551–561. https://doi.org/10.1002/jnr.490180407

Engl, E., & Attwell, D. (2015). Non-signalling energy use in the brain. *The Journal of Physiology*, *593*(16), 3417–3429. https://doi.org/10.1113/jphysiol.2014.282517

Exton, J. H., Friedmann, N., Wong, E. H.-A., Brineaux, J. P., Corbin, J. D., & Park, C. R. (1972). Interaction of Glucocorticoids with Glucagon and Epinephrine in the Control of Gluconeogenesis and Glycogenolysis in Liver and of Lipolysis in Adipose Tissue. *Journal of Biological Chemistry*, *247*(11), 3579–3588. https://doi.org/10.1016/S0021-9258(19)45180-6

Fabricius TW, Verhulst CEM, Kristensen PL, Tack CJ, McCrimmon RJ, Heller S, Evans ML, Amiel SA, Pieber TR, de Galan BE, Pedersen-Bjergaard U; Hypo-RESOLVE consortium. Hyperinsulinaemic-hypoglycaemic glucose clamps in human research: a systematic review of the literature. Diabetologia. 2021 Apr;64(4):727 736. doi: 10.1007/s00125-020-05361-8. Epub 2021 Feb 10. PMID: 33566134; PMCID: PMC7940281.

Fassbender, K., Ries, S., Schminke, U., Schneider, S., & Hennerici, M. (1996). Inflammatory cytokines in CSF in bacterial meningitis: Association with altered blood flow velocities in basal cerebral arteries. *Journal of Neurology, Neurosurgery & Psychiatry*, *61*(1), 57–61. https://doi.org/10.1136/jnnp.61.1.57

Fernie, A. R., Carrari, F., & Sweetlove, L. J. (2004). Respiratory metabolism: Glycolysis, the TCA cycle and mitochondrial electron transport. *Current Opinion in Plant Biology*, *7*(3), 254–261. https://doi.org/10.1016/j.pbi.2004.03.007

Fick, A. (1870). Ueber die Messung des Blutquantums in den Herzventrikeln. *Sitzungsberichte Der Physikalisch-Medizinischen Gesellschaft Zu Würzburg*, 16.

Ford AC, Talley NJ, Schoenfeld PS, Quigley EM, Moayyedi P. Efficacy of antidepressants and psychological therapies in irritable bowel syndrome: systematic review and meta analysis. Gut. 2009 Mar;58(3):367-78. doi: 10.1136/gut.2008.163162. Epub 2008 Nov 10. PMID: 19001059.

Fox, P., & Raichle, M. E. (1986). Focal physiological uncoupling of cerebral blood flow and oxidative metabolism during somatosensory stimulation in human subjects. *Proceedings of the National Academy of Sciences*, *83*(4), 1140–1144. https://doi.org/10.1073/pnas.83.4.1140

Fox, P., Raichle, M., Mintun, M., & Dence, C. (1988). Nonoxidative glucose consumption during focal physiologic neural activity. *Science*, *241*(4864), 462–464. https://doi.org/10.1126/science.3260686

Friedman, H. I., & Nylund, B. (1980). Intestinal fat digestion, absorption, and transport A review. *The American Journal of Clinical Nutrition*, *33*(5), 1108–1139. https://doi.org/10.1093/ajcn/33.5.1108

Fujioka M, Okuchi K, Hiramatsu KI, Sakaki T, Sakaguchi S, Ishii Y. Specific changes in human brain after hypoglycemic injury. Stroke. 1997 Mar;28(3):584-7. doi: 10.1161/01.str.28.3.584. PMID: 9056615.

Fujita, N., Matsumoto, K., Tanaka, H., Watanabe, Y., & Murase, K. (2006). Quantitative study of changes in oxidative metabolism during visual stimulation using absolute relaxation rates. *NMR in Biomedicine*, *19*(1), 60–68. https://doi.org/10.1002/nbm.1001

Gao, J., Zhao, L., Cheng, Y., Lei, W., Wang, Y., Liu, X., Zheng, N., Shao, L., Chen, X., Sun, Y., Ling, Z., & Xu, W. (2023). Probiotics for the treatment of depression and its comorbidities: A systemic review. *Frontiers in Cellular and Infection Microbiology*, *13*, 1167116. https://doi.org/10.3389/fcimb.2023.1167116

Garcia Corrales, A. V., Haidar, M., Bogie, J. F. J., & Hendriks, J. J. A. (2021). Fatty Acid Synthesis in Glial Cells of the CNS. *International Journal of Molecular Sciences*, *22*(15), 8159. https://doi.org/10.3390/ijms22158159

García-Cáceres, C., Quarta, C., Varela, L., Gao, Y., Gruber, T., Legutko, B., Jastroch, M., Johansson, P., Ninkovic, J., Yi, C.-X., Le Thuc, O., Szigeti-Buck, K., Cai, W., Meyer, C. W., Pfluger, P. T., Fernandez, A. M., Luquet, S., Woods, S. C., Torres-Alemán, I., … Tschöp, M. H. (2016). Astrocytic Insulin Signaling Couples Brain Glucose Uptake with Nutrient Availability. *Cell*, *166*(4), 867–880. https://doi.org/10.1016/j.cell.2016.07.028

Garg, R., Chaudhuri, A., Munschauer, F., & Dandona, P. (2006). Hyperglycemia, Insulin, and Acute Ischemic Stroke: A Mechanistic Justification for a Trial of Insulin Infusion Therapy. *Stroke*, *37*(1), 267–273. https://doi.org/10.1161/01.STR.0000195175.29487.30

Genuth, S. (2006). Insights from The Diabetes Control and Complications Trial/Epidemiology of Diabetes Interventions and Complications Study on The Use of Intensive Glycemic Treatment to Reduce The Risk of Complications of Type 1 Diabetes. *Endocrine Practice*, *12*, 34–41. https://doi.org/10.4158/EP.12.S1.34

Gerich JE, Lorenzi M, Hane S, Gustafson G, Guillemin R, Forsham PH. Evidence for a physiologic role of pancreatic glucagon in human glucose homeostasis: studies with somatostatin. Metabolism. 1975 Feb;24(2):175-82. doi: 10.1016/0026 0495(75)90018-9. PMID: 1113681.

Ghimire P, Dhamoon AS. Ketoacidosis. 2023 Aug 8. In: StatPearls [Internet]. Treasure Island (FL): StatPearls Publishing; 2024 Jan–. PMID: 30521269.

Gibney, M. J. (n.d.). *Introduction to Human Nutrition*.

Ginter E, Simko V. Type 2 diabetes mellitus, pandemic in 21st century. Adv Exp Med Biol. 2012;771:42-50. doi: 10.1007/978-1-4614-5441-0_6. PMID: 23393670.

Gray, G. M. (1970). Carbohydrate Digestion and Absorption. *Gastroenterology*, *58*(1), 96–107. https://doi.org/10.1016/S0016-5085(70)80098-1

Hahn, A., Gryglewski, G., Nics, L., Hienert, M., Rischka, L., Vraka, C., Sigurdardottir, H., Vanicek, T., James, G. M., Seiger, R., Kautzky, A., Silberbauer, L., Wadsak, W., Mitterhauser, M., Hacker, M., Kasper, S., & Lanzenberger, R. (2016). Quantification of Task-Specific Glucose Metabolism with Constant Infusion of 18F-FDG. *Journal of Nuclear Medicine*, *57*(12), 1933–1940. https://doi.org/10.2967/jnumed.116.176156

Hahn, A., Gryglewski, G., Nics, L., Rischka, L., Ganger, S., Sigurdardottir, H., Vraka, C., Silberbauer, L., Vanicek, T., Kautzky, A., Wadsak, W., Mitterhauser, M., Hartenbach, M., Hacker, M., Kasper, S., & Lanzenberger, R. (2017). Task-relevant brain networks identified with simultaneous PET/MR imaging of metabolism and connectivity. *Brain Structure and Function*. https://doi.org/10.1007/s00429-017-1558-0

Hasselbalch, S. G., Madsen, P. L., Hageman, L. P., Olsen, K. S., Justesen, N., Holm, S., & Paulson, O. B. (1996). Changes in cerebral blood flow and carbohydrate metabolism during acute hyperketonemia. *American Journal of Physiology-Endocrinology and Metabolism*, *270*(5), E746–E751. https://doi.org/10.1152/ajpendo.1996.270.5.E746

Heise, T., Zijlstra, E., Nosek, L., Heckermann, S., Plum-Mörschel, L., & Forst, T. (2016). Euglycaemic glucose clamp: What it can and cannot do, and how to do it. *Diabetes, Obesity and Metabolism*, *18*(10), 962–972. https://doi.org/10.1111/dom.12703

Hems DA, Whitton PD. Control of hepatic glycogenolysis. Physiol Rev. 1980 Jan;60(1):1 50. doi: 10.1152/physrev.1980.60.1.1. PMID: 6243781.

Hinkle, P. C. (2005). P/O ratios of mitochondrial oxidative phosphorylation. *Biochimica et Biophysica Acta (BBA) - Bioenergetics*, *1706*(1–2), 1–11. https://doi.org/10.1016/j.bbabio.2004.09.004

Hitze B, Hubold C, van Dyken R, Schlichting K, Lehnert H, Entringer S, Peters A. How the selfish brain organizes its supply and demand. Front Neuroenergetics. 2010 Jun 9;2:7. doi: 10.3389/fnene.2010.00007. PMID: 20616886; PMCID: PMC2899523.

Herrera Moro Chao, D., Kirchner, M. K., Pham, C., Foppen, E., Denis, R. G. P., Castel, J., Morel, C., Montalban, E., Hassouna, R., Bui, L.-C., Renault, J., Mouffle, C., García-Cáceres, C., Tschöp, M. H., Li, D., Martin, C., Stern, J. E., & Luquet, S. H. (2022). Hypothalamic astrocytes control systemic glucose metabolism and energy balance. *Cell Metabolism*, *34*(10), 1532-1547.e6. https://doi.org/10.1016/j.cmet.2022.09.002

Herscovitch, P., Markham, J., & Raichle, M. E. (n.d.). *BrainBloodFlow Measuredwith IntravenousH2'50. I. TheoryandErrorAnalysis*. *24*(9).

Hirsch, N. M., Toth, V., Förschler, A., Kooijman, H., Zimmer, C., & Preibisch, C. (2014). Technical considerations on the validity of blood oxygenation level-dependent-based MR assessment of vascular deoxygenation: BOLD-BASED ASSESSMENT OF VASCULAR DEOXYGENATION. *NMR in Biomedicine*, *27*(7), 853–862. https://doi.org/10.1002/nbm.3131

Hochachka, P. W. (1998). Mechanism and Evolution of Hypoxia-Tolerance in Humans. *Journal of Experimental Biology*, *201*(8), 1243–1254. https://doi.org/10.1242/jeb.201.8.1243

Huang, S., & Czech, M. P. (2007). The GLUT4 Glucose Transporter. *Cell Metabolism*, *5*(4), 237–252. https://doi.org/10.1016/j.cmet.2007.03.006

Huber, L., Goense, J., Kennerley, A. J., Ivanov, D., Krieger, S. N., Lepsien, J., Trampel, R., Turner, R., & Möller, H. E. (2014). Investigation of the neurovascular coupling in

positive and negative BOLD responses in human brain at 7T. *NeuroImage*, *97*, 349–362. https://doi.org/10.1016/j.neuroimage.2014.04.022

Hyder, F., Herman, P., Bailey, C. J., Møller, A., Globinsky, R., Fulbright, R. K., Rothman, D. L., & Gjedde, A. (2016). Uniform distributions of glucose oxidation and oxygen extraction in gray matter of normal human brain: No evidence of regional differences of aerobic glycolysis. *Journal of Cerebral Blood Flow & Metabolism*, *36*(5), 903–916. https://doi.org/10.1177/0271678X15625349

Iqbal, A., Prince, L. R., Novodvorsky, P., Bernjak, A., Thomas, M. R., Birch, L., Lambert, D., Kay, L. J., Wright, F. J., Macdonald, I. A., Jacques, R. M., Storey, R. F., McCrimmon, R. J., Francis, S., Heller, S. R., & Sabroe, I. (2019). Effect of Hypoglycemia on Inflammatory Responses and the Response to Low-Dose Endotoxemia in Humans. *The Journal of Clinical Endocrinology & Metabolism*, *104*(4), 1187–1199. https://doi.org/10.1210/jc.2018-01168

Jamadar, S. D., Ward, P. G., Carey, A., McIntyre, R., Parkes, L., Sasan, D., Fallon, J., Li, S., Chen, Z., & Egan, G. F. (2019). *Constant Infusion Radiotracer Administration for High Temporal Resolution Positron Emission Tomography (PET) of the Human Brain: Application to [18F]-Fluorodexoyglucose PET (FDG-PET)* [Preprint]. Neuroscience. https://doi.org/10.1101/667352

Jamadar, S. D., Ward, P. GD., Li, S., Sforazzini, F., Baran, J., Chen, Z., & Egan, G. F. (2019). Simultaneous task-based BOLD-fMRI and [18-F] FDG functional PET for measurement of neuronal metabolism in the human visual cortex. *NeuroImage*, *189*, 258–266. https://doi.org/10.1016/j.neuroimage.2019.01.003

Jamadar, S. D., Zhong, S., Carey, A., McIntyre, R., Ward, P. G. D., Fornito, A., Premaratne, M., Jon Shah, N., O'Brien, K., Stäb, D., Chen, Z., & Egan, G. F. (2021). Task-evoked simultaneous FDG-PET and fMRI data for measurement of neural metabolism in the human visual cortex. *Scientific Data*, *8*(1), 267. https://doi.org/10.1038/s41597-021-01042-2

Johnson, T. A., Jinnah, H. A., & Kamatani, N. (2019). Shortage of Cellular ATP as a Cause of Diseases and Strategies to Enhance ATP. *Frontiers in Pharmacology*, *10*, 98. https://doi.org/10.3389/fphar.2019.00098

Kaczmarz, S., Hyder, F., & Preibisch, C. (2020). Oxygen extraction fraction mapping with multi-parametric quantitative BOLD MRI: Reduced transverse relaxation bias using 3D-GraSE imaging. *NeuroImage*, *220*, 117095. https://doi.org/10.1016/j.neuroimage.2020.117095

Khakh, B. S., & Burnstock, G. (2009). The Double Life of ATP. *Scientific American*, *301*(6), 84–92. https://doi.org/10.1038/scientificamerican1209-84

Kim, S.-G., Rostrup, E., Larsson, H. B. W., Ogawa, S., & Paulson, O. B. (1999). Determination of relative CMRO2 from CBF and BOLD changes: Significant increase of oxygen consumption rate during visual stimulation. *Magnetic Resonance in Medicine*, *41*(6), 1152–1161. https://doi.org/10.1002/(SICI)1522-2594(199906)41:6<1152::AID-MRM11>3.0.CO;2-T

Kind, K. L., Roberts, C. T., Sohlstrom, A. I., Katsman, A., Clifton, P. M., Robinson, J. S., & Owens, J. A. (2005). Chronic maternal feed restriction impairs growth but increases adiposity of the fetal guinea pig. *American Journal of Physiology-Regulatory, Integrative and Comparative Physiology*, *288*(1), R119–R126. https://doi.org/10.1152/ajpregu.00360.2004

Koepsell, H. (2020). Glucose transporters in brain in health and disease. *Pflügers Archiv - European Journal of Physiology*, *472*(9), 1299–1343. https://doi.org/10.1007/s00424-020-02441-x

Kolb, H., Kempf, K., Röhling, M., Lenzen-Schulte, M., Schloot, N. C., & Martin, S. (2021). Ketone bodies: From enemy to friend and guardian angel. *BMC Medicine*, *19*(1), 313. https://doi.org/10.1186/s12916-021-02185-0

Kolwicz, S. C. (2021). Ketone Body Metabolism in the Ischemic Heart. *Frontiers in Cardiovascular Medicine*, *8*, 789458. https://doi.org/10.3389/fcvm.2021.789458

Kraegen, E. W., Sowden, J. A., Halstead, M. B., Clark, P. W., Rodnick, K. J., Chisholm, D. J., & JAMESt, D. E. (n.d.). *Glucose transporters and in viva glucose uptake in skeletal and cardiac muscle: Fasting, insulin stimulation and immunoisolation studies of GLUT1 and GLUT4*.

Krebs, H. A. (1966). The regulation of the release of ketone bodies by the liver. *Advances in Enzyme Regulation*, *4*, 339–353. https://doi.org/10.1016/0065-2571(66)90027-6

Laffel, L. (1999). Ketone bodies: A review of physiology, pathophysiology and application of monitoring to diabetes. *Diabetes/Metabolism Research and Reviews*, *15*(6), 412–426. https://doi.org/10.1002/(SICI)1520-7560(199911/12)15:6<412::AID-DMRR72>3.0.CO;2-8

Laitinen, T., Lyyra-Laitinen, T., Huopio, H., Vauhkonen, I., Halonen, T., Hartikainen, J., Niskanen, L., & Laakso, M. (2008). Electrocardiographic Alterations during Hyperinsulinemic Hypoglycemia in Healthy Subjects. *Annals of Noninvasive Electrocardiology*, *13*(2), 97–105. https://doi.org/10.1111/j.1542-474X.2008.00208.x

Laybutt DR, Thompson AL, Cooney GJ, Kraegen EW. Selective chronic regulation of GLUT1 and GLUT4 content by insulin, glucose, and lipid in rat cardiac muscle in vivo. Am J Physiol. 1997 Sep;273(3 Pt 2):H1309-16. doi: 10.1152/ajpheart.1997.273.3.H1309. PMID: 9321820.

LeMay, D. R., Gehua, L., Zelenock, G. B., & D'Alecy, L. G. (1988). Insulin administration protects neurologic function in cerebral ischemia in rats. *Stroke*, *19*(11), 1411–1419. https://doi.org/10.1161/01.STR.19.11.1411

Lima, F. D., Correia, A. L. M., Teixeira, D. da S., Silva Neto, D. V. da, Fernandes, Í. S., Viana, M. B., Petitto, M., Sampaio, R. A., Chaves, S. N., Alves, S. T., Dantas, R. A. E., & Mota, M. R. (2015). Acute metabolic response to fasted and postprandial exercise. *International Journal of General Medicine*, 255. https://doi.org/10.2147/IJGM.S87429

Liu, E. Y., Guo, J., Simon, A. B., Haist, F., Dubowitz, D. J., & Buxton, R. B. (2020). The potential for gas-free measurements of absolute oxygen metabolism during both baseline and activation states in the human brain. *NeuroImage*, *207*, 116342. https://doi.org/10.1016/j.neuroimage.2019.116342

Lopaschuk, G. D., Ussher, J. R., Folmes, C. D. L., Jaswal, J. S., & Stanley, W. C. (2010). Myocardial Fatty Acid Metabolism in Health and Disease. *Physiological Reviews*, *90*(1), 207–258. https://doi.org/10.1152/physrev.00015.2009

Maier, N., Nimmrich, V., & Draguhn, A. (2003). Cellular and Network Mechanisms Underlying Spontaneous Sharp Wave–Ripple Complexes in Mouse Hippocampal Slices. *The Journal of Physiology*, *550*(3), 873–887. https://doi.org/10.1113/jphysiol.2003.044602

Masino, S. A., & Rho, J. M. (n.d.). Mechanisms of Ketogenic Diet Action. *Jasper's Basic Mechanisms of the Epilepsies*.

Masood W, Annamaraju P, Khan Suheb MZ, Uppaluri KR. Ketogenic Diet. 2023 Jun 16. In: StatPearls [Internet]. Treasure Island (FL): StatPearls Publishing; 2024 Jan–. PMID: 29763005.

McNay, E. C. (2007). Insulin and ghrelin: peripheral hormones modulating memory and hippocampal function. *Current Opinion in Pharmacology, 7*(6), 628-632. https://doi.org/10.1016/j.coph.2007.10.009.

McNay, E. C., Fries, T. M., & Gold, P. E. (2000). Decreases in rat extracellular hippocampal glucose concentration associated with cognitive demand during a spatial task. *Proceedings of the National Academy of Sciences*, *97*(6), 2881–2885. https://doi.org/10.1073/pnas.050583697

McNay, E. C., & Pearson-Leary, J. (2020). GluT4: A central player in hippocampal memory and brain insulin resistance. *Experimental Neurology*, *323*, 113076. https://doi.org/10.1016/j.expneurol.2019.113076

Melanson, K. J., Westerterp-Plantenga, M. S., Campfield, L. A., & Saris, W. H. M. (1999). Appetite and blood glucose profiles in humans after glycogen-depleting exercise. *Journal of Applied Physiology*, *87*(3), 947–954. https://doi.org/10.1152/jappl.1999.87.3.947

Melkonian EA, Schury MP. Biochemistry, Anaerobic Glycolysis. 2023 Jul 31. In: StatPearls [Internet]. Treasure Island (FL): StatPearls Publishing; 2024 Jan–. PMID: 31536301.

Miller, S. L., Green, L. R., Peebles, D. M., Hanson, M. A., & Blanco, C. E. (2002). Effects of chronic hypoxia and protein malnutrition on growth in the developing chick. *American Journal of Obstetrics and Gynecology*, *186*(2), 261–267. https://doi.org/10.1067/mob.2002.119629

Mitrakou A, Ryan C, Veneman T, Mokan M, Jenssen T, Kiss I, Durrant J, Cryer P, Gerich J. Hierarchy of glycemic thresholds for counterregulatory hormone secretion, symptoms, and cerebral dysfunction. Am J Physiol. 1991 Jan;260(1 Pt 1):E67-74. doi: 10.1152/ajpendo.1991.260.1.E67. PMID: 1987794.

Napoli, E., DueÃ±as, N., & Giulivi, C. (2014). Potential Therapeutic Use of the Ketogenic Diet in Autism Spectrum Disorders. *Frontiers in Pediatrics*, *2*. https://doi.org/10.3389/fped.2014.00069

Navarro, F., Liu, Y., & Rhoads, J. M. (2016). Can probiotics benefit children with autism spectrum disorders? *World Journal of Gastroenterology*, *22*(46), 10093. https://doi.org/10.3748/wjg.v22.i46.10093

Norton JE, Gonzalez Espinosa Y, Watson RL, Spyropoulos F, Norton IT. Functional food microstructures for macronutrient release and delivery. Food Funct. 2015 Mar;6(3):663-78. doi: 10.1039/c4fo00965g. PMID: 25553863.

Nyenwe, E. A., & Kitabchi, A. E. (2016). The evolution of diabetic ketoacidosis: An update of its etiology, pathogenesis and management. *Metabolism*, *65*(4), 507–521. https://doi.org/10.1016/j.metabol.2015.12.007

Orii, K. E., Fukao, T., Song, X.-Q., Mitchell, G. A., & Kondo, N. (2008). Liver-Specific Silencing of the Human Gene Encoding Succinyl-CoA: 3-Ketoacid CoA Transferase. *The Tohoku Journal of Experimental Medicine*, *215*(3), 227–236. https://doi.org/10.1620/tjem.215.227

Öz, G., Seaquist, E. R., Kumar, A., Criego, A. B., Benedict, L. E., Rao, J. P., Henry, P.-G., Van De Moortele, P.-F., & Gruetter, R. (2007). Human brain glycogen content and metabolism: Implications on its role in brain energy metabolism. *American Journal of Physiology-Endocrinology and Metabolism*, *292*(3), E946–E951. https://doi.org/10.1152/ajpendo.00424.2006

Padamsey, Z., & Rochefort, N. L. (2023). Paying the brain's energy bill. *Current Opinion in Neurobiology*, *78*, 102668. https://doi.org/10.1016/j.conb.2022.102668

Papatheodoropoulos, C., & Kostopoulos, G. (2002). Spontaneous GABAA-dependent synchronous periodic activity in adult rat ventral hippocampal slices. *Neuroscience Letters*, *319*(1), 17–20. https://doi.org/10.1016/S0304-3940(01)02505-8

Pei, D., Chen, T.-W., Kuo, Y.-L., Hung, Y.-J., Hsieh, C.-H., Wu, L.-Y., Chang, J.-B., Chou, T.-C., Chen, Y.-D. I., & Kuo, S.-W. (2003). The effect of surgical stress on insulin sensitivity, glucose effectiveness and acute insulin response to glucose load. *Journal of Endocrinological Investigation*, *26*(5), 397–402. https://doi.org/10.1007/BF03345193

Peirce, J. M., & Alviña, K. (2019). The role of inflammation and the gut microbiome in depression and anxiety. *Journal of Neuroscience Research*, *97*(10), 1223–1241. https://doi.org/10.1002/jnr.24476

Pellerin, L., & Magistretti, P. J. (1994). Glutamate uptake into astrocytes stimulates aerobic glycolysis: A mechanism coupling neuronal activity to glucose utilization. *Proceedings of the National Academy of Sciences*, *91*(22), 10625–10629. https://doi.org/10.1073/pnas.91.22.10625

Peters, A., Bosy-Westphal, A., Kubera, B., Langemann, D., Goele, K., Later, W., Heller, M., Hubold, C., & Müller, M. J. (2011). Why Doesn't the Brain Lose Weight, When Obese People Diet? *Obesity Facts*, *4*(2), 2–2. https://doi.org/10.1159/000327676

Peters, A., Schweiger, U., Pellerin, L., Hubold, C., Oltmanns, K. M., Conrad, M., Schultes, B., Born, J., & Fehm, H. L. (2004). The selfish brain: Competition for energy resources. *Neuroscience & Biobehavioral Reviews*, *28*(2), 143–180. https://doi.org/10.1016/j.neubiorev.2004.03.002

Peters, A., Sprengell, M., & Kubera, B. (2022). The principle of 'brain energy on demand' and its predictive power for stress, sleep, stroke, obesity and diabetes. *Neuroscience & Biobehavioral Reviews*, *141*, 104847. https://doi.org/10.1016/j.neubiorev.2022.104847

Petersen, M. C., Vatner, D. F., & Shulman, G. I. (2017). Regulation of hepatic glucose metabolism in health and disease. *Nature Reviews Endocrinology*, *13*(10), 572–587. https://doi.org/10.1038/nrendo.2017.80

Petersen, O. H., & Verkhratsky, A. (2016). Calcium and ATP control multiple vital functions. *Philosophical Transactions of the Royal Society B: Biological Sciences*, *371*(1700), 20150418. https://doi.org/10.1098/rstb.2015.0418

Pfeiffer T, Schuster S, Bonhoeffer S. Cooperation and competition in the evolution of ATP producing pathways. Science. 2001 Apr 20;292(5516):504-7. doi: 10.1126/science.1058079. Epub 2001 Mar 29. Erratum in: Science 2001 Aug 24;293(5534):1436. PMID: 11283355.

Profenno, L. A., Porsteinsson, A. P., & Faraone, S. V. (2010). Meta-Analysis of Alzheimer's Disease Risk with Obesity, Diabetes, and Related Disorders. *Biological Psychiatry*, *67*(6), 505–512. https://doi.org/10.1016/j.biopsych.2009.02.013

Pulikkan J, Mazumder A, Grace T. Role of the Gut Microbiome in Autism Spectrum Disorders. Adv Exp Med Biol. 2019;1118:253-269. doi: 10.1007/978-3-030 05542-4_13. PMID: 30747427.

Raichle, M. E., Martin, W. R. W., Herscovltch, P., Mintun, M. A., & Markham, J. (n.d.). *BrainBlOOdFlowMeasuredwith IntravenousH2150. II. ImplementationandValidation*. *24*(9).

Ratter, J. M., Rooijackers, H. M. M., Tack, C. J., Hijmans, A. G. M., Netea, M. G., de Galan, B. E., & Stienstra, R. (2017). Proinflammatory Effects of Hypoglycemia in Humans With or Without Diabetes. *Diabetes*, *66*(4), 1052–1061. https://doi.org/10.2337/db16-1091

Rhea, E. M., Rask-Madsen, C., & Banks, W. A. (2018). Insulin transport across the blood–brain barrier can occur independently of the insulin receptor. *The Journal of Physiology*, *596*(19), 4753–4765. https://doi.org/10.1113/JP276149

Rischka, L., Gryglewski, G., Pfaff, S., Vanicek, T., Hienert, M., Klöbl, M., Hartenbach, M., Haug, A., Wadsak, W., Mitterhauser, M., Hacker, M., Kasper, S., Lanzenberger, R., & Hahn, A. (2018). Reduced task durations in functional PET imaging with [18F]FDG approaching that of functional MRI. *NeuroImage*, *181*(June), 323–330. https://doi.org/10.1016/j.neuroimage.2018.06.079

Schönfeld, P., & Reiser, G. (2013). Why does Brain Metabolism not Favor Burning of Fatty Acids to Provide Energy? - Reflections on Disadvantages of the Use of Free Fatty Acids as Fuel for Brain. *Journal of Cerebral Blood Flow & Metabolism*, *33*(10), 1493–1499. https://doi.org/10.1038/jcbfm.2013.128

Schreiner, T., Griffiths, B. J., Kutlu, M., Vollmar, C., Kaufmann, E., Quach, S., Remi, J., Noachtar, S., & Staudigl, T. (2023). *Spindle-locked ripples mediate memory reactivation during human NREM sleep*. https://doi.org/10.1101/2023.01.27.525854

Schrieks, I. C., Heil, A. L. J., Hendriks, H. F. J., Mukamal, K. J., & Beulens, J. W. J. (2015). The Effect of Alcohol Consumption on Insulin Sensitivity and Glycemic Status: A Systematic Review and Meta-analysis of Intervention Studies. *Diabetes Care*, *38*(4), 723–732. https://doi.org/10.2337/dc14-1556

Schulingkamp, R. J., Pagano, T. C., Hung, D., & Raffa, R. B. (2000). Insulin receptors and insulin action in the brain: Review and clinical implications. *Neuroscience & Biobehavioral Reviews*, *24*(8), 855–872. https://doi.org/10.1016/S0149-7634(00)00040-3

Schutz Y. Protein turnover, ureagenesis and gluconeogenesis. Int J Vitam Nutr Res. 2011 Mar;81(2-3):101-7. doi: 10.1024/0300-9831/a000064. PMID: 22139560.

Schwingshackl, L., Zähringer, J., Beyerbach, J., Werner, S. W., Heseker, H., Koletzko, B., & Meerpohl, J. J. (2021). Total Dietary Fat Intake, Fat Quality, and Health Outcomes: A Scoping Review of Systematic Reviews of Prospective Studies. *Annals of Nutrition and Metabolism*, *77*(1), 4–15. https://doi.org/10.1159/000515058

Sharma, C., Kim, S., Nam, Y., Jung, U. J., & Kim, S. R. (2021). Mitochondrial Dysfunction as a Driver of Cognitive Impairment in Alzheimer's Disease. *International Journal of Molecular Sciences*, *22*(9), 4850. https://doi.org/10.3390/ijms22094850

Shulman, R. G., Hyder, F., & Rothman, D. L. (2001). Lactate efflux and the neuroenergetic basis of brain function. *NMR in Biomedicine*, *14*(7–8), 389–396. https://doi.org/10.1002/nbm.741

Sokoloff, L. (n.d.). *Energetics of Functional Activation in Neural Tissues*.

Sommerfield, A. J., Deary, I. J., McAulay, V., & Frier, B. M. (2003a). Moderate hypoglycemia impairs multiple memory functions in healthy adults. *Neuropsychology*, *17*(1), 125–132. https://doi.org/10.1037/0894-4105.17.1.125

Sommerfield, A. J., Deary, I. J., McAulay, V., & Frier, B. M. (2003b). Short-Term, Delayed, and Working Memory Are Impaired During Hypoglycemia in Individuals With Type 1 Diabetes. *Diabetes Care*, *26*(2), 390–396. https://doi.org/10.2337/diacare.26.2.390

Standl, E., Khunti, K., Hansen, T. B., & Schnell, O. (2019). The global epidemics of diabetes in the 21st century: Current situation and perspectives. *European Journal of Preventive Cardiology*, *26*(2_suppl), 7–14. https://doi.org/10.1177/2047487319881021

Stapleton, J. M., Morgan, M. J., Liu, X., Yung, B. C. K., Phillips, R. L., Wong, D. F., Shaya, E. K., Dannals, R. F., & London, E. D. (1997). Cerebral Glucose Utilization Is Reduced in Second Test Session. *Journal of Cerebral Blood Flow & Metabolism*, *17*(6), 704–712. https://doi.org/10.1097/00004647-199706000-00012

Su, S. W., Cilio, M. R., Sogawa, Y., Silveira, D., Holmes, G. L., & Stafstrom, C. E. (2000). Timing of ketogenic diet initiation in an experimental epilepsy model. *Developmental Brain Research*.

Suzuki, A., Stern, S. A., Bozdagi, O., Huntley, G. W., Walker, R. H., Magistretti, P. J., & Alberini, C. M. (2011). Astrocyte-Neuron Lactate Transport Is Required for Long-Term Memory Formation. *Cell*, *144*(5), 810–823. https://doi.org/10.1016/j.cell.2011.02.018

Svart, M., Gormsen, L. C., Hansen, J., Zeidler, D., Gejl, M., Vang, K., Aanerud, J., & Moeller, N. (2018). Regional cerebral effects of ketone body infusion with 3-hydroxybutyrate in humans: Reduced glucose uptake, unchanged oxygen consumption and increased blood flow by positron emission tomography. A randomized, controlled trial. *PLOS ONE*, *13*(2), e0190556. https://doi.org/10.1371/journal.pone.0190556

Thomas, M., Sherwin, R. S., Murphy, J., & Kerr, D. (1997). *Importance of Cerebral Blood Flow to the Recognition of and Physiological Responses to Hypoglycemia*. *46*.

Thomsen, H. S. (2017). Generic gadolinium-based contrast agents: The future? *Acta Radiologica*, *58*(11), 1285–1287. https://doi.org/10.1177/0284185117719576

Thorens, B., & Mueckler, M. (2010). Glucose transporters in the 21st Century. *American Journal of Physiology-Endocrinology and Metabolism*, *298*(2), E141–E145. https://doi.org/10.1152/ajpendo.00712.2009

Tyler, J. L., Strother, S. C., Zatorre, R. J., Alivisatos, B., Worsley, K. J., Diksic, M., & Yamamoto, Y. L. (n.d.). *Measuredby Positron Emission Tomography*. *29*.

van Hall, G., Strømstad, M., Rasmussen, P., Jans, Ø., Zaar, M., Gam, C., Quistorff, B., Secher, N. H., & Nielsen, H. B. (2009). Blood Lactate is an Important Energy Source for the Human Brain. *Journal of Cerebral Blood Flow & Metabolism*, *29*(6), 1121–1129. https://doi.org/10.1038/jcbfm.2009.35

Velu, L., Pellerin, L., Julian, A., Paccalin, M., Giraud, C., Fayolle, P., Guillevin, R., & Guillevin, C. (2024). Early rise of glutamate-glutamine levels in mild cognitive impairment:

Evidence for emerging excitotoxicity. *Journal of Neuroradiology, 51*(2), 168-175. https://doi.org/10.1016/j.neurad.2023.09.003

Villien, M., Wey, H.-Y., Mandeville, J. B., Catana, C., Polimeni, J. R., Sander, C. Y., Zürcher, N. R., Chonde, D. B., Fowler, J. S., Rosen, B. R., & Hooker, J. M. (2014). Dynamic functional imaging of brain glucose utilization using fPET-FDG. *NeuroImage*, *100*, 192–199. https://doi.org/10.1016/j.neuroimage.2014.06.025

Voll, C. L., Whishaw, I. Q., & Auer, R. N. (1989). Postischemic insulin reduces spatial learning deficit following transient forebrain ischemia in rats. *Stroke*, *20*(5), 646–651. https://doi.org/10.1161/01.STR.20.5.646

White BC, Wiegenstein JG, Winegar CD. Brain ischemic anoxia. Mechanisms of injury. JAMA. 1984 Mar 23-30;251(12):1586-90. PMID: 6366268.

Won, S. J., Yoo, B. H., Kauppinen, T. M., Choi, B. Y., Kim, J. H., Jang, B. G., Lee, M. W., Sohn, M., Liu, J., Swanson, R. A., & Suh, S. W. (2012). Recurrent/moderate hypoglycemia induces hippocampal dendritic injury, microglial activation, and cognitive impairment in diabetic rats. *Journal of Neuroinflammation*, *9*(1), 182. https://doi.org/10.1186/1742-2094-9-182

World Health Organization. (n.d.). Mean fasting blood glucose (mmol/L)(age standardized estimate). WHO. www.who.int/data/gho/indicator- metadata-registry/imr-details/2380

Xu, F., & Rhodes, E. C. (1999). Oxygen Uptake Kinetics During Exercise: *Sports Medicine*, *27*(5), 313–327. https://doi.org/10.2165/00007256-199927050-00003

Yaffe, K. (2013). Association Between Hypoglycemia and Dementia in a Biracial Cohort of Older Adults With Diabetes Mellitus. *JAMA Internal Medicine*, *173*(14), 1300. https://doi.org/10.1001/jamainternmed.2013.6176

Yang, S., Xia, J., Zhang, Y., Fan, J., Wang, H., Yuan, J., Zhao, Z., Pan, Q., Mu, Y., Xin, L., Chen, Y., & Li, K. (2015). Hyperinsulinemia shifted energy supply from glucose to ketone bodies in early nonalcoholic steatohepatitis from high-fat high-sucrose diet

induced Bama minipigs. *Scientific Reports*, *5*(1), 13980. https://doi.org/10.1038/srep13980

Yang, W., Sun, C., Huszár, R., Hainmueller, T., Kiselev, K., & Buzsáki, G. (2024). Selection of experience for memory by hippocampal sharp wave ripples. *Science*, *383*(6690), 1478–1483. https://doi.org/10.1126/science.adk8261

Yu, L.-Y., & Pei, Y. (2015). Insulin Neuroprotection and the Mechanisms. *Chinese Medical Journal*, *128*(7), 976–981. https://doi.org/10.4103/0366-6999.154323

Zajac, A., Poprzecki, S., Maszczyk, A., Czuba, M., Michalczyk, M., & Zydek, G. (2014). The Effects of a Ketogenic Diet on Exercise Metabolism and Physical Performance in Off-Road Cyclists. *Nutrients*, *6*(7), 2493–2508. https://doi.org/10.3390/nu6072493

Zhang, X., Yang, S., Chen, J., & Su, Z. (2019). Unraveling the Regulation of Hepatic Gluconeogenesis. *Frontiers in Endocrinology*, *9*, 802. https://doi.org/10.3389/fendo.2018.00802

Zhang, Z., Cheng, J., Xu, F., Chen, Y., Du, J., Yuan, M., Zhu, F., Xu, X., & Yuan, S. (2011). Red blood cell extrudes nucleus and mitochondria against oxidative stress. *IUBMB Life*, *63*(7), 560–565. https://doi.org/10.1002/iub.490

Zhu, C. Z., & Auer, R. N. (1994). Intraventricular Administration of Insulin and IGF-1 in Transient Forebrain Ischemia. *Journal of Cerebral Blood Flow & Metabolism*, *14*(2), 237–242. https://doi.org/10.1038/jcbfm.1994.30

Acknowledgements

In science, people are used to statements about probabilities, but they rarely start sentences with "*It is safe to say that …*". On these last pages of my dissertation, I would like to defy these principles. Because it *is* safe to say that this thesis, representing the past five years, would not have been possible without the infinite and unconditional support of many people. I want to take this chance to thank them.

First of all, I want to thank you, Valentin, for your open door, ear and mind. In addition to your scientific visions, you have a talent for bringing together people that just click. Thank you for the trust you put into each of us, for always having our backs, and for reminding us that taking time off is important, whether that is for an ice cream break or a proper vacation. You lead this lab by example and I repeat myself when I say that you set the bar quite high for any future supervisor.
Further, I want to thank Dr. Roman Iakoubov for hearing me out when I showed up in his office unannounced and pitched him the idea of not only inducing hypoglycemia in perfectly healthy people but also putting them into the MR scanner while doing so. Thank you for believing in the project and for all your support. Thank you, Dr. Stefanie Haschka, Dr. Johanna Köhler, Dr. Felix Hesse and all my medical students for scanning 198 MR sessions with me and for making the early mornings even fun (after we had our first cup of coffee).
A huge thanks goes to the GSN for enabling me to learn and work in an international and interdisciplinary environment and, of course, for financial support. To the entire GSN staff, thank you for your kindness and patience, for organizing countless events, and for putting up with my many questions. Additionally, I would like to thank my TAC members Prof. Dr. Tobias Bonhoeffer and Prof. Dr. Tobias Staudigl for their guidance and support throughout my PhD journey. Thank you for staying open to my research projects despite the turn they took from cognitive to biomedical neuroscience, eventually combining the two fields. Thank you for all of your input, both scientifically and personally. I never would have thought TAC meetings could be fun, but I ended up looking forward to them.

I honestly do not know how I got this lucky but during these last couple of years I got to work alongside the best lab I could have imagined. Thank you, André, that I could always

turn to you (quite literally as we sat back to back) and that you would face each question, whether brain- or food-related, with equal amounts of joy. A big thanks goes to Samira for her commitment towards our research and for creating room for conversations about science as well as the truly important topics in life. Thank you, Mahnaz, for staying way longer than initially intended and for sharing lots of laughs and mirza ghasemi. Thank you, Gabi and Roman, for never getting tired of answering my technical questions (and there were loads). A special thanks goes to Laura and her snack drawer for ensuring constantly high levels of motivation. I promise that I always refilled it. Also, thank you for answering my countless biochemistry questions. Further thanks go to Franziska, Eric, Kasia, Jingxian and the entire TUM Neuroimaging Center. I am especially grateful for Alyssa and Dani, who started out as the lab adoptees and ended up as close friends. Thank you for this joint PhD ride; for being there on the hard days and for celebrating the tiniest wins. Further, I would like to thank everyone else who is still friends with me despite potential social withdrawal during hectic phases of the PhD, especially Leo, Kimi, Marlon, Jenny and Keanu.

None of this would have been possible without the infinite support of my family – Valli, Alina, Hannah and my Mom. It is mentioned quite often that first generation academics have to work hard towards their goals. What is not emphasized enough, though, is how much hard work, dedication and love it takes from their parents to enable their kids to receive the education of their dreams. Not once did my mom let us doubt that we could go to university and achieve our goals. You did it all by yourself and I am so, so proud of you. Thank you for teaching me to dream big and that et hätt noch immer jot jejange.
Last, but surely not least, Felix, you first met me when I was a couple of weeks into my PhD so you have no idea how easygoing I actually am. Prepare to be stunned. You dealt with me being sleep deprived, happily discussed MRI data at the dinner table and not once complained about the alarm clock ringing at 3:15am on a Sunday “morning“ so that I could go acquire my data. This thesis would have never seen the light of day without you covering my back – especially during these last couple of weeks before submission. Thank you for believing in me when I didn't and for never mocking my code.

List of publications

Bose, A., Epp, S. M., Belenya, R., Kurcyus, K., Ceballos Dominguez, E., Ranft, A., Salas Villa, E., Bursche, M., Preibisch, C., Castrillón, G., & Ri*edl, V. (2024).* Simultaneous quantification of oxygen and glucose consumption during visual stimulation in the human cortex*.* **bioRxiv**. https://doi.org/10.1101/2024.10.11.617828

Castrillon, G., Epp, S., **Bose, A.**, Fraticelli, L., Hechler, A., Belenya, R., Ranft, A., Yakushev, I., Utz, L., Sundar, L., Rauschecker, J. P., Preibisch, C., Kurcyus, K., & Riedl, V. (2023). An energy costly architecture of neuromodulators for human brain evolution and cognition. *Science Advances*, *9*(50), eadi7632. https://doi.org/10.1126/sciadv.adi7632

Declaration of author contributions

Manuscript I: Quantifying the effects of hypoglycemia on cerebral oxygen metabolism

Bose, A., Haschka, S.J., Köhler, J., Hesse, F.A., Martin, S., Steinberg, L., Iakoubov, R., Riedl, V.

AB, VR designed the study. AB, IR, VR implemented glucose clamping within the MR scanner. AB designed all experiments and coded all cognitive tasks. AB acquired all data with help of SH, JK, FH, SM, LS, IR. During data acquisition, SH, JK, FH, IR were responsible for glucose clamping. AB was responsible for participant management, supported by LS. AB preprocessed, analyzed and interpreted all data, performed all data visualizations and wrote the present manuscript. VR provided supervision, funding and writing review.

My contributions to this manuscript in detail:

For this manuscript, I designed the study, implemented the clamping procedure within the MR scanner, designed all experiments and coded all cognitive tasks. Moreover, I was responsible for participant and data management and acquired all data. Subsequently, I preprocessed, analyzed and interpreted all data, performed data visualizations and wrote this manuscript.

Munich, May 15, 2024

Antonia Bose

Prof. Dr. Valentin Riedl, PhD

Manuscript II: Simultaneous quantification of oxygen and glucose consumption during visual stimulation in the human cortex

Bose, A. & Epp, S.M.*, Belenya, R., Castrillón, G., Kurcuys, K., Ceballos Dominguez, E., Ranft, A., Salas Villa, E., Bursche, M., Preibisch, C., Riedl, V.

*shared first authorship between AB and SE

SE & AB were responsible for data collection, design optimization, participant organization and data analysis. AB and SE wrote the manuscript with contributions of GC and VR. SE finalized all figures. RB performed the quantification of the fPET data. GC assisted with data analysis, data management and manuscript editing. KK assisted with conceptualization of the design. ECD assisted with the quantification of the fPET data. AR was the responsible medical doctor during data collection, ESV helped with the quantification of the fPET data, MB helped with data collection, CP was responsible for sequence optimization and for the mqBOLD analysis pipeline. VR supervised the project, was responsible for conceptualization, funding and manuscript review.

My contributions to this manuscript in detail:

In this project, I took care of design optimization, participant management, data acquisition, preprocessing and analysis. I wrote this manuscript with contributions of SE.

Munich, May 15, 2024

Antonia Bose Dr. Samira M. Epp Prof. Dr. Valentin Riedl, PhD